The Effect of Rosiglitazone on Bone Quality in a Rat Model of Insulin Resistance and Osteoporosis

by

Laura Donata Sardone

A thesis submitted in conformity with the requirements
for the degree of Master of Science

Department of Laboratory Medicine and Pathobiology
University of Toronto

The Effect of Rosiglitazone on Bone Quality in a Rat Model of Insulin Resistance and Osteoporosis

Laura Donata Sardone

Master of Science

Department of Laboratory Medicine and Pathobiology
University of Toronto

2010

Abstract

Rosiglitazone (RSG) is an insulin-sensitizing drug used to treat Type 2 Diabetes Mellitus (T2DM). Clinical trials show that women taking RSG experience more limb fractures than patients taking other T2DM drugs. The purpose of this study is to understand how RSG (3mg/kg/day and 10mg/kg/day) and the bisphosphonate alendronate (0.7mg/kg/week) alter bone quality in the male, female and female ovariectomized (OVX) Zucker fatty rat model over a 12 week period.

Bone quality was evaluated by mechanical testing of cortical and trabecular bone. Microarchitecture, bone mineral density (BMD), cortical bone porosity, bone formation/resorption and mineralization were also measured.

Female OVX RSG10mg/kg rats had significantly lower vertebral BMD and compromised trabecular architecture versus OVX controls. Increased cortical porosity and decreased mechanical properties occurred in these rats. ALN treatment prevented these negative effects in the OVX RSG model. Evidence of reduced bone formation and excess bone resorption was detected in female RSG-treated rats.

Acknowledgments

I would first like to thank my supervisor, Dr. Marc Grynpas for the plethora of support and encouragement that he has given me these past two years. My time in the Grynpas lab has been both challenging and rewarding and I owe much of this incredcible experience to the exceptional learning environment fostered by Dr. Grynpas. I would also like to thank my committee members, Dr. Rita Kandel and Dr. George Fantus, for their time, expert advice and suggestions regarding this thesis.

This project would not have been possible without techincal assistance. Thank you to Dr. Richard Renlund and the Department of Comparative Medicine at UofT for their instrumental role in the care and treatment of the rats used for this study. I would like to thank Mr.Doug Holmyard for his help with scanning electron microscopy and for always enthusiastically answering my numerous and frequent questions. Thank you to Mircea Dumitriu for performing the mineralization and strut analysis for this project and for never lacking in interesting conversation. Also, thank you to Dr. David Cole and Dr. Reinhold Vieth for performing the blood serum assays for this project.

I would also like to extend my sincere thanks to the entire Grynpas lab for being a pillar of support throughout my graduate studies. I would specifically like to thank my lab manager, Mr. Richard Cheung for his countless hours of assistance as well as Dr. Tom Willett for his expertise in mechanical testing and MicroCT analysis which were essential to this project. I am especially grateful for the guidance and friendship that I received from Kimberly Kyle and Chrystia Wynnychyj who were instrumental in making my time in Grynpasland both a valuable learning experience and enjoyable at the same time.

Lastly, I would like to whole heartedly acknowledge my family and friends for their love and support and for simply being there for me during stressful times. Thank you to my parents for having the extraordinary ability to encourage me to do my best without ever putting pressure on me. Finally, thank you to Greg for understanding me better than anyone and for being unconditionally supportive of me over these last two years.

Table of Contents

List of Tables

List of Figures

List of Abbreviations

ALN	Alendronate
BFR	Bone formation rate
BMC	Bone Mineral Content
BMD	Bone Mineral Density
BMI	Body Mass Index
BSE	Back-scatter Electron Imagaing
BV/TV	Bone Volume/Tissue Volume
CTSK	Cathepsin K
CTX	Carboxyterminal cross-linking telopeptide of bone collagen
ES	Eroded surface
FWHMH	Full width at half maximum height
I.P.	Intraperitoneal injection
JNK	c-Jun N-terminal kinases
MAP	Mineral Aposition Rate
Mpa	Mega pascals
MS	Mineralized surface
N	Newtons
NFATc1	Nuclear factor of activated T-cells, cytoplasmic 1
NF-κB	Nuclear Factor κB
NTX	Aminoterminal cross-linking telopeptide of bone collagen
OS/BS	Osteoid surface/bone surface
OV	Osteoid Volume
OVX	Ovariectomized
PMMA	Poly(methyl methacrylate)
RSG	Rosiglitazone
SEM	Scanning Electron Microscope
T2DM	Type 2 Diabetes Mellitus
Tb.N.	Trabecular Number
Tb.Sp.	Trabecular Separation
Tb.Th.	Trabecular Thickness
TNF-α	Tumor Necrosis Factor alpha
TRAF6	TNF receptor associated factor 6
TRAP	Tartrate-Resistant Acidic Phosphatase

Chapter 1: Introduction

1.1 Motivation and Rationale

In 2008, 51.1% of adults over the age of 18 were reported as obese as well as a startling 19.3% of youth aged 12-17, as diagnosed by body mass index (BMI) (Statistics Canada, 2008). Accompanying these growing rates of obesity is an increasing number of people with Type 2 diabetes mellitus. According to the Public Health Agency of Canada in 2009, 2 million Canadians have been diagnosed with diabetes and 90% of these cases are Type 2. This growing epidemic presents a need for effective anti-diabetic drugs for use when patients are beyond the ability to control the disease with diet and exercise alone. Rosiglitazone is a Type 2 diabetes drug that is currently in use for reducing insulin resistance and improving glycemic control. However, rosliglitazone appears to have skeletal effects, especially in women (Viberti, 2002). Therefore, it is necessary to examine the effect of rosiglitazone treatment on bone quality in an animal model of human obesity and Type 2 diabetes. A thorough understanding of bone biology and bone quality is necessary for this analysis.

1.2 Bone Biology

1.2.1 Composition of Bone

Bone is a composite material that consists of 65% mineral and 35% organic matrix and small solutes. The mineral phase is largely made up of hydroxyapatite [$Ca_{10}(PO_4)_6(OH)_2$]. The

hydroxyapatite provides rigidity to the collagen framework that makes up the organic matrix. The organic matrix consists of 90% collagen and 10% non-collagenous proteins. The collagen in bone is predominantly Type 1 collagen and it is the collagen fibers themselves that form the structural framework in which hydroxyapetite is inserted (Cowin, 2001). The most abundant non-collagenous proteins are osteocalcin, osteonectin and osteopontin. The levels of these proteins in either blood serum or urine are commonly used as markers for bone remodeling, however, their exact function is still poorly understood (Bilezikian, 2002).

1.2.2 Bone Structure

Macrostructure

At the macrostructure level, bone is divided into 2 types: cortical bone and trabecular bone (Figure 1-1). Cortical bone is the compact bone that is found in the shafts of long bones, such as humerus, femur and tibia and on the outside of vertebrae. Long bones consist of the diaphysis (the cylindrical shaft) and the epiphysis (the wider ends). The metaphysis connects the diaphysis with the epiphysis. The diaphysis is mainly composed of cortical bone whereas the majority of the metaphysis and epiphysis are trabecular bone, explained below. Inbetween the metaphysis and epiphysis is the growth plate, which is the region where cancellous bone production and cortex elongation occurs during growth. This region becomes closed in adult humerus when bone growth is no longer occurring (Rho, 1997).

Cortical bone is dense and only contains microscopic channels. Cortical bone comprises 80% of the human skeleton and is responsible for the supportive and protective functions of the skeleton (Cowin, 2001). It is made up of only approximately 10% soft tissue and contains

haversian systems complete with interstitial and circumferential lamellae. This type of bone has very low porosity as well as fatty bone marrow. Bone turnover in cortical bone is very slow.

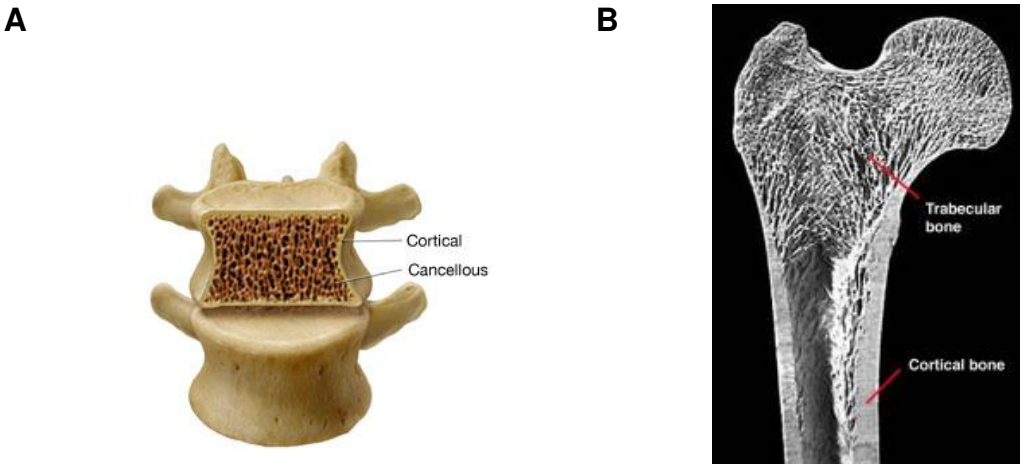

Figure 1-1. Cortical bone and trabecular (cancellous) bone in vertebra (A) and femur (B) (International Osteoporosis Foundation 2007, http://stg.centrax.com/ama/osteo/part4/module03/images/m3_02path_02.jpg)

Trabecular (a.k.a. cancellous) bone is the spongy and porous bone that is found in the ends of long bones (epiphysis and metaphysis) and on the inside of vertebrae. Trabecular bone makes up the remaining 20% of the human skeleton and consists of several interconnected trabecula. Trabecular bone is approximately 75% soft tissue and is made up of curved plates and rods and contains only interstitial lamellae. This type of bone has very high porosity, rapid bone turnover and its bone marrow is hematopoietic. The distribution of cortical and trabecular bone changes depending on the particular bone (Cowin, 2001) and, at the macrostructure of bone, mechanical properties can vary from one bone to another as well as within different regions of the same bone (Rho, 2007).

Microstructure

Both cortical and trabecular bone are made up of woven bone or lamellar bone. New bone is deposited in woven form which is a matrix of interwoven collagen fibers with randomly distributed osteocytes. This type of bone is less organized and shorter lived than lamellar bone and is eventually replaced by lamellar bone.

Lamellar bone is formed in layers of lamellae and contains mineralized collagen fibers that run in the same direction as the lamellae (Figure 1-2). Sometimes these fibers wrap in concentric layers around a central canal which makes up a haversian system (Rho, 1997).

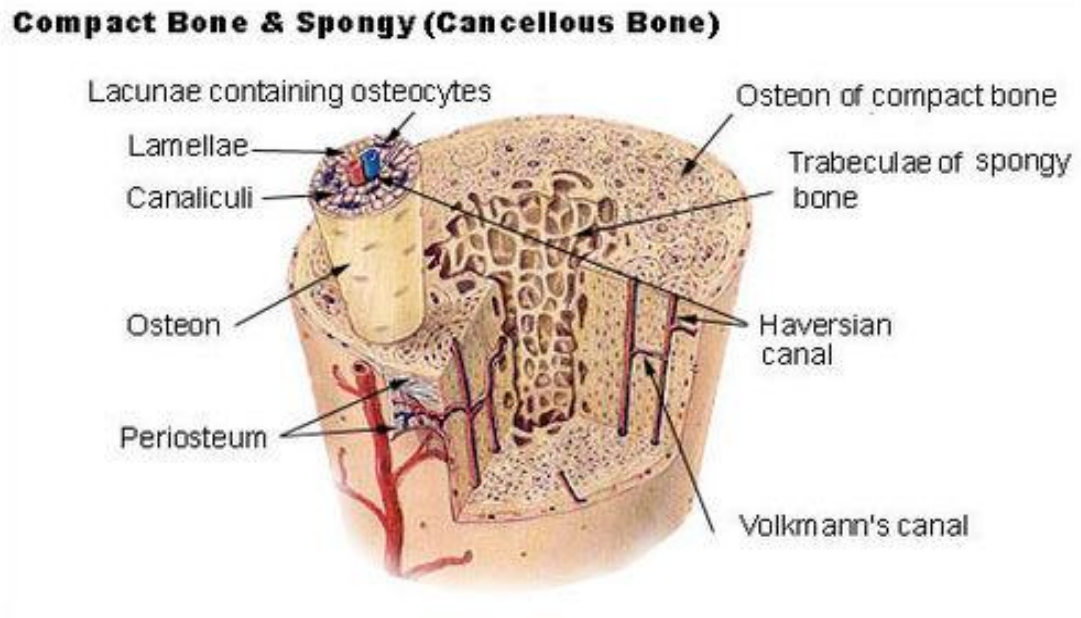

Figure 1-2. Compact and trabecular bone showing haversion system
(U.S. National Institute of Health, http://www.web-books.com/eLibrary/Medicine/Physiology/Skeletal/compact_spongy_bone.jpg)

1.2.3 Bone Cells

Bone is made up of three distinct cell types: osteoblasts, osteocytes and osteoclasts. These cells are responsible for the bone remodeling process and their regulation is very important. Osteoblasts and osteoclasts arise from different cell lineages.

Osteoblasts are mononucleated cuboidal cells that are responsible for bone formation (Bilezikian, 2002). These cells arise from osteoprogenitor cells that are of mesenchymal origin. Under the influence of growth factors (eg. bone morphogenic proteins, BMPs), the progenitor cells differentiate into osteoblasts which express a variety of genetic markers including osteopontin, osteonectin and osteocalcin. They are strongly positive for the alkaline phosphatase enzyme which is a marker enzyme for cells that produce mineralized matrices (Cowin, 2001).

Bone formation by osteoblasts occurs in two stages. First, osteoblast cells lay down osteoid, an organic matrix, which acts as a template for the mineral phase that is subsequently formed. The osteoblast cells are then responsible for facilitating the deposition of mineral within the osteoid.

Osteoblasts that become entrapped within the bone matrix become osteocytes. They are the most abunddant cell type in bone (Bilezikian, 2002). These cells lose a number of osteoblastic characteristics and become stellate shaped. Osteocytes may be responsible for maintaining a low level of bone remodelling in their confined environment. (Cowin, 2001).

Osteoclasts are multinucleated bone-resorbing cells that arise from the monocyte-macrophage lineage (Figure 1-3). The cytoplasm of these cells is characterized by its homogenous, foamy

apperance (Bilezikian, 2002). These cells are strongly positive for tartrate resistant acid phosphatase (TRAP) and cathepsin K.

Signalling of NF-$_K$B by RANKL (Receptor Activator for Nuclear Factor κ B Ligand) is a key factor for stimulating the differentiation and activation of osteoclasts (Suda, 1999). Osteoclast precursors are guided to resorption sites and are induced to mature by osteoblastic cells (Rifkin and Gay, 1992). The osteoclast cell forms a "ruffled" border at the site of bone resorption in order to increase the surface area at the cell-bone interface. The osteoclast then releases hydrogen ions through the ruffled border which allows for the dissolution of the mineralized bone matrix. The release of hydrolytic enzymes also aids in this process.

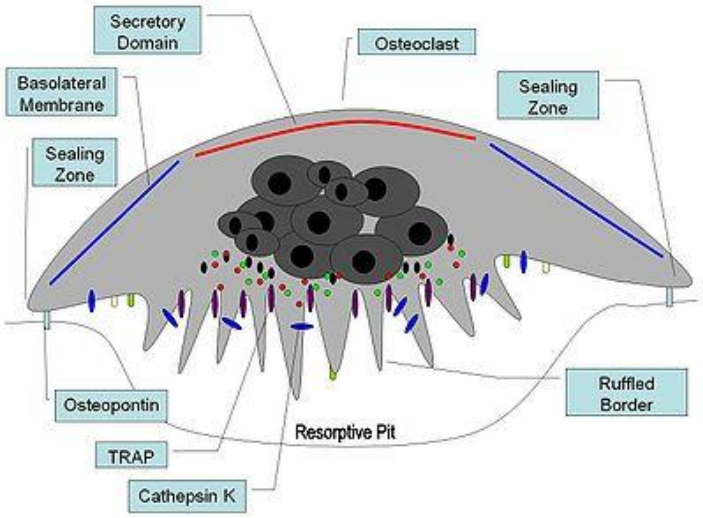

Figure 1-3. Diagram of osteoclast
(Merck Frosst, 2010, http://knol.google.com/k/-/-/3fy5eowy8suq3/wbysga/792px-osteoclast1.jpg)

1.2.4 Bone Remodeling

Bone is a dynamic tissue that is constantly undergoing the process of remodeling (Figure 1-4). Old bone is resorbed by osteoclasts and new bone is layed down by osteoblasts. This process is

necessary in order to repair bone micro-damage that occurs during normal daily activity and also to replace bone during the growth process and following fracture injuries. Precise signalling between osteoblasts and osteoclasts is imperative for this process to be effective (Hill, 1998).

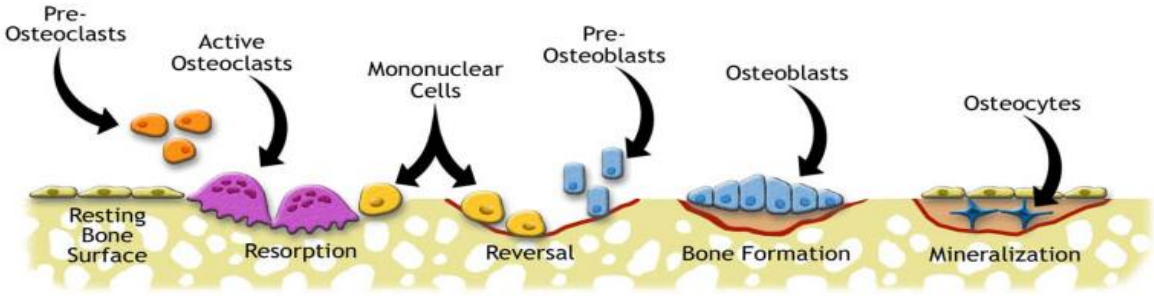

Figure 1-4. Bone remodeling cycle
(http://www.ns.umich.edu/Releases/2005/Feb05/img/bone.jpg)

During the resting stage of remodeling, the bone surface is inactive and is covered by bone-lining cells. The activation phase occurs next and is thought to be induced by structural or biomechanical requirements of the skeleton. During this phase, the mineralized bone surface is exposed and pre-osteoclasts are recruited to the resorption site. Once osteoclasts come in contact with the bone surface, they become active and begin the resorption phase of the cycle. Once resorption is complete, there is a 1-2 week period before formation commences. This period is termed reversal. The formation stage then occurs in 2 stages: the synthesis of bone matrix by osteoblasts and the subsequent mineralization of the matrix as mentioned previously (Cowin, 2001).

An imbalance between formation and resorption can lead to various bone diseases including osteoporosis which results from an excess of bone resorption without adequate formation to compensate.

1.3 Osteoporosis

Osteoporosis is a metabolic bone disease that is characterized by low bone mineral density, weakened trabecular microarchitecture and altered material properties. These changes ultimately result in an increased fracture risk associated with this disease (Grynpas, 2000). There are 2 distinct types of osteoporosis: Type 1 and Type 2 osteoporosis. Type 1 osteopososis, also called post-menopausal osteoporosis, affects post-menopausal women and is most notably characterized by increased bone turnover leading to bone loss. Type 2 osteoporosis is a disease that affects older men and women where hip fracture is the most common occurence.

1.3.1 Post-menopausal Osteoporosis

Post-menopausal osteoporosis arises in older women due to the estrogen deificency that accompanies menopause. Estrogen deficiency causes an increase in the production of cytokines that are involved with the proliferation of osteoblasts and osteoclasts. The osteoblasts, however, do not replace as much bone as is resorbed and an increased rate of bone turnover leading to decreased bone mass ensues. Osteoclastic cytokines (such as tumor necrosis factor, IL-1 and IL-6) are normally suppressed by estrogen. Estrogen also suppresses RANKL, providing an inhibitory effect on osteoclastogenesis (Nirupama, 2000). Important to note is that there are other factors aside from estrogen deficiency that come into play with this disease as all post-menopausal women do not develop osteoporosis (Bilezikian, 2002).

This disease is characterized by decreased bone mineral density (BMD), deterioration of trabecular architecture in the vertebrae and changes in the material properties (eg.

mineralization levels) of bone. All of these changes can affect bone's mechanical properties and lead to an increased risk of fracture (Grynpas 2000).

The most common fractures that occur with this disease are those of the spine and the hip. These fractures are especially prominent due to the substantial amount of trabecular bone in the vertebrae, which is more susceptible to bone loss than cortical bone. The femoral head which comprises part of the hip joint also contains substantial trabecular bone. The shape and structure of this joint also add to its susceptibility to fracture (Peacock, 1995).

1.3.2 The Aged Rat Model of Osteoporosis

The use of animal models is necessary when examining or developing new drugs in order to predict the risk of fracture in humans (Grynpas, 2000 and Iwaniec, 2008). The ovariectomized (OVX) aged rat is a well-accepted model for post-menopausal osteoporosis as it mimics many of the clinical features of the estrogen-depleted human skeleton (Cowin, 2001). This model exhibits increased bone turnover where an excess of bone resorption is not adequately matched by bone formation. The bone loss is more prominent in trabecular bone than in cortical bone and initiates as a rapid phase of bone loss followed by a slower phase. Griffin et al. demonstrated the minimal effects of OVX on cortical bone in the diaphysis of long bones (Griffin, 1993). The bone loss in these rats also occurs in a similar fashion to that of humans, with increased endocortical resorption with little or no change in periosteal area (Szulc, 2006). These rats also demonstrate similar responses to anti-resorptive therapies such as bisphosphonates.

The OVX model is also useful due to the fact that once rats reach 9 months of age they are skeletally mature and more closely mimic the bone loss seen in humans once skeletal maturity has been reached. At 3 months of age, bone growth rapidly slows and growth plateaus by 12 months (Kalu, 1989). The stable skeletal structure observed in the aged rat model ensures that skeletal changes are due to the effects of ovariectomy. Other advantages to the OVX rat model are its convenience, its relatively low cost and its rapid response to ovariectomy and therapy, although, aged rats respond more slowly than young rats (Grynpas, 2000).

There are some limitations to this model: 1) rats have very low levels of haversion remodeling, especially in cortical bone, so the bone loss induced by OVX can be slow to develop in the shafts of long bones, 2) the OVX rat does not develop fragility fractures and 3) there are processes of skeletal bone growth that occur in the rat that do not occur in humans (Cowin, 2001 and Martin, 2003). Since spontaneous fractures do not occur in any species other than humans, the use of sufficient techniques is imperative for the assessment of the effects of therapy on bone. In humans, the amount of bone present along with the probability of a fracture causing fall both contribute to fracture risk. Fracture incidence, however, is not useful for the evaluation of the effects of therapy on bone in animal models, so a collective of parameters known as bone quality is examined instead (Grynpas, 2000).

1.4 Bone Quality

Bone quality is a term that encompasses all of the structural and material properties of bone that contribute to fracture risk (Heaney 1993, Figure 1-5). The main parameters that collectively contribute to bone quality are bone microarchitecture, bone mineralization and bone mechanical properties (Grynpas, 2000). While bone strength is measured by evaluating bone mineral

density (BMD) in a clinical setting, this does not provide an accurate assessment of fracture risk. First, the BMD measurements that are taken in a clinical setting are two-dimensional in nature and additionally, they do not provide a comprehensive analysis of both material and structural properties that contribute to the intrinsic strength of bone. This intrinsic strength is dependent on structural properties (bone geometry and connectivity) and material properties (mineralization) which are all influenced by the process of bone remodeling. An evaluation of bone quantity and bone quality is necessary to adequately predict fracture risk.

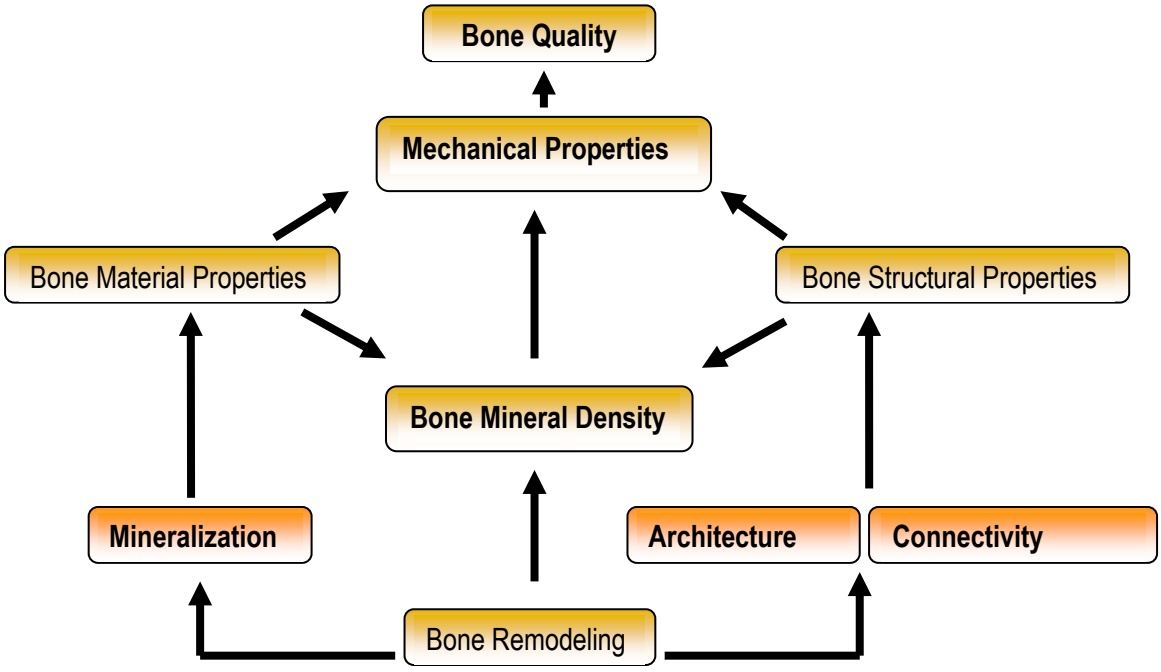

Figure 1-5. Schematic diagram of factors that influence bone quality

1.4.1 Assessment of Bone Mineral Density (BMD)

Dual Energy X-Ray Absorptiometry (DEXA) provides a two-dimensional analysis of BMD (Nagy, 2001). BMD as evaluated by DEXA is a measure of the amount of bone mineral projected in a given area and is not sensitive to density changes in all dimensions, providing an

assessment of the amount of bone present with no suggestion of bone quality. Still, this technique is the most widely used clinical tool for the evaluation of bone mass.

The Piximus mouse densitometer works by passing a cone beam x-ray that generates two different energies onto the bone sample. Photons from this beam are either absorbed or scattered by the tissue depending on the type of tissue (bone mineral or soft tissue). The ratio of the 2 energy x-ray attenuation coefficients provides a measurement of bone mineral content (BMC) which, when divided by the bone area, gives the BMD.

Micro-computed tomography (MicroCT) can also be used to evaluate BMD and is a more accurate tool as it provides a three-dimensional measurement (Thomsen, 2005).

1.4.2 Assessment of Bone Mechanical Properties

Biomechanical parameters such as ultimate load, failure displacement (see page 36) and energy to failure (see page 37) are large contributors to bone fragility (Turner, 2002). Bone fracture, as a result of fragility, occurs when an applied load exceeds the strength of the bone. Both the material properties and structural properties of bone have influence on mechanical properties and bone fragility. The most effective treatment for bone fragility should improve the structural properties of bone without negatively affecting the material properties, although this combined effect is difficult to achieve (Turner, 2002).

The aforementioned mechanical properties of bone that influence bone fragility as well as stiffness (see page 36), which is not a direct measure of fragility, can be evaluated through mechanical testing where bones are loaded until failure (Turner, 1993). The data obtained from

these tests is used to construct a load-displacement curve (see page 37) from which the mechanical properties are derived.

There are four mechanical tests that are commonly used to test the mechanical properties of bone. Three-point bending is used to test long bones in bending until failure. Torsion testing is used to test long bones in shear. Both of these tests are used to evaluate the mechanical integrity of cortical bone. Vertebral compression is used to test vertebrae in compression. This test is not run until failure but rather until a 10% drop in load is achieved. Femoral neck fracture is used as a clinically relevant test to mimic the fracture that occurs following a fall to the hip. Vertebral compression and femoral neck fracture are considered tests of trabecular bone, however, cortical bone does play a small role in both of these tests as well. As mentioned previously, data from these tests generates a load-displacement curve from which the mechanical properties are obtained. This load-displacement curve can then be normalized to account for any structural changes in order to obtain a stress-strain curve (see page 38) from which material properties (such as ultimate stress and strain and toughness, see page 38) can be obtained. The results from femoral neck fracture testing cannot be normalized due to the complex geometry of the femoral head and neck.

1.4.3 Assessment of Bone Material Properties

Bone material properties are the intrinsic properties of bone, independent of shape and size that influence bone's susceptibility to fracture. These properties consist of the characteristics of bone at the tissue level. The quality of the mineral phase of bone is an important contributor to mechanical strength. Back-scatter electron imaging (BSE) evaluates the mineral content of bone. BSE generates a distribution of mineralization values over a cross-section of bone area.

These measurements allow for the determination of the age of the mineral distribution as well as the amount of homogeneity in a given area. The brightness of a given area is related to molecular weight and the degree of mineralization (Grynpas, 2000). Histograms of grey level produce a mineralization profile. An increase in grey level indicates a higher degree of mineralization. While BSE is only a semi-quantitative technique, it is sufficient for detecting mineralization changes as a result of drug treatment.

A scanning electron microscope (SEM) is used for this analysis and works through a focused beam that is continuously scanned over the surface of the bone cross-section. This scanning results in the backscatter of some of the primary electrons and the ejection of some of the secondary electrons. The backscattered electrons are collected and used to distinguish between regions that possess different chemical compositions.

1.4.4 Assessment of Bone Structural Properties

Bone structural properties are the extrinsic characteristics of bone that influence its susceptibility to fracture. An increase in bone mass is most beneficial for bone strength when there is an effective distribution of that bone mass. An assessment of bone geometrical parameters, as well as trabecular architecture and cortical bone porosity allow for the evaluation of the extrinsic properties of bone (Turner, 2002).

Micro-computed tomography (MicroCT) is used to evaluate these parameters. This imaging technique is performed on excised vertebra and femora in order to obtain a three-dimensional image of the specimen. The technique is based on the principle of the collection of the projection of x-rays through a specimen at a very high resolution. These x-rays create cross

sections of the specimen and are later reconstructed into a three-dimensional image of the bone. From these images, cortical bone parameters such as cortical thickness and cross sectional area can be measured. Parameters such as moment of area (see page 40) and polar moment of inertia (see page 45) are also measured and represent the distribution of bone mass around the central axis of the femur. This technique also allows for the evaluation of cortical bone porosity which can be determined through thresholding the reconstructed image to obtain a binary image that distinguishes between bone and empty space.

MicroCT images of vertebrae allow for the determination of trabecular parameters such as trabecular thickness and trabecular number as well as trabecular separation. BSE images are also used to perform strut analysis which gives a measure of the degree of connectivity of trabecular bone. More connected trabeculae add to the mechanical strength of bone.

1.4.5 Assessment of Bone Remodeling and Growth

Bone remodeling and the rate of bone growth are also very important contributors to bone quality. As mentioned previously, an unbalance in the bone remodeling process can lead to many bone diseases such as osteoporosis (Hill, 1998). Bone remodeling, as assessed by static histomorphometry, allows for the measurement of the amount of osteoid (which is an indicator of bone formation) as well as eroded surface (which is an indicator of bone resorption). Dynamic histomorphometry allows for the assessment of bone growth rate by measuring the distance between fluorescent calcein green mineralization markers. For the purposes of this study, proximal tibiae are used for histological analysis. As mentioned previously, the effects of OVX in the aged rat model are more apparent in certain skeletal sites. Even though mechanical testing confirms a loss of strength in rat vertebrae, histomorphological assessment of bone loss

in the tibiae is much more pronounced and thus, more useful to measure than bone loss in the vertebrae (Grynpas, 2000).

1.5 Type 2 Diabetes (T2DM)

Type 2 Diabetes (aka. Non-insulin dependent diabetes mellitus) is a metabolic disorder consisting of a combination of insulin resistance and insulin deficiency. The insulin resistance results in high levels of circulating blood glucose (Figure 1-6).

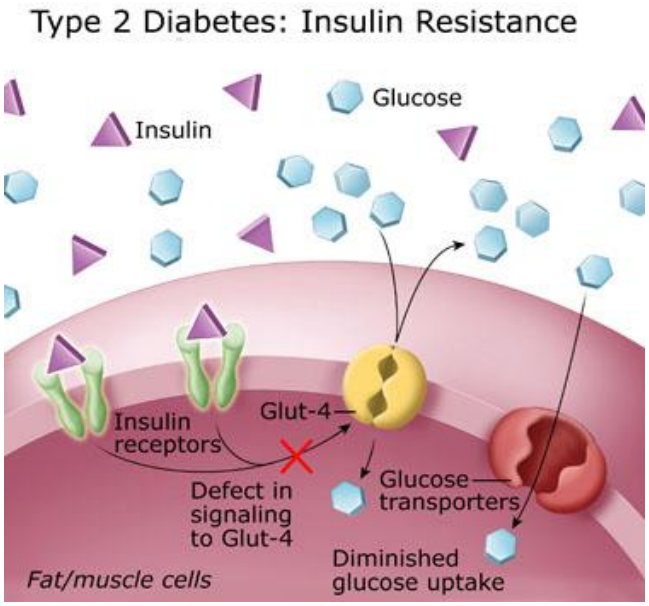

Figure 1-6. Insulin resistance in Type 2 Diabetes (Diabetes Education Online, http://blogs.monografias.com/sistema-limbico-neurociencias/files/2010/04/type-2-diabetes.jpg)

Unlike Type 1 Diabetes, Type 2 Diabetes does not involve the auto-immune destruction of insulin-producing beta cells. Type 2 diabetes is usually accompanied by obesity, especially in the abdominal region. Obesity arises through the processes of adipocyte hypertrophy and hyperplasia (increased number and size of adipocytes) and is the result of energy imbalance in the body (MacKellar, 2009). The partitioning of energy (input versus output) is key for determining if an individual will develop type 2 diabetes (Reddy, 2001).

1.5.1 The Zucker Fatty Rat Model of Insulin Resistance

This study uses Zucker fatty (ZF) rats . The ZF rat is an accepted model for obesity and insulin resistance. The ZF rat is characterized by hyperinsulinemia, hyperlipedemia and very mild hyperglycemia. In this particular strain, adiopcytes are increased in size and in number. The ZF rat has a mutated leptin receptor and is also hyperphagic, obese, hyperlipidemic and insulin resistant. This model is useful for this study due to the ZF rats ability to mimic the effects of non-insulin dependent diabetes (Kurtz, 1989).

Previous studies have demonstrated that ZF rats that are pre-diabetic exhibit increased BMD in long bones and this increase corresponded with high blood serum insulin levels (Prisby, 2008). A study by Reinwald et al showed decreased breaking strength of long bones which was accompanied by decreased BMD (Reinwald, 2009). Another study by Liu et al (2007) showed reduced bone formation in ZF rats compared to their lean counterparts as well as increased adipose volume in bone marrow. All of this evidence shows many similarities to the findings in human studies of increased fracture risk, decreased bone formation and the varying effects of T2DM on BMD which makes the ZF an excellent model for studying the effects of T2DM on bone.

1.5.2 Type 2 Diabetes and Bone

T2DM is associated with an increased risk of osteoporotic fractures despite and increase in BMD (Kawashima, 2009). Interestingly, T2DM is associated with increased body weight which normally protects against fracture risk (Schwartz, 2004). However, some studies (Schwartz, 2001 and Nicodemus, 2001) have found increased fracture risk in women with the disease, the majority of which were non-vertebral in nature. The association of fractures with T2DM,

despite elevated BMD, remained even after correction for increased BMI due to obesity. Certain factors are known to contribute to the fracture risk associated with diabetes such as the number of falls, poor vision and peripheral neuropathy (Shwartz, 2004). The increased fracture risk observed in The Study of Osteoporotic Fractures were not accounted for by these factors. These fractures may be a result of inferior bone quality.

Animal studies have shown similar results. A study of Wistar rats demonstrated increased BMD compared to non-diabetic controls (Sottile, 2004). Decreased bending strength was observed in these rats with energy absorption also being affected indicating that the bones were brittle and thus, more susceptible to fracture. It is unlikely that this decrease in strength is related to BMD, especially since BMD was elevated. Therefore, the reduction in strength may be due to altered bone composition (Bilezikian, 2002). Bones of diabetic rats contain a hypermineralized matrix, which could be negatively affecting the plastic properties of the bone.

Studies show that the increased BMD seen in T2DM is positively correlated with fasting serum insulin (Bilezikian, 2002). This could also explain the decreased BMD seen in individuals with Type 1 Diabetes since they are not producing adequate amounts of insulin. Insulin may have an anabolic effect on bone. It is suspected that insulin's effects on bone are specific to bone size, not necessarily true bone density (Liefde, 2005).

In addition to regulating plasma glucose concentrations, insulin can also influence the functions of other cells such as those of osteoblastic lineage, subsequently affecting the bone formation process (Schwartz, 2003). Evidence of decreased bone formation, as assessed by histomorphometry, in T2DM subjects indicates that the factors responsible for the decreaed

formation are present in the bone serum (Bilezikian, 2002). Decreased osteocalcin concentrations have been found in hyperinsulinemic Wistar fatty diabetic rats. There are various other ways that diabetes can affect bone and possibly lead to bone loss in older diabetic women. Some of these factors include obesity, abnormal insulin levels, hypercalciuria, inflammation, lower levels of insulin-like growth factor 1 and reduced renal function (Schwartz, 2003).

The relationship between fat and bone is important for the assessment of bone quality in type 2 diabetes as obesity often accompanies the disease. As mentioned previously, increased body weight is protective against fracture risk. However, various cytokines that are produced by fat cells (adipokines) have been shown to affect bone quality (Leidig-Bruckner, 2001 and Hamrick, 2008). Leptin, which increases with increased fat mass, can increase the proliferation and differentiation of osteoblasts and inhibit osteoclastogenesis by decreasing RANK expression (Cornish, 2009). Adiponectin is secreted almost exclusively by adipocytes and plasma concentrations are inversely related to visceral fat mass (Cornish, 2009). There is controversy, however, regarding the effects of adiponectin on bone with some studies showing increased bone mass (Williams, 2009) and some showing decreased bone mass with increased serum adiponectin (Cornish, 2009). TNF-α is a bone-resorbing cytokine which increases proportionately to fat mass and interferes with insulin signaling (Epstein, 1995 and Fujiwara, 2000).

The formation of advanced glycation end products (AGEs) can be elevated in subjects with diabetes. They are formed through normal metabolism and can accumulate in bone due to increased levels of circulating glucose. AGEs are thought to alter the physical properties of

bone collagen (Vashishth, 2001). Some studies have also demonstrated the potential for these molecules to increase bone resorption (Miyata, 1997). Treatment for T2DM can involve lifestyle and dietary changes as well as medications to improve insulin sensitivity such as metformin, sulfonylureas and thiazolidinediones.

1.6 Rosiglitazone

Rosiglitazone (RSG) is an insulin-sensitizing drug that is used to treat patients with T2DM to improve glycemic control. It is a member of the thiazolidinedione (TZD) class of drugs which includes other drugs such as pioglitazone and troglitazone. The TZDs are able to enhance insulin action without directly stimulating insulin secretion from the pancreas. These drugs are advantageous for the treatment of T2DM because their effect does not alter the negative feedback system between glucose and insulin, eliminating the possibility of hypoglycemia which commonly occurs with other T2DM drugs such as insulin and sulfonylureas (Saltiel, 1996).They serve as activators for the the peroxisome proliferator-activated receptors (PPAR) and alter the expression of insulin responsive genes, allowing for the uptake of glucose into skeletal muscle (Saltiel, 1996) and preventing fatty acid-induced insulin resistance (Ye, 2004). Three types of PPAR have been identified (alpha, gamma and beta/delta). PPAR α is expressed in liver, kidney, heart, muscle and adipose tissue. PPAR β/δ is mainly expressed in the brain, adipose tissue, and skin (Tontonoz, 2008). Lastly, PPARγ is expressed in 3 different forms: PPARγ 1 is expressed in virtually all tissues, PPARγ 2 is expressed in adipose tissue and PPARγ 3 is expressed in macrophages, large intestine and white adipose tissue (Kawai, 2009). Pioglitazone and troglitazone bind to PPARγ but to a lesser extent, to PPAR α as well whereas rosiglitazone only binds to PPARγ. Recently, TZDs have been implicated in causing liver damage, increasing fatalities from heart disease and increased fracture risk.

1.6.1 Rosiglitazone as Diabetes Treatment

RSG is an agonist for the peroxisome proliferator-activated receptor isoform γ (PPARγ) receptor. PPAR γ is a member of the nuclear receptor family of transcription factors (Mayerson, A.B. et al, 2002) and regulates mRNA expression levels of its target genes with ligand activation (Wan, 2007). The nuclear receptor family are a class of proteins that regulate the expression of specific genes involved in homeostasis, development and metabolism (Green, 1988, Figure 1-7). Activation of PPAR γ by RSG allows for the regulation of insulin-responsive genes (Rzonca, 2005).

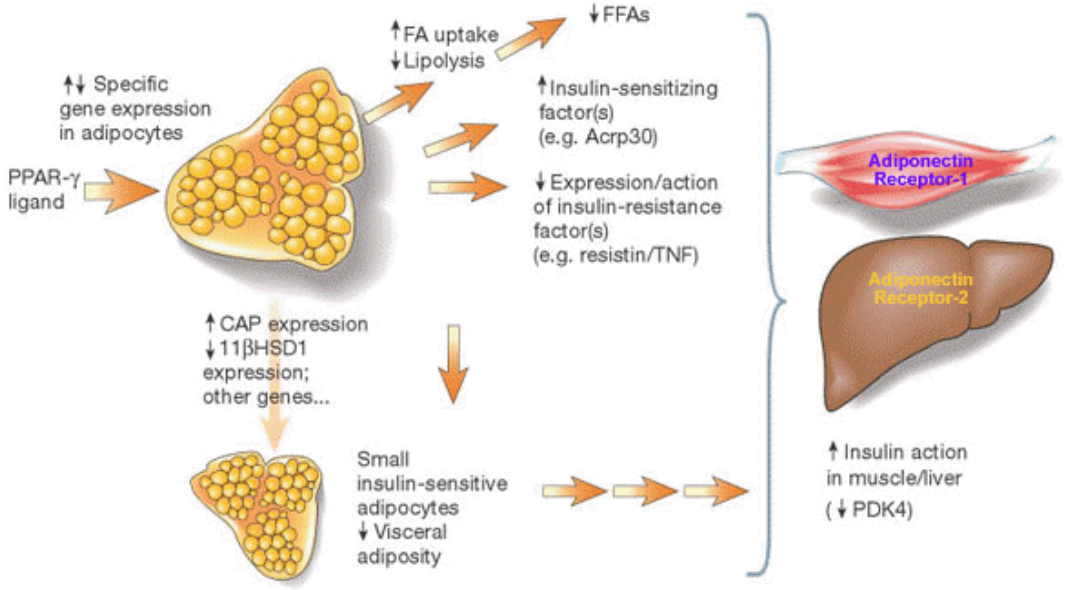

Figure 1-7. The effects of PPARγ agonist in muscle, liver and adipose tissue
Reprinted by permission from Macmillan Publishers Ltd: Nature (Moller DE. New drug targets for type 2 diabetes and the metabolic syndrome, Volume 414, Number 6865) © 2001

1.6.2 Rosiglitazone's Effect on Bone

Previous studies have shown that female patients taking RSG experience more fractures than patients taking other T2DM drugs (Viberti, 2002). These were not the usual osteoporotic fractures of the spine and hip but rather, occurred in the upper and lower limbs. The increase in fractures was significant in women but not in men. RSG may cause decreased osteoblast

formation leading to bone loss. Activation of PPAR γ by RSG can stimulate mesenchymal cells to preferentially differentiate into marrow adipocytes instead of osteoblasts (Ali, 2008). This decrease in osteoblast formation may result in bone loss. These findings have been discovered via *in vitro* studies.

1.6.3 PPARγ and Osteoclastogenesis

There have been conflicting studies, however, suggesting that activation of PPAR γ by RSG regulates osteoclastogenesis *in vivo* which could subsequently affect bone resorption. It has been shown that PPAR γ is expressed in osteoclast precursor cells (Wan, 2007). A study by Sottile et al. showed increases in bone resorption markers (osteoclast number and % eroded surface) in OVX Wistar rats following RSG treatment indicating that observed bone loss is associated with increased bone resorption (Sottile, 2004).

In the study by Wan et al. an important regulator of the osteoclast lineage, c-fos, was indentified as a target gene of PPAR γ. Activation of PPARγ can regulate c-fos levels, part of the RANKL signaling pathway, which can lead to increased osteoclastogenesis (Wan 2007, Figure 1-8). This provides one possible mechanism of RSG's effect on bone though PPAR γ activation. It is possible that both bone formation and bone resorption are being affected thus contributing to altered bone remodeling.

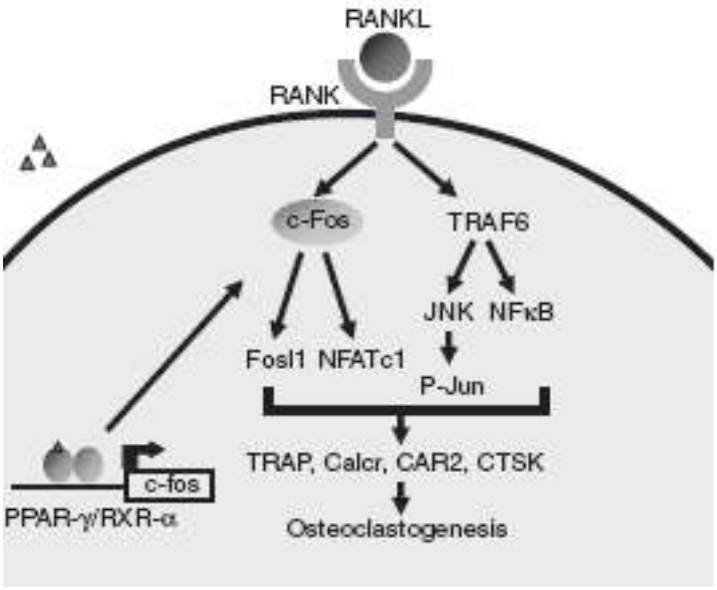

Figure 1-8. The influence of PPARγ on osteoclastogenesis
Reprinted by permission from Macmillan Publishers Ltd: Nature Medicine (Wan Y, Chong LW, Evans RM. PPAR-gamma regulates osteoclastogenesis in mice, Volume 13, Number 12) © 2007

1.7 Alendronate

Bisphosphonates have been shown to enhance mechanical strength of bone through decreasing bone resorption (Azuma et al., 1995). For the purposes of this study, we found it useful to examine the effects of the bisphosphonate alendronate (ALN) on both male and female ZF rats to see if ALN protects against the effects of RSG on bone, thus providing insight into the mechanism by which RSG leads to bone loss.

Bisphosphonates are widely used treatments for osteoporosis. They are bone resorption inhibitors that have been shown to reduce fracture risk and reduce bone turnover by 80-90% (Chavassiuex, 1997). They preferentially target bone by binding apatite which is predominantly stored in bone. Due to their high affinity binding to the mineral surface, they are internalized by the bone-resorbing osteoclasts. They act by interfering with various biochemical processes that occur in the osteoclast and can also encourage osteoclasts to undergo apoptosis (Graham,

2007). While these drugs inhibit resorption, chronic use also results in decreased bone formation (Sahni, 1993) due to the close coupling that exists between bone resoprtion and bone formation. This decreased bone turnover results in increased mineralization (Turner, 2002).

Treatment of post-menopausal women with alendronate has resulted in increased spine, hip and total body BMD as well as decreased risk of both vertebral and non-vertebral fracture. Bisphosphonate treatment has also been shown to enhance the mineralization of bone which could subsequently affect mechanical properties (Turner, 2002).

1.8 Objectives and Hypothesis

The objectives of this study are:

1. To determine if RSG given at doses known to improve insulin resistance will induce bone loss in the ZF and the ZF OVX rat.
2. To determine if RSG will enhance changes in bone architecture and volumetric density in the ZF and ZF OVX rat.
3. To determine if RSG treatment will decrease the mechanical properties of bone in the ZF and ZF OVX rat.
4. To determine if RSG treatment will enhance changes in mineralization, histomorphometry and connectivity parameters of bone in the ZF and ZF OVX rat.
5. To determine if adding alendronate along with RSG prevents the deleterious effects of RSG on the skeleton.

We hypothesize that RSG treatment will induce bone loss, enhance the changes in bone architecture and volumetric density and decrease bone mechanical properties in our female rat model of OVX and insulin resistance. We suspect that this potentially deleterious effect of RSG on bone is due to increased bone resorption and decreased formation and we also suspect that the addition of alendronate will prevent the detrimental effects of RSG due to its anti-resorptive capabilities.

Chapter 2 : Materials and Methods

2.1 Animal Care and Housing

This study involved 50 male and 91 female Zucker fatty rats that were purchased from Charles River. The 50 male rats arrived at the Department of Comparative Medicine at the University of Toronto at 16 weeks of age. The 91 rats arrived at the Department of Comparative Medicine at the University of Toronto at 15 weeks of age. All rats were initially housed in pairs on cornmeal bedding in plastic cages that contained a hide-away tube. Lab chow and an unlimited supply of water were available to all of the rats. The rats were aged for 9 weeks before beginning treatment. One week following arrival, 71 of the female rats were ovariectomized.

2.1.1 Pre-treatment Period

For the first 9 weeks, all rats were fed a 1ml piece of reduced calorie (87% less calorie) strawberry Jello, 5 days a week. 5 weeks after delivery, the rats were split up and housed singly which allowed for proper monitoring of their Jello intake. 4 male rats and 2 female rats died naturally during the 9 week pre-treatment period.

Male Treatment Groups

After the 9 week period, the remaining 46 rats were randomly assigned to one of 4 treatment groups according to Table 2-1. One group was a control and the other 3 groups received various doses of Rosiglitazone (RSG) and Alendronate (ALN). The RSG doses were chosen based on previous studies that demonstrated that these doses were effective for improving insulin sensitivity (Sottile, 2004). The treatment period lasted for a total of 12 weeks. Throughout this 12 week period, all of the rats were transferred to paper bedding to avoid bed sores due to their increasing body weight.

Table 2-1. Male Zucker fatty (ZF) rat treatment chart

GROUP	NUMBER OF RATS	MODEL	TREATMENT
1	11	ZF	Vehicle
2	11	ZF	RSG 3mg/kg
3	12	ZF	RSG 10mg/kg
4	12	ZF	RSG 10mg/kg + ALN 0.7mg/kg

Male Project Timeline

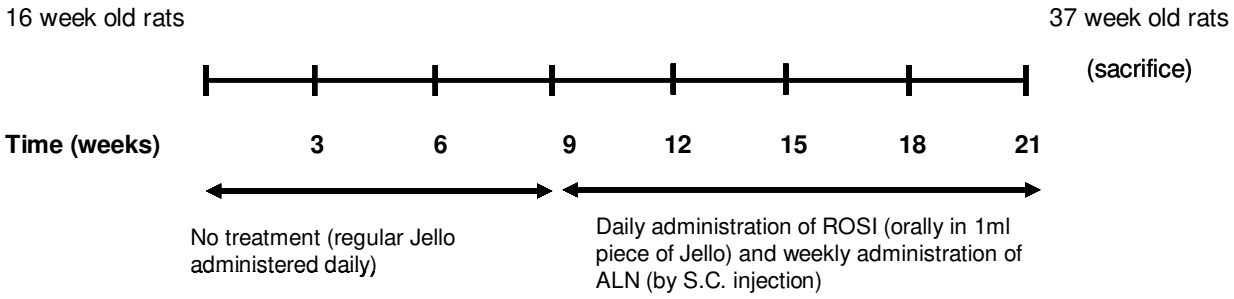

Figure 2-1. Male project timeline

Female Treatment Groups

After the 9 week period, the remaining 89 rats were randomly assigned to one of 8 treatment groups according to Table 2-2. The treatment period lasted for a total of 12 weeks. Throughout this 12 week period, some of the rats were transferred to paper bedding to avoid bed sores due to their increase in body weight.

Table 2-2. Female Zucker fatty (ZF) rat treatment chart

GROUP	NUMBER OF RATS	MODEL	TREATMENT
1	10	ZF sham	Vehicle
2	10	ZF sham	RSG 10mg/kg
3	11	ZF OVX	Vehicle
4	12	ZF OVX	ALN 0.7mg/kg
5	12	ZF OVX	RSG 3mg/kg
6	12	ZF OVX	RSG 3mg/kg + ALN 0.7mg/kg
7	12	ZF OVX	RSG 10mg/kg
8	12	ZF OVX	RSG 10mg/kg + ALN 0.7mg/kg

Female Project Timeline

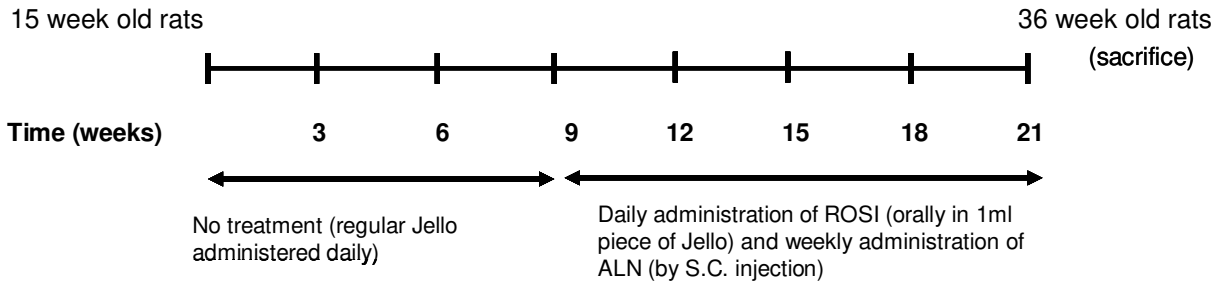

Figure 2-2. Female project timeline

2.1.2 Treatment Period

Drug Preparation and Administration

All of the Jello was administered to the rats orally. 1mL pieces of Jello were placed on the inside of each plastic cage and ingestion of the Jello was monitored for each rat to ensure that the piece had been consumed.

A dose of 0.7mg/kg alendronate was administered via sub-cutaneous injection once a week to the 12 rats in the ALN groups once a week for 12 weeks. Alendronate powder was weighed and added to saline solution to achieve the desired concentration. When the powder had fully dissolved it was injected with a syringe through a syringe filter with a 0.2um supor membrane into a sterile vial. This was all done in a sterile fume hood.

Calcein Green (10mg/kg), a bone mineralization marker, was administered to all rats via I.P. injection 12 days and 2 days before the end of the experiment. The Calcein Green was also prepared as a sterile solution.

Complications During the Treatment Period for Males

Throughout the treatment period, 7 additional rats died naturally leaving a total of 39 rats at experiment termination. The final treatment groups with number of rats in each group are presented in Table 2-3.

Table 2-3. Final male Zucker Fatty rat treatment chart

GROUP	NUMBER OF RATS	MODEL	TREATMENT
1	8	ZF	Vehicle
2	10	ZF	RSG 3mg/kg
3	11	ZF	RSG 10mg/kg
4	10	ZF	RSG 10mg/kg + ALN 0.7mg/kg

Complications During the Treatment Period for Females

Throughout the treatment period, 8 additional rats died naturally leaving a total of 81 rats at experiment termination. The final treatment groups with number of rats in each group are presented in Table 2-4.

Table 2-4. Final female Zucker Fatty (ZF) rat treatment chart

GROUP	NUMBER OF RATS	MODEL	TREATMENT
1	9	ZF sham	Vehicle
2	8	ZF sham	RSG 10mg/kg
3	9	ZF OVX	Vehicle
4	12	ZF OVX	ALN 0.7mg/kg
5	12	ZF OVX	RSG 3mg/kg
6	8	ZF OVX	RSG 3mg/kg + ALN 0.7mg/kg
7	11	ZF OVX	RSG 10mg/kg
8	12	ZF OVX	RSG 10mg/kg + ALN 0.7mg/kg

2.2 Tests Performed Prior to and During Treatment Period for Males and Females

Weight Testing

Prior to beginning the treatment period, all of the rats were weighed. These weights were used to determine the initial concentration of RSG and ALN to be administered to the rats. The rats were also weighed every 4 weeks throughout the treatment period and the RSG and ALN doses were adjusted accordingly as the study progressed.

Blood Testing

Prior to beginning treatment, 1.5mL of blood was taken from each rat via the tail vein. This blood was used to test for determination of insulin and lipids (cholesterol and triglycerides). These blood samples were also used to measure bone formation (osteocalcin) and bone resorption (serum CTX). One drop of blood from the tail vein was used to measure plasma glucose levels via an Accu-check blood glucose meter. Additionally, throughout the study, monthly blood samples were taken for determination of plasma glucose.

2.3 Sacrifice and Dissection for Males and Females

Following the 12 week treatment period, each rat was euthanized in a CO_2 chamber. This was followed by exsanguination via cardiac puncture and cervical dislocation. The blood that was taken at termination was used to test for insulin and lipids (cholesterol and triglycerides), adiponectin and leptin as well as osteocalcin and bone resorption CTX. A final blood glucose test using the glucometer was also performed 2 days before sacrifice.

The femora, humeri, tibiae, and the lumbar vertebrae were dissected out. Both tibia were cleaned immediately of adherent soft tissue. The right tibia were cut in half and immediately

fixed in 70% ethanol. The left tibia were immediately fixed in formalin. The femora and lumbar vertebrae were cleaned of adherent soft tissue and stored in saline solution at -20ºC for the bone studies.

2.4 Assessment of Bone Quality

In order to perform a complete assessment of bone quality, all of the techniques in Figure 2-3 were performed. All 39 male and 81 female samples were evaluated using the following techniques.

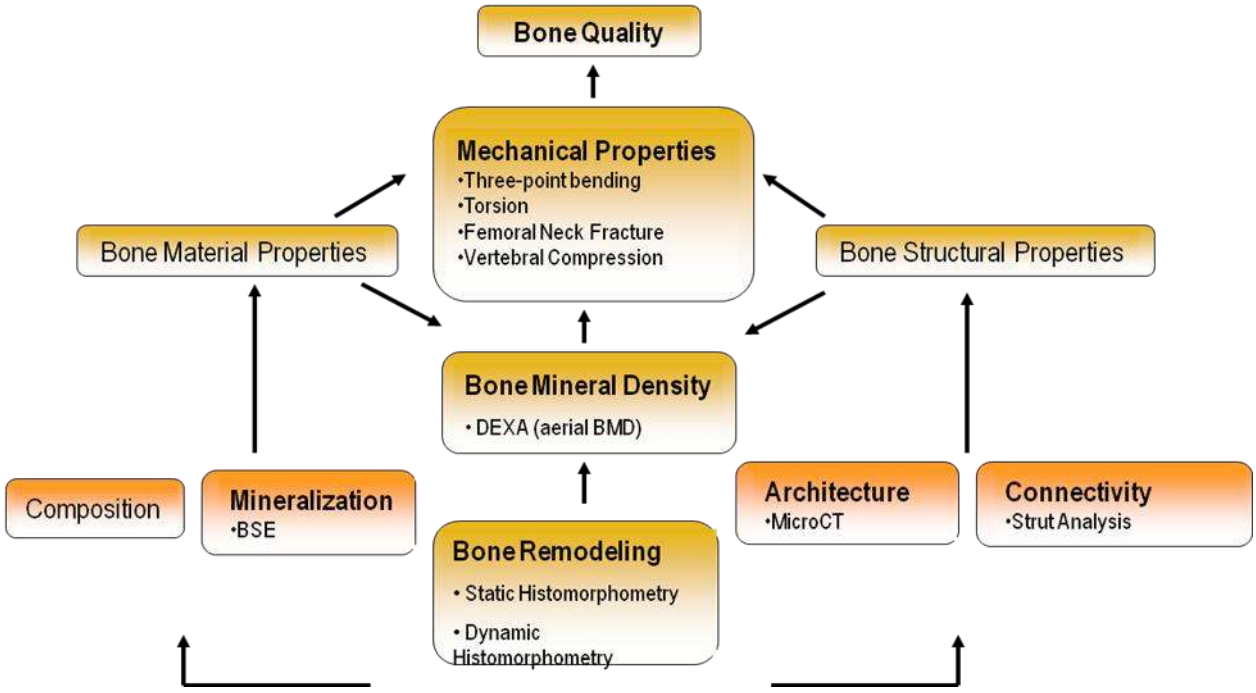

Figure 2-3. Summary of techniques used to assess bone quality

2.4.1 Assessment of Areal BMD : Dual Energy X-Ray Absorptiometry (DEXA)

Dual Energy X-Ray Absorptiometry was performed on all right femora and all L5 and L6 lumbar vertebrae. The cleaned femora and lumbar vertebrae were removed from the -20ºC freezer the night before testing and were kept in the fridge overnight.

DEXA testing was performed using the PIXImus Densitometer. Every time that the machine was turned on, it was calibrated by placing a phantom plate in the scanning area and then running the calibration scan. This was done prior to any testing of bone samples.

Prior to scanning, the bones were placed on a polystyrene plate. The DEXA plate was arranged as follows for femora and lumbar vertebrae respectively.

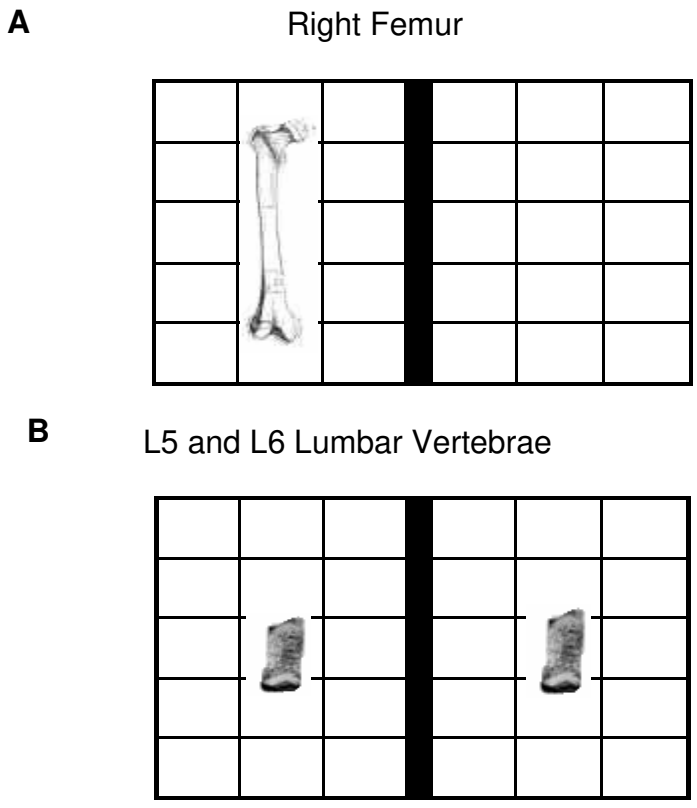

Figure 2-4. Preparation of femur (A) and vertebrae (B) for DEXA analysis

Each right femur was placed individually on the plate with the anterior side facing up. One L5 and one L6 lumbar vertebrae were placed on the plate side by side. Once the scans were run, the software generated the data for Bone Mineral Content (BMC) and bone area. Following each scan, the bones were re-wrapped in saline soaked gauze. All bones were then placed in the -20ºC freezer.

The scans were analyzed using PIXImus software. Bone mineral density was determined by dividing the BMC by the bone area. The values for BMD, BMC and bone area were averaged for L5 and L6 lumbar vertebrae.

2.4.2 Assessment of Volumetric BMD and Bone Structural Properties

Microcomputed tomography (MicroCT)

All right femora and L6 lumbar vertebrae were scanned using MicroCT. The femora and the vertebrae were wrapped in saline soaked gauze and secured in plastic tubes to prevent movement during scanning and to maintain an upright position. All scans were reconstructed and were also calibrated using a hydroxyapatite standard in order to assess volumetric bone mineral density. The images obtained from scanning were analyzed using CTscan software. For femur analysis, the region of interest was defined as 1mm on each side of the midpoint for each sample and was analyzed to obtain structural properties of the bone as well as volumetric BMD. This region of interest surrounded the fracture site from three-point bending tests. The parameters that were obtained from the femur scans were volumetric BMD, anterior/posterior diameter, medial/lateral diameter, the polar moment of inertia (mm^4), the cross-sectional area (mm^2) and the elliptical moment of inertia (mm^4). These geometrical parameters were used to normalize the results from three-point bending and torsion testing.

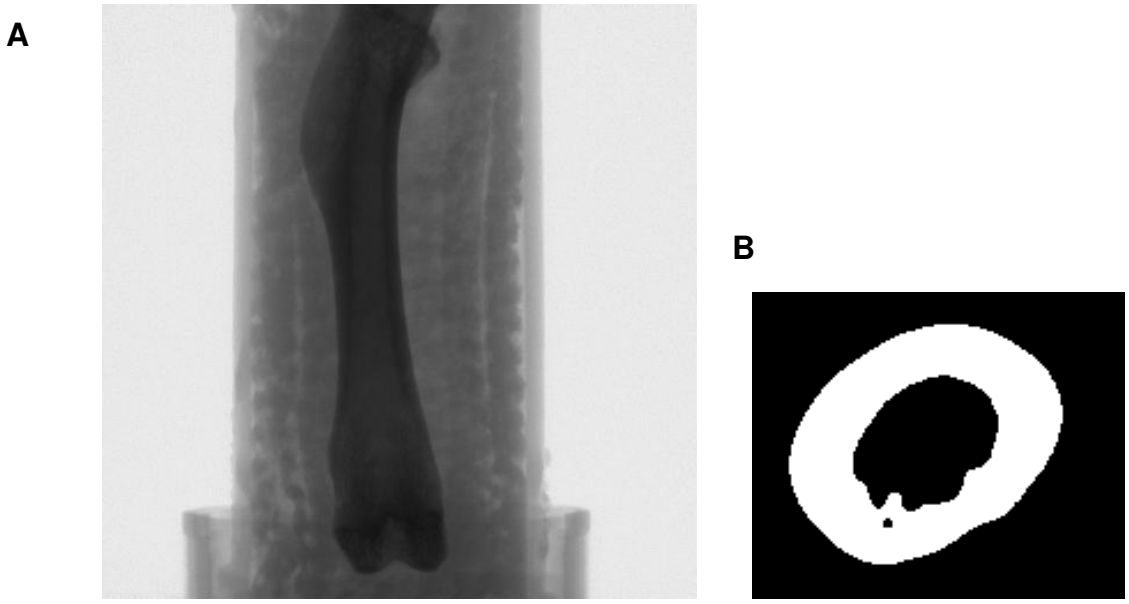

Figure 2-5. Sample image of femur scan (A) and reconstructed image (B)

For vertebrae analysis, the entire length of the vertebrae was used as the region of interest. The parameters that were obtained from the vertebrae scans were total length (mm) and area (mm^2) which were used to normalize the results from vertebral compression testing. Volumetric BMD, percent bone volume, trabecular thickness, trabecular number and trabecular separation were also obtained and were used to evaluate the architecture of each vertebra.

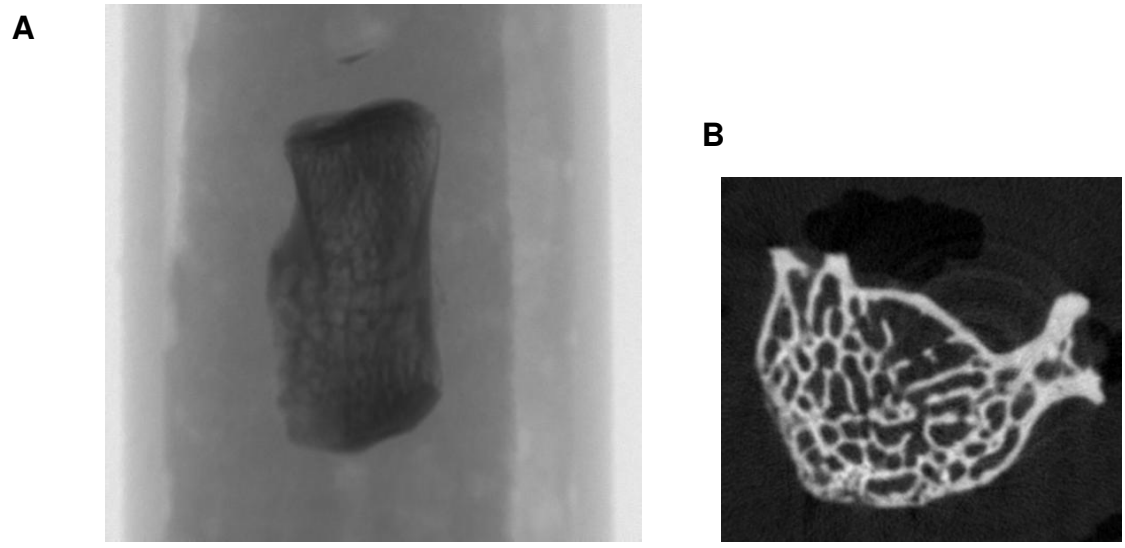

Figure 2-6. Sample image of L6 vertebra scan (A) and reconstructed image (B)

Porosity Measurements

MicroCT was also used to assess the level of porosity in the cortical bone for all right femura. Porosity was analyzed on the same 2mm region of interest that was used for the other MicroCT parameters using Ctan software. The parameters that were obtained from this analysis were % closed porosity, % open porosity and % total porosity. In order to perform this analysis, the region of interest was first thresholded in order to distinguish bone from tissue and the surrounding area. A shrink-wrap was applied to the region of interest in order to stretch over any holes, in order to prevent the program from recognizing the inner cortical space as a pore. A 3-dimensional analysis for porosity was then performed.

2.4.3 Assessment of Mechanical Properties of Cortical Bone

Direct mechanical testing of bone specimens provides a wealth of information regarding bone fragility that cannot be assessed by DEXA alone (Turner, 1993). A load-displacement curve provides information about the relationship between the load applied to a specimen and the resulting deformation in response to that load (Figure 2-7). The parameters that we are most interested in obtaining from the load-displacement curve are; ultimate load, failure load, energy to failure, failure displacement and stiffness. Load is measured in newtons (N) and deformation is measure in millimeters (mm).

The ultimate load represents the maximum load that the specimen sustains whereas the failure load represents the load at which the bone ultimately breaks. The stiffness is determined from the slope of the elastic region of the curve and represents the extrinsic stiffness or the rigidity of the specimen. The failure displacement measures the extent of deformation of the bone at

failure and the energy to failure represents the amount of energy that the specimen can absorb prior to breaking (Turner, 1993).

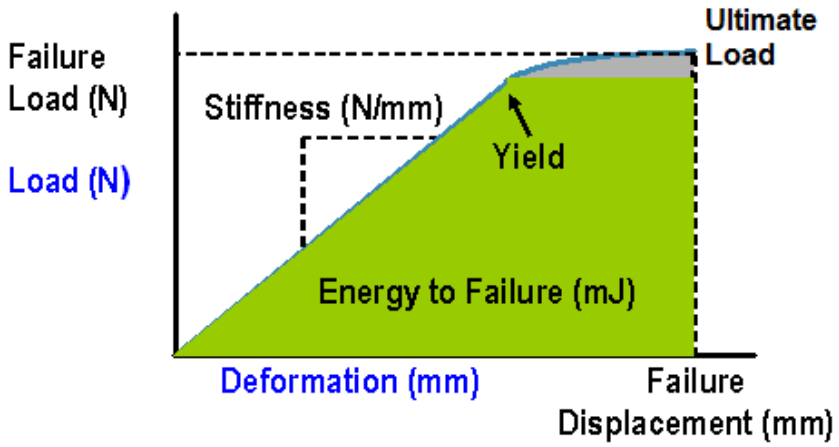

Figure 2-7. Load-displacement curve generated via mechanical testing

Load and deformation can be converted to stress and strain (Figure 2-8) which eliminates the effects of bone size and other extrinsic properties on bone fragility. Stress is defined as force per unit area and is reported in pascals (Pa) or mega pascals (MPa). A specimen can undergo either compressive, tensile or shear stress depending on the direction/orientation of the applied load. These 3 types of stresses, however, often occur in combination and failure often occurs in shear even under compressive forces (Turner, 1993). This is one reason why torsion testing of cortical bone is becoming accepted as a more accurate test than bending or compression as there is no influence of compression on the shear stress that this test aims to measure (Lind, 2001). Strain is defined as the deformation or the percent change in length of a specimen (Turner, 1993) and has no units. The information that we are interested in obtaining from the stress-strain curve are; ultimate stress, failure stress, Young's modulus, and toughness.

The ultimate stress indicates the maximum amount of stress that the bone can withstand and the failure stress is the stress at which the bone actually breaks. The Young's modulus is determined from the slope of the elastic region of the stress-strain curve and is a measure of the intrinsic stiffness of the material. The toughness is a measure of the amount of energy required to cause fracture and is calculated from the total area under both the elastic and plastic regions of the stress-strain curve. A tougher bone is generally more resistant to fracture (Turner, 1993).

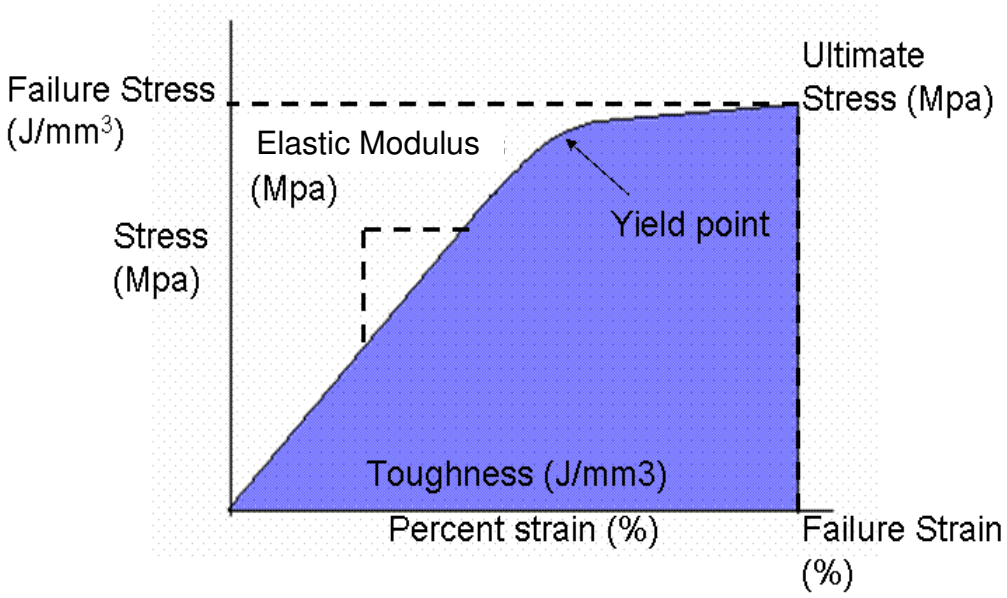

Figure 2-8. Stress-strain curve generate via normalization data

Three-point bending and torsion testing are used to test the mechanical integrity of the cortical bone found in the shafts of long bones. Vertebral compression and femoral neck fracture are accepted tests for the assessment of the mechanical integrity of trabecular bone in the lumbar vertebrae and femoral head/neck respectively.

Three-point Bending

Three point bending was used to test the cortical bone of the right femur (Figure 2-9). This test was used to measure the mechanical properties of the femoral shaft using an Instron 4465 with

a 1000N load cell. Right femora were removed from the -20ºC freezer 2 hours prior to testing and were kept wrapped in saline soaked gauze while they thawed. The length, medial-lateral diameter and anterior-posterior diameter of each femur was measured using digital calipers. The midpoint of each femur was marked with a waterproof marker.

The entire right femur was placed, with anterior side facing up, on two supports 15.6mm apart. A preload between 1N and 2N was applied to the midpoint of the bone and the bone was loaded in bending until failure at a rate of 1mm/min. Immediately after testing, the proximal half of the femur was re-wrapped in saline soaked gauze and placed back in the -20ºC freezer for femoral neck fracture testing.

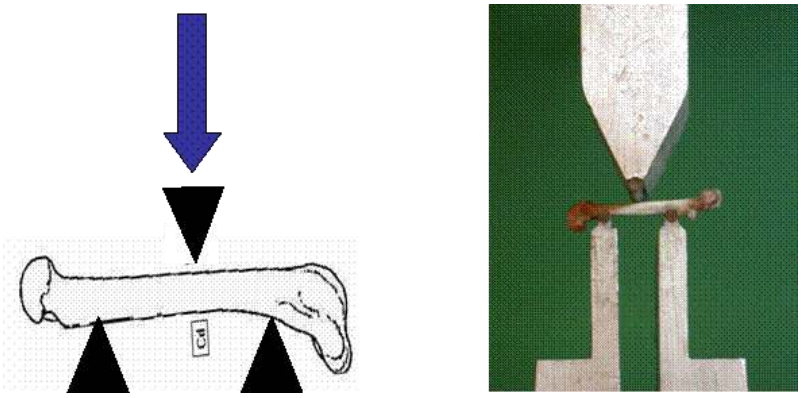

Figure 2-9. Schematic diagram (left) and photograph (right) of three point bending

A load displacement curve (Figure 2-10) was generated using Lab View 5.0 software. The mechanical properties of the bone (ultimate load, failure load, failure deformation, total energy to failure, and stiffness) were calculated from the load displacement curve.

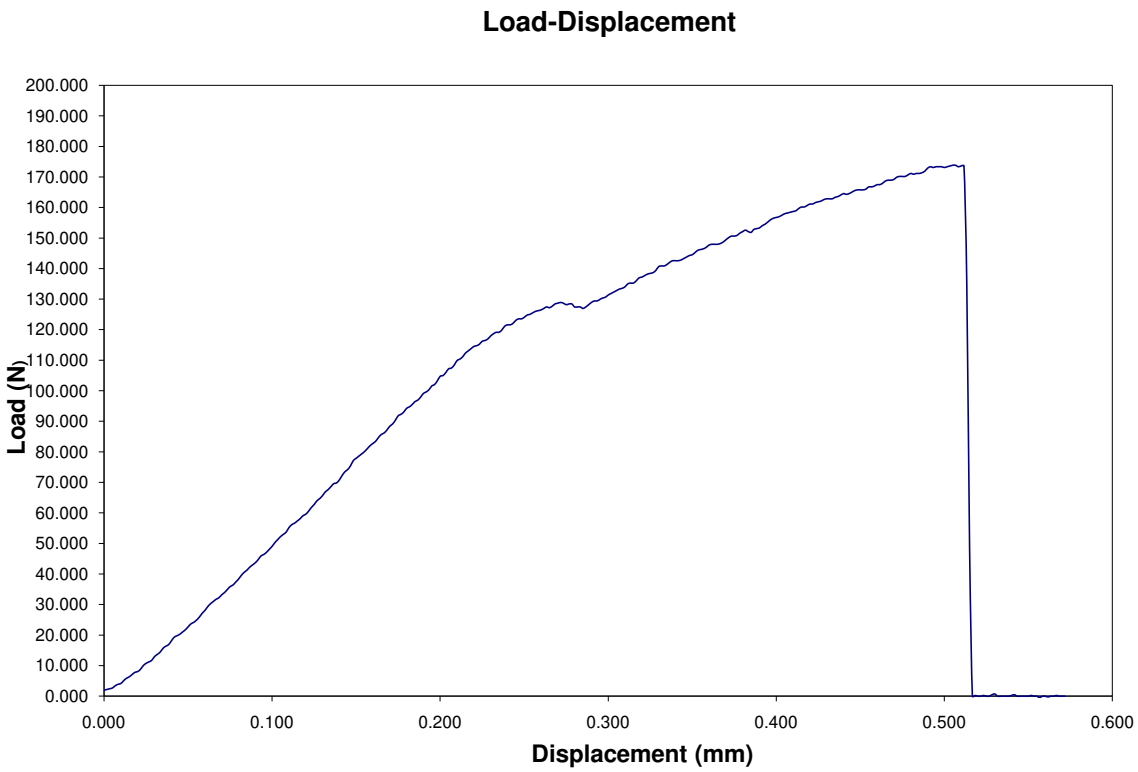

Figure 2-10. Load displacement curve generated via three-point bending

Normalization of this data is essential in order to compare samples that differ in their geometrical parameters. Cross sectional images of distal femora were obtained via microcomputed tomography. This allowed for the determination of the diameter (anterior-posterior and medial-lateral) of the femur as well as the moment of inertia (mm^4) which were used to normalize the load-displacement data (Figure 2-11). This data was then used to create a stress-strain curve (Figure 2-12). The normalized mechanical properties of the bone were determined from the stress-strain curve.

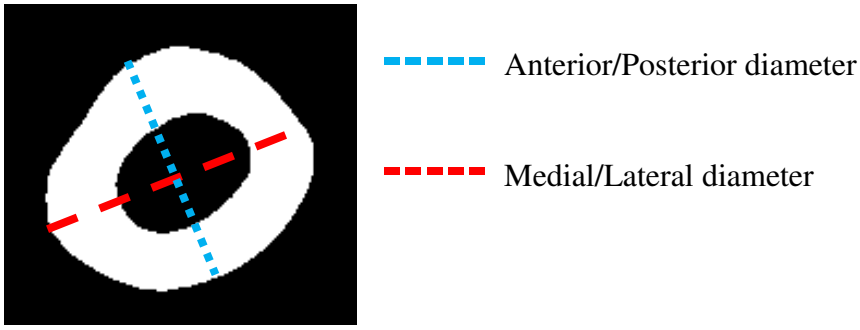

Figure 2-11. Femur cross section used to generate normalization data

The following calculations were used to determine the normalized parameters using the geometrical properties listed above.

$$\sigma_f = \frac{F_f l_o \phi_{AP}}{8 I_{xx}}$$

σ_f : *Failure stress* (MPa)
F_f : *Measured failure load* (N) [Equation 1]
l_o : *Gauge length* (mm)
ϕ_{AP} : *External diameter in anterior – posterior direction* (mm)
I_{xx} : *Elliptical moment of inertia* (mm^4)

$$\varepsilon_f = \frac{6 \phi_{AP} \delta_f}{l_o^2} \cdot 100$$

ε_f : *Failure strain* $(\%)$ [Equation 2]
ϕ_{AP} : *External diameter in anterior – posterior direction* (mm)
δ_f : *Failure displacement* (mm)
l_o : *Gauge length* (mm)

$$E = \frac{Kl_o^3}{48I}$$

E : *Elastic* modulus (MPa) [Equation 3]

K : *Stiffness* (*slope of load – deformation curve*) (N/mm)

l_o : *Gauge length* (mm)

I : *Elliptical moment of inertia* (mm^4)

$$\mu_f = \sum_{j=1}^{n} (\sigma_{j-1})(\varepsilon_{j-1} - \varepsilon_j) + \left[\frac{(\sigma_{j-1} - \sigma_j)(\sigma_{j-1} - \sigma_j)}{2} \right]$$

μ_f : *Toughness* (mJ/mm^3)

σ : *Stress* (MPa) [Equation 4]

ε : *Strain*

n : *Total number of data points to yield*

j : *Integer increments from* 1 *to* n

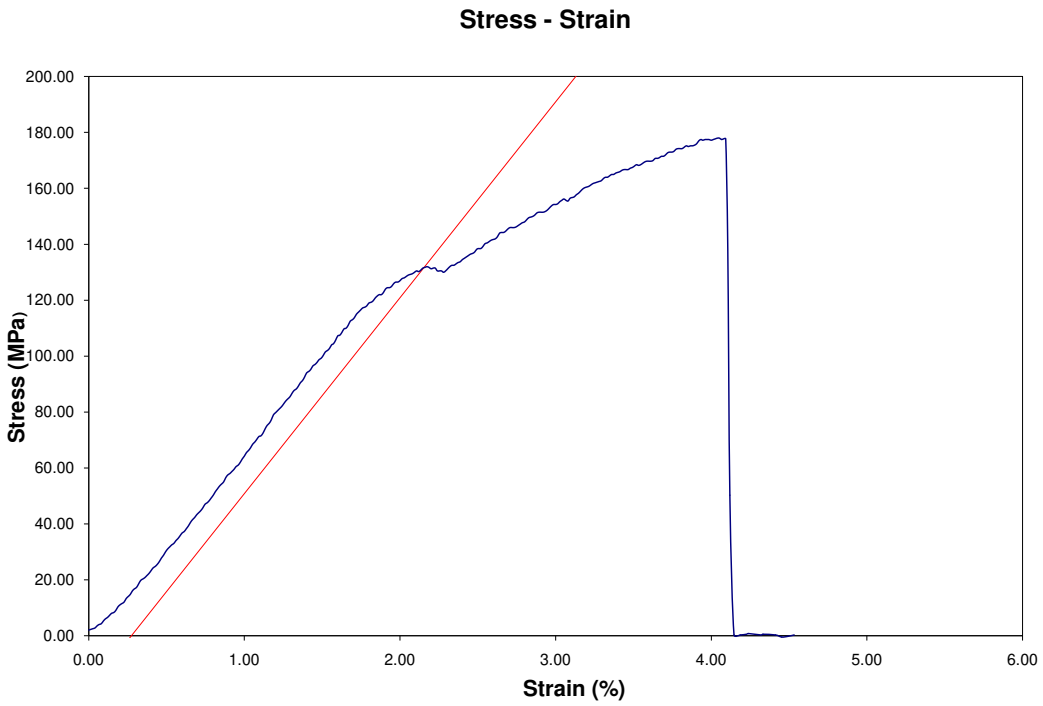

Figure 2-12. Stress-Strain curve (showing 0.2% offset for yield point determination) following normalization of Three-point Bending

Torsion Testing

Torsion testing was used to test the cortical bone of the left femur. All left femora were removed from the -20ºC freezer 2 hours prior to testing and were kept wrapped in saline soaked gauze while they thawed. While femora were thawing, the total length of each bone was measured using digital calipers. The midpoint of the bone was marked as was an 18 mm gauge length (amount of exposed bone) and the outer ends of the femur were removed using an Isomet low speed saw. The bones were then rewrapped in saline soaked gauze around the gauge length and were kept moist until testing.

The proximal end of each femur was secured into a bolt head using PMMA and the same was done with the distal end. The PMMA was allowed to dry for at least 10 minutes per end. Saline soaked gauze was kept moist throughout this process (Figure 2-13).

Torsion tests were performed on a custom machine loaded with a 20in.lb. load cell. The machine consists of one stationary chuck and one rotating chuck and was calibrated before use. The femur, encapsulated by the two bolts, was secured into the two chucks and, immediately before testing, the gauze was removed. The exact gauge length was measured with digital calipers. The tests were run at a speed of approximately 1.5 degrees/sec until failure. Data files containing the time, torque and rotation information were acquired using LabView data acquisition software. The parameters that were evaluated are Failure Torque (N·mm), Angular Deformation at Failure (rad), Energy to Failure (N·mm·rad) and Stiffness (N/mm) (Figure 2-14).

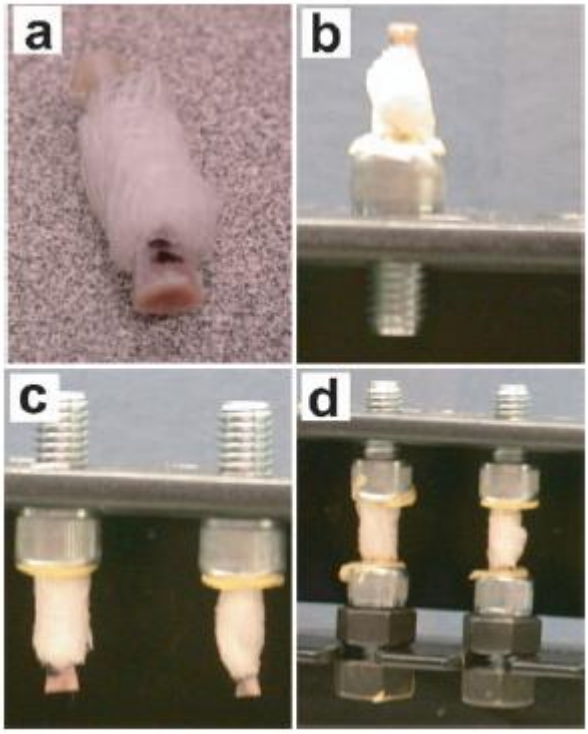

a) Epiphyses of bone are removed and bone is wrapped in saline soacked gauze until testing.
b) Bone is inserted into bolt and is left to dry right-side up.
c) Bolts are turned upside down.
d) Bones are secured into second bolt and left to dry.

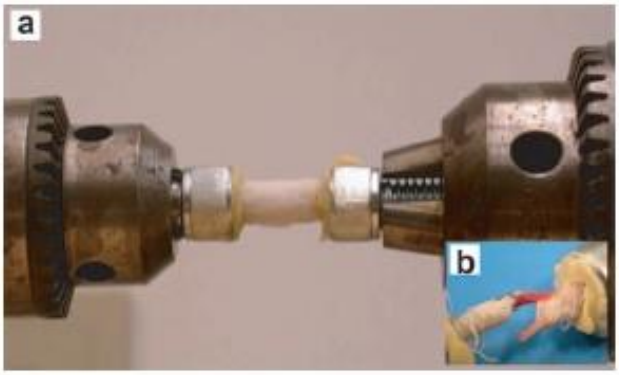

a) Bone and bolt set-up is inserted into jigs on torsion machine.
b) Broken bone following torsion testing.

Figure 2-13. Preparation of femora for torsion testing

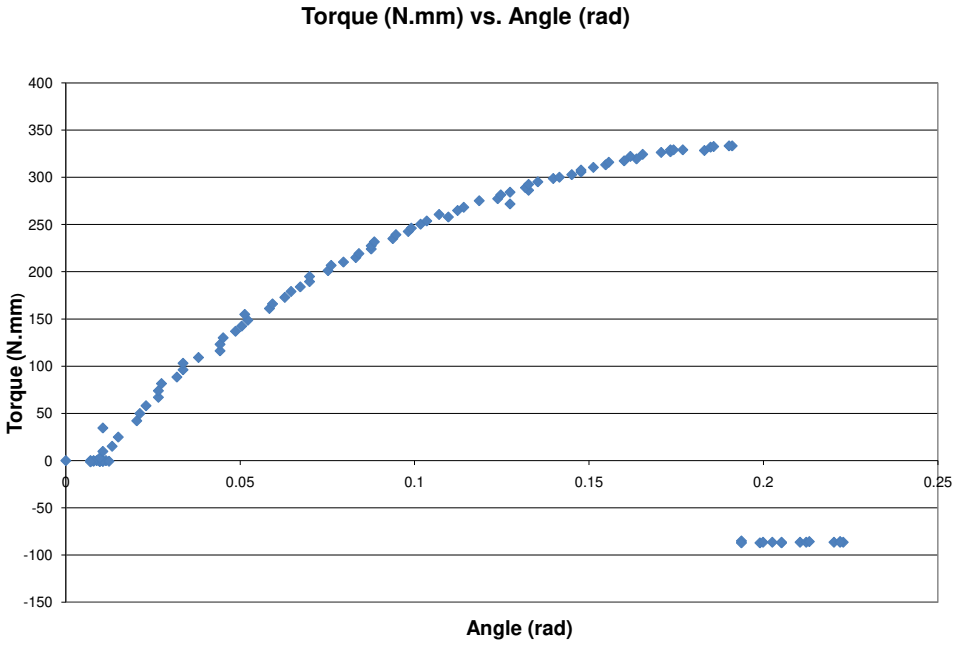

Figure 2-14. Torque vs. Angle curve generated from torsion testing

The data from torsion testing was normalized using data obtained from MicroCT testing including the polar moment of inertia (mm^4), cross sectional area (mm^2) as well as the medial/lateral diameter of the femur and the gauge length. The following equations were used to determine the normalized parameters.

$$\sigma_f = \frac{\phi_{ML}}{2} \cdot \frac{T_f}{J}$$

[Equation 5]

σ_f : *Failure shear stress* (MPa)

T_f : *Failure torque* $(N \cdot mm)$

ϕ_{ML} : *External diameter in medial – lateral (major) direction* (mm)

J : *Polar moment of inertia* (mm^4)

$$\varepsilon_f = \frac{\phi_{ML}}{2} \cdot \frac{\alpha_f}{l_o} \cdot 100$$

γ_f : *Failure shear strain* (%) [Equation 6]

ϕ_{ML} : *External diameter in medial – lateral* (*major*) *direction* (*mm*)

α_f : *Failure rotation* (*mm*)

l_o : *Gauge length* (*mm*)

$$G = \frac{sl_o}{J}$$

G : *Shear* mod *ulus*(*GPa*)

s : *Stiffness* ($N \cdot mm/rad$) *or* (mJ/rad) [Equation 7]

l_o : *Gauge length* (*mm*)

J : *Polar moment of inertia* (mm^4)

$$\mu_f = \sum_{j=1}^{n} (\sigma_{j-1})(\varepsilon_{j-1} - \varepsilon_j) + \left[\frac{(\sigma_{j-1} - \sigma_j)(\sigma_{j-1} - \sigma_j)}{2} \right]$$

μ_f : *Toughness* (mJ/mm^3)

σ : *Stress* (*MPa*) [Equation 8]

ε : *Strain*

n : *Total number of data po* int *s to yield*

j : *Integer increments from* 1 *to n*

2.4.4 Assessment of Mechanical Properties of Trabecular Bone

Vertebral Compression

Vertebral compression was used to test the trabecular bone of the L6 lumbar vertebrae. L6 lumbar vertebrae were removed from the -20ºC freezer 2 hours prior to testing and were kept wrapped in saline soaked gauze while they thawed. A plate with multiple holes of varying sizes

was placed on top of a solid plate and both were clamped onto the base of the Instron 4465 with a 1000N load cell. Small bolts were filled with PMMA and the L6 lumbar vertebrae were secured in the PMMA with the narrow side down. PMMA was left to dry for 10 minutes while the bone was covered with saline soaked gauze (Figure 2-15). Before testing, the gauge length of the vertebra was measured and recorded.

The bolt containing the vertebra was then screwed into the jig, which was then inserted into the 1000N load cell. The plate on the base of the Instron was aligned such that the vertebra would fit snugly into the appropriate hole. The jig and bone setup was then lowered so that the vertebra came in contact with the plate. A preload of 5N was applied and the vertebra was loaded until a 10% drop in load was achieved at a rate of 1 mm/min.

A load displacement curve was generated using Lab View 5.0 software (Figure 2-16). The mechanical properties of the bone (ultimate load, failure load, failure deformation, total energy to failure, and stiffness) were calculated from the load displacement curve. As mentioned previously, this test is not run until failure but rather until a 10% drop in load is achieved.

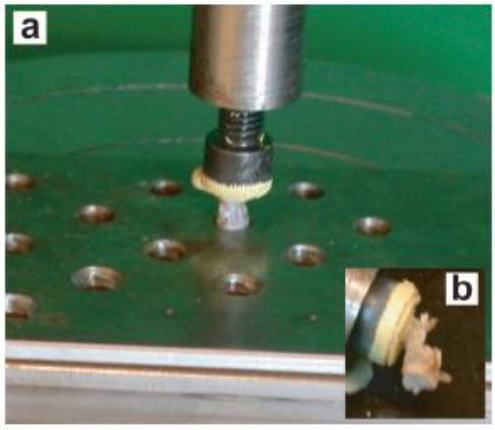

Figure 2-15. Preparation of L6 vertebra for vertebral compression testing

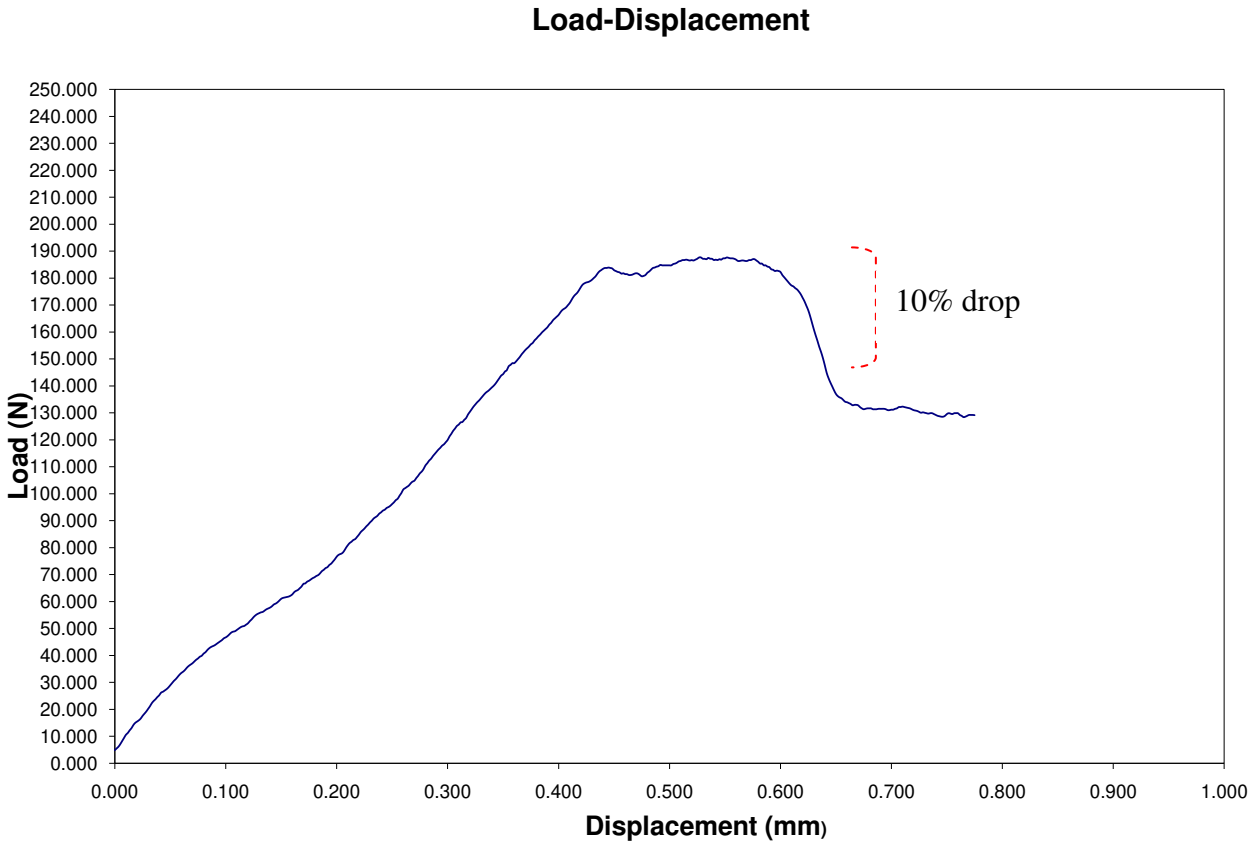

Figure 2-16. Load-displacement curve generated via vertebral compression

This data was normalized using data from MicroCT testing including the area of the bone (mm^2) and the total height (mm) of the vertebrae. A stress strain curve was generated and the normalized parameters were determined based on this curve. The following equations were used to calculate the normalized parameters.

$$\sigma_f = \frac{F_f}{A_{cs}}$$

$\sigma_f : Failure\ stress\ (MPa)$ [Equation 9]

$F_f : Bending\ moment\ (N \cdot mm)$

$A_{cs} : Cross-sectional\ area\ (mm^2)$

$$\varepsilon_f = \frac{\delta_f}{h_\upsilon} \cdot 100$$

$\varepsilon_f : Failure\ strain\ (\%)$ [Equation 10]
$\delta_f : Displacement\ at\ failure\ (mm)$
$h_\upsilon : Height\ of\ vertebra\ (mm)$

$$E = \frac{h_\upsilon}{A_{cs}} K$$

$E : Elastic\ \mathrm{mod}ulus\ (MPa)$ [Equation 11]
$h_\upsilon : Height\ of\ the\ vertebra\ (mm)$
$K : Stiffness\ (N/mm)$
$A_{cs} : Cross-\mathrm{sec}tional\ area\ (mm^2)$

Femoral Neck Fracture

Femoral neck fracture is another test that is used to obtain load-deformation data. This test is clinically relevant since it mimics the common hip fracture. Femoral neck fracture was administered to the proximal half of all right femora using an Instron 4465 with a 1000N load cell. Right proximal femora were removed from the -20ºC freezer 2 hours prior to testing and were kept wrapped in saline soaked gauze while they thawed. A square piece of cardboard was placed in the bottom of a jig that had been coated with Vaseline. The proximal end of the right femur was fixed in the jig with 4 screws. The jig was filled with polymethylmethacrylate (PMMA) and was left to dry for 10 minutes while covered in saline soaked gauze.

Before testing, the gauge length was measured and recorded. The jig was then loaded into the Instron 4465 so the femoral head was facing downwards. A plate with a hole in it was placed on the base of the Instron 4465. The jig and bone setup was then lowered so that the femoral head came in contact with the plate and the rest of the proximal femur passed through the hole in the plate (Figure 2-17). A preload between 0.5 and 1N was applied and the femoral head was loaded until failure at a rate of 2.5 mm/min.

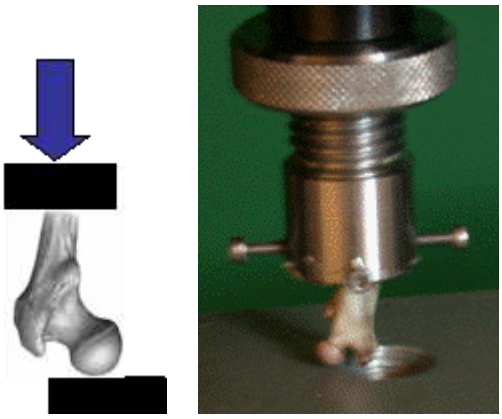

Figure 2-17. Schematic diagram (left) and photograph (right) of femoral neck fracture of proximal femur

A load displacement curve (Figure 2-18) was generated using Lab View 5.0 software. The mechanical properties of the bone (ultimate load, failure load, failure deformation, total energy to failure, and stiffness) were calculated from the load displacement curve. Unlike the three-point bending data, femoral neck fracture data cannot be normalized due to the irregular geometry and angle of the femoral neck. Variations in the sites of fracture and the composition of the femoral head/neck (cortical bone and trabecular bone) also prevent this data from being normalized.

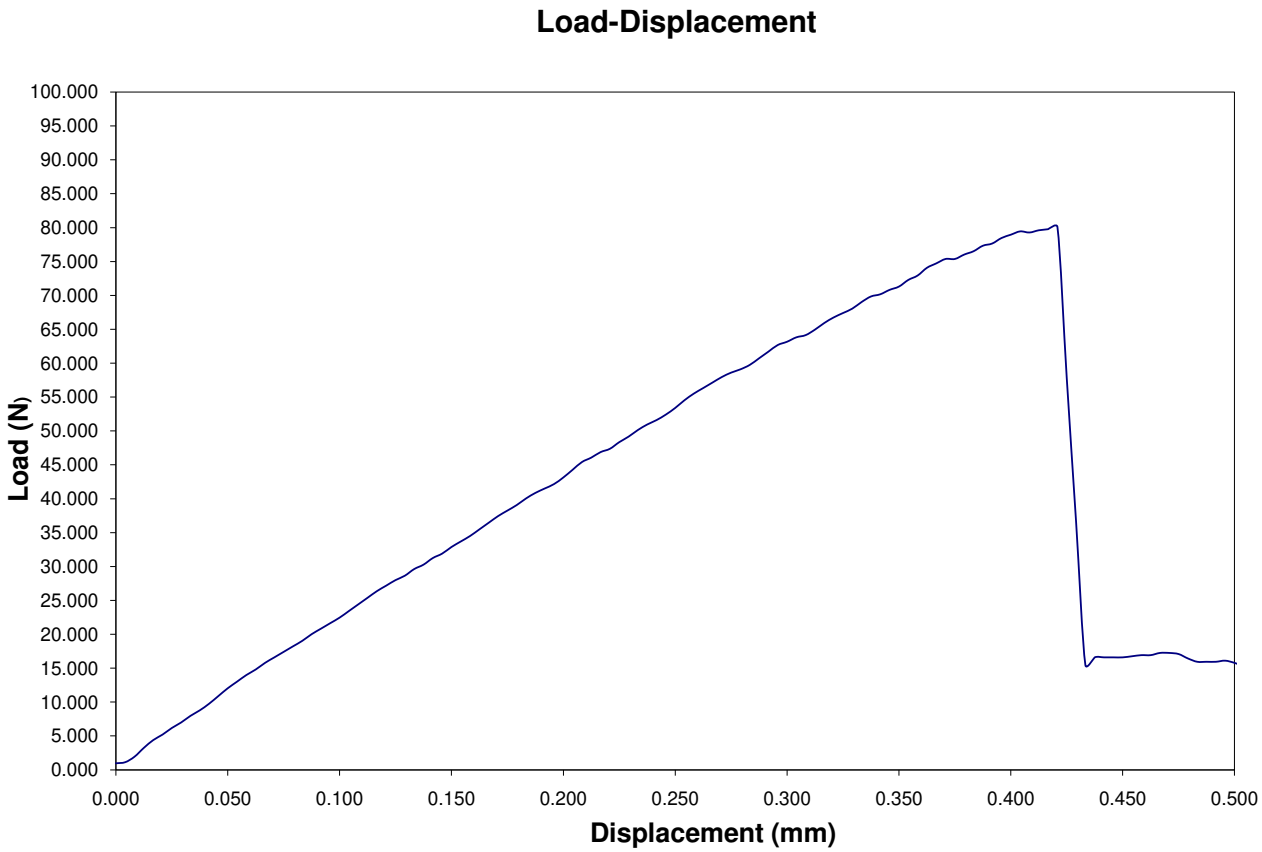

Figure 2-18. Load-displacement curve generated via femoral neck fracture

2.4.5 Assessment of Bone Remodeling: Static and Dynamic Histomorphometry

Histomorphometry was used to assess bone structure as well as parameters that give insight into bone remodeling (bone formation and resorption). Static and Dynamic histomorphometry are both *ex vivo* techniques.

Specimen Processing

After dissection, all right tibiae were cut in half, the proximal end of each tibia was cut coronally using an Isomet low speed bone saw (Buehler Ltd.) and was placed in 70% ethanol for 1 week. The proximal cranial sections were then dehydrated and embedded in spurr. Samples were subjected to increasing concentrations of acetone (70%, 90%, 100%, 100%) at 3-4 day intervals. Samples were then subjected to increasing concentrations of spurr resin (50%, 80%, 100%, 100%) at 3-4 day intervals. The remainder of the solution consisted of 100% acetone. Throughout this process, the samples were placed in cassettes that allowed for infiltration of acetone and spur resin. The dehydration and spurr infiltration procedures were performed under vacuum. Samples were then embedded in 100% spur resin, inferior side down in an embedding mold and the molds were placed in a 50°C oven for 2 days in order for the spurr to harden.

Slide preparation and staining procedure

The spurr blocks containing the tibia samples were sectioned using a Leica RM2265 microtome. Blocks were first trimmed using a coarse blade in order to expose the bone surface. Once exposed, the blocks were trimmed using a fine blade in order to obtain three 5 micron sections for static histomorphometry and one 7 micron section for dynamic histomorphometry. All sections were first placed in a 60°C water bath containing 1 tablespoon of gelatin and were

then adhered to gelatinized slides and were placed in a 60°C oven for 48 hours. All of the 5 micron sections were stained with Goldner's Trichrome for static histomorphometry analysis and were cover-slipped using permount.

Static Histomorphometry

Static histomorphometry was performed using Bioquant morphometry program computer software (Bioquant Nova Prime, version 6.50.10). Slides were placed on a Zeiss microscope which is attached to a video camera which allows the computer to acquire the image on the slide. All specimens were analyzed using the 10x objective lens. Analysis consisted of the bone area that was 1mm under the growth plate and 1mm from each side of the cortical shaft to ensure that only trabecular bone was being analyzed. Four images were taken and careful consideration was taken to ensure that these images matched up but did not overlap (Figure 2-19).

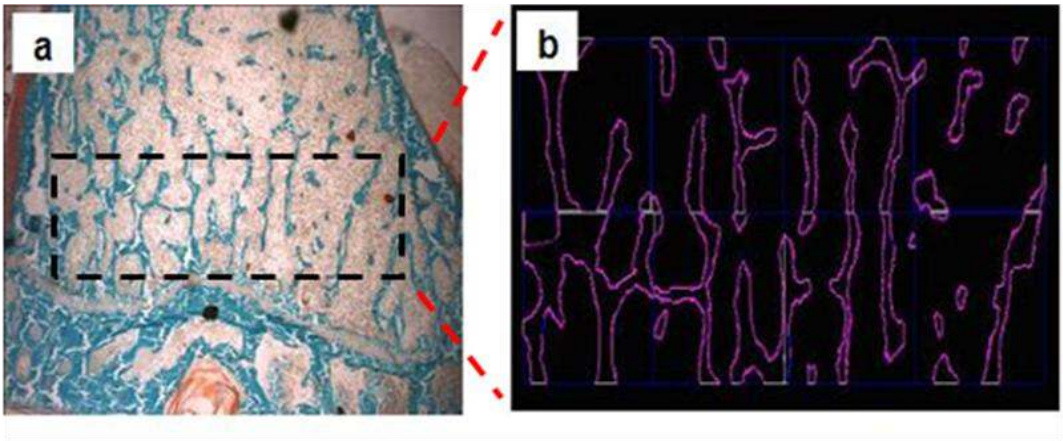

Figure 2-19. Example image of proximal tibia (A) and region of interest (B) from static histomorphometry

The Goldner's Trichrome stain makes mineralized bone appear green/blue and unmineralized osteoid appear red. Eroded surfaces of active bone resorption appear as a ruffled edge on the bone trabeculae as opposed to the normal smooth appearance of these edges. Structural

parameters such as %BV/TV, Tb.Th., Tb. N. and Tb.Sp. were also quantified using these images. The formation parameters obtained from this technique are Osteoid volume (%OV), Osteoid thickness (O.Th.) and Osteoid surface (OS/BS). Eroded surface (%ES) is obtained as an indicator of bone resorption. All measurements were completed following the nomenclature and guidelines from the American Society for Bone Mineral (ASBMR) (Parfitt, 1987).

Dynamic Histomorphometry

All of the 7 micron slides were left unstained and were also cover-slipped using permount for dynamic histomorphometry analysis. Dynamic histomorphometry was performed using Bioquant morphometry program computer software (Bioquant Nova Prime, version 6.50.10). Slides were analyzed using a 10x objective lens for a total magnification of 100x. For this technique, fluorescent microscopy was used to measure the bone labels that were generated as a result of the calcein green injections that all rats received 12 days and 2 days prior to sacrifice. Fluoresent labels represent mineralized bone surface. The same bone area under the growth plate was used for analysis in this technique as was used for static histomorphometry explained above and 4 serial images were analyzed (Figure 2-20).

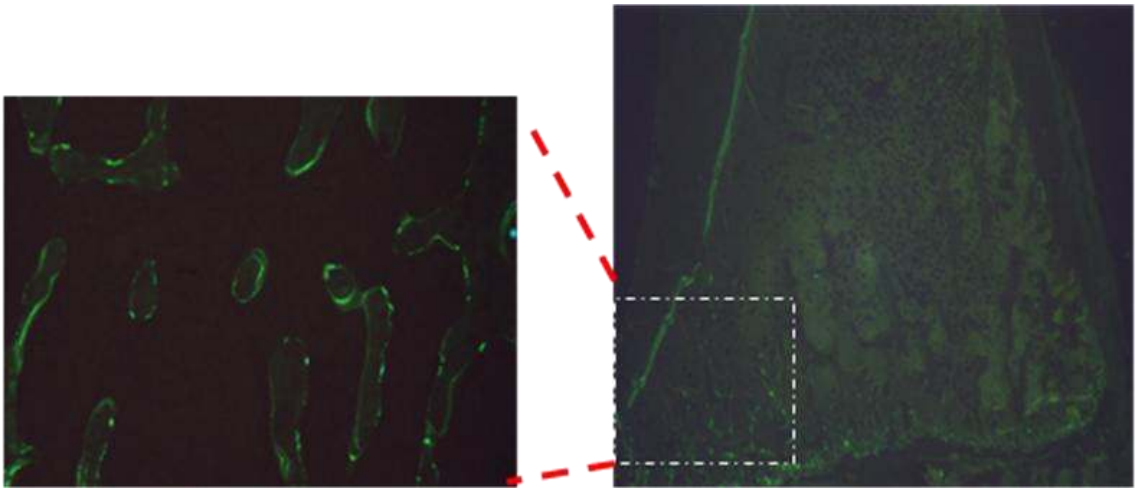

Figure 2-20. Sample image of proximal tibia showing fluorescent labels from dynamic histomorphometry analysis

Single fluorescent labels and double labels on bone trabeculae were measured separately. The distance between the double labels gives insight into the mineral aposition rate. The formation parameters obtained from this technique are mineralizing surface (%MS), mineral apposition rate (MAP, mcm/day) and bone formation rate (BFR, mcm/day). All measurements were completed following the nomenclature and guidelines from the American Society for Bone Mineral (ASBMR) (Parfitt, 1987).

2.4.6 Assessment of Bone Mineralization and Connectivity

Backscatter Electron Imaging (BSE)

Backscatter electron imaging (BSE) generates a mineralization profile for cross sections on bone area. The mineralization profile allows for the analysis of the distribution of mineral throughout the sample. Following trimming for histomorphometry, the same spurr blocks were used for Quantitative BSE. Blocks were ground and polished with a grinder/polisher. The surface of the block that contained the exposed bone was ground first on 400 grade grinding paper, then 600 grade and finally 1200 grade paper. The same surface of the block was then polished using first a 6 μm followed by a 1 μm diamond polish on the same machine. Blocks were then mounted, face up, onto square, plexiglass plates using Fimo (Fimo Classic, Eberhard Faber). Careful care was taken to ensure that the surfaces of all blocks on a given plate were level with each other. Finally, the blocks were connected to the plastic plate using carbon tape and the plate/block complex was carbon coated in preparation for BSE.

BSE was performed on a FEI XL300ESEM (solid state BSE detector, FEI Company, Hillsboro, OR, USA). Prior to scanning, a silicon dioxide (SiO_2) and MgF_2 standard was attached to the plexiglass plate in order to calibrate the BSE for brightness and contrast. An embedded and

polished tooth was also used as an internal reference standard. The scan was set to BSE, the beam was set at 20kv and the spot size was set at 6.2. A working distance of 15mm was used for all samples.

Four serial images of each proximal tibia specimen were taken at 80x magnification. An image of the SiO_2 and MgF_2 standard was taken in between each sample image to ensure no variation between specimens. After images had been taken of all specimens, an image of the embedded tooth standard was taken at 200x magnification. Following this process, the 4 serial images from each specimen were stitched together to make 1 image.

Figure 2-21. Image of proximal tibia generated from Back-scatter electron imaging

Regions of cortical bone and trabecular bone were isolated by creating a mask over the stitched image. In Figure 2-21, unmineralized surfaces appear black whereas mineralized surfaces appear grey. Surfaces that are lighter grey to white represent bone that is hyperminralized

whereas darker grey regions represent bone that is less mineralized. Mineralization profiles were created for each specimen in the form of a histogram and shifts in these profiles were compared using the logit value.

$$\text{logit} = \ln \frac{area \leq cutoff}{area > cutoff}$$

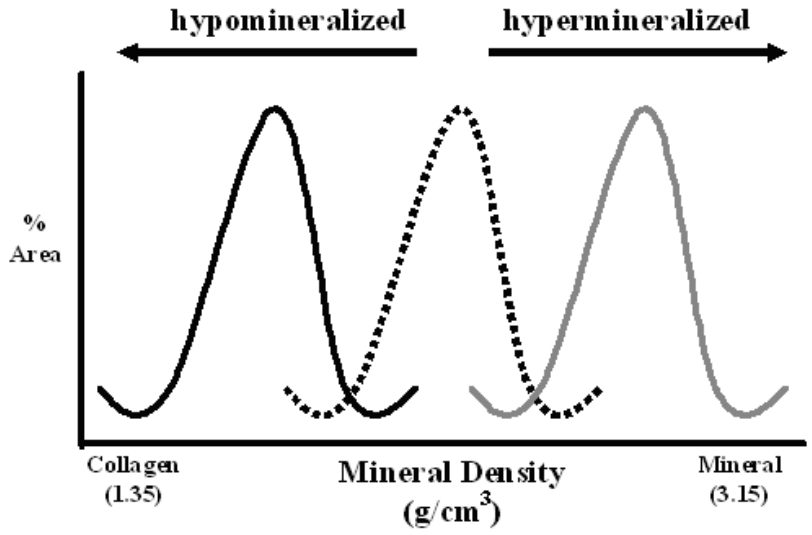

Figure 2-22. Schematic mineralization profiles from BSE

The cutoff values used in the above equation were chosen based on the average grey level for either cortical bone, trabecular bone or both in the control group. A more negative logit value represents hypermineralization and a shift of the histogram to the right whereas a more positive logit value represents hypomineralization and a shift of the histogram to the left (Figure 2-22). The peak grey level for each specimen was also determined as was the full width at half the maximum height (FWHMH) (Figure 2-23). The latter parameter gives insight into the level of heterogeneity of the grey level distribution for that particular specimen.

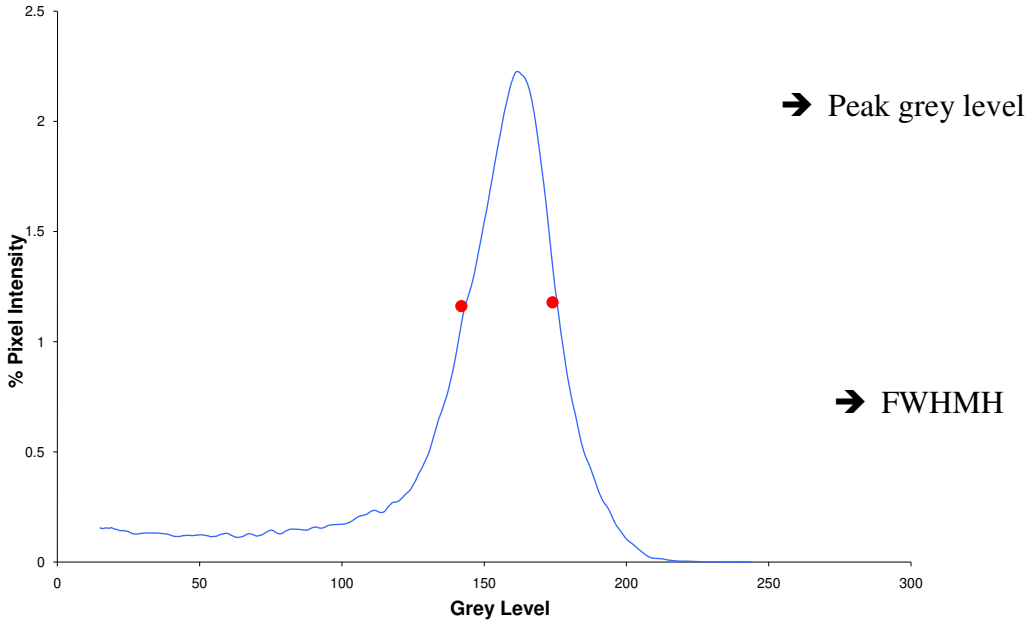

Figure 2-23. Sample histogram of proximal tibia generated by BSE
FWHMH= full width at half maximum height

Strut Analysis

Strut analysis allows for the quantification of connectivity parameters of the trabecular bone area located beneath the growth plate. This is especially important since trabecular bone architecture is an important determinant of bone strength (Croucher, 2007). This technique is a 2-dimensional analysis that is performed on tibiae images that were obtained from Back-scatter electron imaging (BSE) analysis. The parameters that were analyzed are nodes, free ends, node-node struts (NNS), node-free end struts (NFS), and free-free struts (FFS) (Figure 2-24).

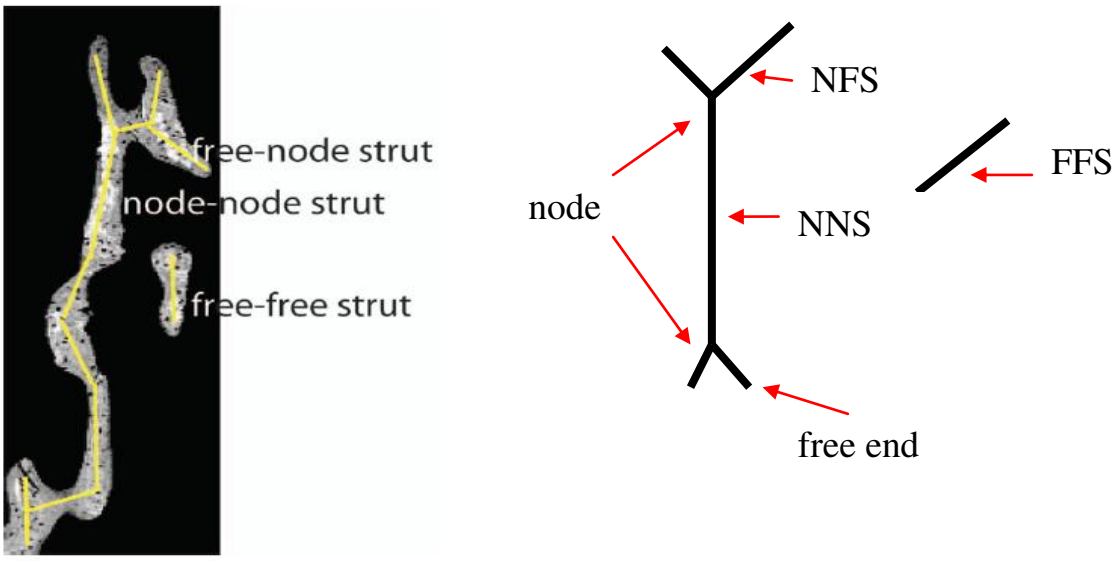

Figure 2-24. Example of parameters obtained from strut analysis

2.5 Statistical Analysis

SPSS version 17.0 software was used to perform statistical analysis. For the male study, one-way analysis of variance (ANOVA) was used to determine if there were any differences in mean responses among the groups for each experiment. Fisher's LSD post-hoc test was used for multiple comparisons. Student's T-test was used to evaluate differences between the 2 female Sham groups and between the female Sham control and OVX control groups. For the female OVX study, a 2-way ANOVA was used to determine if there were any differences in mean responses among the two treatments (RSG and ALN) and to determine if there was any interaction between the two drugs. Multiple comparisons were performed using Fisher's LSD post-hoc test. A p value less than 0.05 was used to indicate significance and a p value less than 0.1 was used to denote a trend. Data are presented as mean ± standard deviation.

Chapter 3 : Results from the Male Study

3.1 The Effect of Rosiglitazone on Body Weight

A summary of the 4 weights taken for each rat throughout the treatment period is displayed in Table 3-1.

Table 3-1. Summary of rat weights for all male groups

	Weight (g)			
	1(onset)	**2**	**3**	**4**
Control	726.27 ± 83.52	794.27 ± 83.43	828.36 ± 106.12	888.00 ± 111.93
RSG 3mg/kg	711.42 ± 69.73	784.73 ± 73.5	840.09 ± 87.24	891.10 ± 101.95
RSG 10mg/kg	721.58 ± 89.47	807.92 ± 84.16	883.08 ± 113.29	974.55 ± 120.13
RSG 10mg/kg + ALN	706.42 ± 84.29	801.58 ± 89.1	893.42 ± 114.21	985.40 ± 121.33

Data are presented as mean ± standard deviation.

At the onset of treatment as well as for the 3 other weight tests, there were no significant differences in weight (g) between any of the groups. The average weight for the control group and all 3 treatment groups increased throughout the experiment.

3.2 The Effect of Rosiglitazone on Blood Biochemistry

3.2.1 Glucose Testing

A summary for the 4 glucose tests performed on each rat throughout the treatment period is displayed in Table 3-2.

Table 3-2. Summary of glucose tests

	Glucose (mmol/L) baseline	**Glucose (mmol/L) #2**	**Glucose (mmol/L) #3**	**Glucose (mmol/L) #4**
Control	8.57± 3.87	8.66 ± 3.29	8.37 ± 2.84	7.63 ± 1.85
RSG 3mg/kg	10.92 ± 4.47	9.57 ± 3.92	9.63 ± 3.6	10.14 ± 4.80
RSG 10mg/kg	11.63 ± 4.81	**8.67 ± 3.51** **	**8.08 ± 1.04** **	**8.00 ± 1.03** **
RSG 10mg/kg + ALN	8.83 ± 4.55	6.84 ± 3.19	7.36 ± 3.9	7.78 ± 1.82

*Data are presented as mean ± standard deviation. ** indicates a trend ($p<0.1$) when compared to baseline glucose).*

At baseline, there were no significant differences for mean glucose (mmol/L) between any of the groups. For all other glucose tests that were completed 4 weeks apart, there were also no significant differences in mean glucose between any of the groups. The RSG 10mg/kg group did demonstrate a trend of lower blood glucose for the 2nd, 3rd, and 4th test when compared to baseline blood glucose.

For all 3 treatment groups (RSG 3mg/kg, RSG 10mg/kg and RSG 10mg/kg + ALN), there was a decrease in blood glucose from baseline to the second glucose test that was completed 4 weeks after onset of treatment. The 3mg/kg and 10mg/kg + ALN groups demonstrated a slight increase in blood glucose for the third and fourth glucose tests however, the final blood glucose readings were still lower than that taken at baseline of the experiment. The 10mg/kg group demonstrated a decrease in blood glucose for each test following the baseline blood glucose reading. The control group did not demonstrate a decrease in blood glucose between the baseline test and the second blood glucose test.

3.2.2 Remaining Blood Biochemistry

A summary of the remaining blood testing results are displayed in Table 3-3. Blood serum was tested for total cholesterol, total triglycerides, insulin, osteocalcin and serum CTX at baseline

and at termination of the experiment. At experiment termination, serum was also testing for leptin and adiponectin.

Table 3-3. Blood biochemistry results for all male groups, B= baseline, T= termination

		Control	RSG 3mg/kg	RSG 10mg/kg	RSG 10mg/kg + ALN
Cholesterol (mmol/L)	B	11.49 ± 4.15	11.78 ± 4.36	11.54 ± 4.40	10.23 ± 4.24
Cholesterol (mmol/L)	T	**15.59 ± 7.00***	13.37 ± 4.93	11.11 ± 2.68	10.64 ± 4.19
Triglycerides(mmol/L)	B	7.14 ± 4.48	9.76 ± 4.98	9.68 ± 4.79	9.11 ± 4.63
Triglycerides(mmol/L)	T	**12.40 ± 5.49***	12.51 ± 5.71	8.04 ± 1.92	9.53 ± 4.92
Insulin (ng/mL)	B	19.98±10.01	16.70±10.07	13.78±8.87	13.91±8.58
Insulin (ng/mL)	T	15.25 ± 7.93	13.58±9.38	14.24±5.37	12.42±4.54
Osteocalcin (ng/mL)	B	269.64 ± 190.81	188.25 ± 77.87	209.56 ± 80.47	185.27 ± 52.39
Osteocalcin (ng/mL)	T	199.95 ± 100.84	267.77 ± 191.49	175.10 ± 94.01	110.31 ± 108.80
Serum CTX (ng/mL)	B	51.78 ± 24.32	44.08 ± 13.63	47.96 ± 21.00	46.61 ± 14.11
Serum CTX (ng/mL)	T	39.96 ± 13.24	77.50 ± 83.22	49.49 ± 25.91	45.42 ± 27.05
Adiponectin (µg/mL)	T	11.05 ± 2.23	15.21 ± 3.90	**16.90 ± 9.18** [a]	**18.62 ± 3.7** [a]
Leptin(ng/mL)	T	108.13 ± 53.79	120.07 ± 50.51	100.50 ± 48.66	108.41 ± 54.58

Data are presented as mean ± standard deviation. indicates significance vs. baseline blood serum test (p<0.05) .[a] indicates significance vs. male controls (p<0.05).Tests were performed in the laboratories of Dr. Reinhold Vieth and Dr. David Cole at the University of Toronto.*

The Control group was the only group that demonstrated significantly higher serum cholesterol at termination compared to baseline ($p<0.05$). All 3 groups that were treated with RSG did not demonstrate a significant change in serum cholesterol from baseline to termination of the experiment. The Control group also demonstrated higher serum triglycerides at termination compared to baseline ($p < 0.05$). We would expect that RSG treatment would maintain serum levels of cholesterol and triglycerides. Although the findings were not significant, the RSG 10mg/kg group was the only group that showed lower values for serum cholesterol and

triglycerides at termination compared to baseline. All other groups demonstrated increases in these values at termination of the treatment period.

There were also no significant results for serum insulin, osteocalcin or serum CTX for any of the groups from baseline to termination of the treatment period. We would expect a decrease in serum CTX for the ALN group at termination of the experiment. This, however, was not observed. Possible explanations are discussed in Chapter 5. The RSG 10mg/kg and RSG 10mg/kg + ALN group demonstrated significantly higher adiponectin compared to male controls ($p<0.05$).

3.3 The Effect of Rosiglitazone on Bone Mineral Density

Areal Bone Mineral Density

Areal bone mineral density was analyzed via DEXA analysis. A summary of the results from Dual Energy X-Ray Absorptiometry is displayed in Table 3-4. One scan was performed on each right femur and another scan was performed on each L5 and L6 lumbar vertebrae. For L5 and L6, the average values for BMD (g/cm^2), BMC (g) and Bone area (cm^2) were taken and are displayed in Table 3-4.

Table 3-4. DEXA results for all male groups

	Sample	Control	RSG 3mg/kg	RSG 10mg/kg	RSG 10mg/kg + ALN
BMD(g/cm^2)	RF	0.207± 0.01	0.199± 0.01	0.200± 0.01	**0.228± 0.01** [abc]
BMC(g)	RF	0.531± 0.05	0.510± 0.04	0.522± 0.04	**0.590± 0.04** [abc]
B Area(cm^2)	RF	2.559± 0.13	2.558± 0.13	2.605± 0.15	2.583± 0.12
BMD(g/cm^2)	L5 & L6	0.107± 0.01	0.102± 0.01	**0.097± 0.01**[a]	**0.123± 0.01** [abc]
BMC(g)	L5 & L6	0.064± 0.01	0.060± 0.01	**0.056± 0.005**[a]	**0.073± 0.01** [abc]
B Area(cm^2)	L5 & L6	0.599± 0.06	0.585± 0.04	0.580± 0.03	0.593± 0.03

Data are presented as mean ± standard deviation. [a] indicates significance vs. male controls ($p<0.05$). [b] indicates significance vs. male RSG 3mg/kg group ($p<0.05$). [c] indicates significance vs. male RSG 10mg/kg group ($p<0.05$).

The RSG 10mg/kg + ALN group demonstrated significantly higher femur BMD and BMC than all other groups ($p<0.001$). The RSG 10mg/kg + ALN group also demonstrated significantly higher vertebrae BMD and BMC than all other groups ($p<0.001$). The RSG 10mg/kg group showed significantly lower vertebrae BMD and BMC than the Control group ($p<0.05$)

Volumetric Bone Mineral Density

MicroCT analysis allowed for an analysis of volumetric BMD. MicroCT was completed on all 39 L6 vertebrae and all 39 right femora from the male rats. This analysis was used to evaluate the volumetric BMD of the L6 vertebrae and the volumetric BMD of the right femora. The results from these tests are displayed in Table 3-5.

Table 3-5. Volumetric BMD results for all male groups

Volumetric BMD	**Control**	**RSG 3mg/kg**	**RSG 10mg/kg**	**RSG 10mg/kg + ALN**
Trabecular	0.379±0.060	0.350±0.055	0.340±0.042	**0.413±0.045** [bc]
Cortical	1.0179±0.0275	1.0145±0.0148	1.0060±0.0300	1.0208±0.0223

Data are presented as mean ± standard deviation.. [b] indicates significance vs. male RSG 3mg/kg group ($p<0.05$). [c] indicates significance vs. male RSG 10mg/kg group ($p<0.05$).

The RSG 10mg/kg + ALN group showed significantly higher trabecular volumetric BMD than both the RSG 3mg/kg and RSG 10mg/kg groups ($p < 0.01$). There were no significant differences in the femur volumetric BMD between any of the groups.

3.4 Effect of Rosiglitazone on Bone Structural Properties

Trabecular Bone Microarchitecture

The MicroCT results from the L6 vertebrae were used to evaluate the microarchitecture of trabecular bone. These parameters include percent bone volume (BV/TV), trabecular thickness

(Tb.Th.). trabecular number (Tb.N.) and trabecular separation (Tb.Sp.). The results from these tests are displayed in Table 3-6.

Table 3-6. MicroCT results for trabecular bone

Trabecular Bone	Control	RSG 3mg/kg	RSG 10mg/kg	RSG 10mg/kg + ALN
Percent bone volume	32.437±4.790	30.183±4.344	**28.657±2.707**[a]	**35.123±3.800**[bc]
Trabecular thickness	0.108±0.004	0.103±0.005	0.104±0.005	**0.108±0.004**[bc]
Trabecular number	2.990±0.357	2.922±0.284	2.745±0.198	**3.242±0.255**[bc]
Trabecular separation	0.261±0.028	0.268±0.023	**0.284±0.022**[a]	**0.240±0.020**[bc]

Data are presented as mean ± standard deviation. [a] indicates significance vs. male controls ($p<0.05$). [b] indicates significance vs. male RSG 3mg/kg group ($p<0.05$). [c] indicates significance vs. male RSG 10mg/kg group ($p<0.05$).

The RSG 10mg/kg group demonstrated significantly lower BV/TV than the Control group ($p = 0.046$), a trend of lower trabecular thickness ($p = 0.083$) and a trend of lower trabecular number ($p = 0.063$) than the Control group. The RSG 10mg/kg group also showed significantly higher trabecular separation than the Control group ($p = 0.045$). The RSG 10mg/kg + ALN group demonstrated significantly higher BV/TV, higher trabecular thickness, higher trabecular number and significantly lower trabecular separation than both the RSG 3mg/kg and RSG 10mg/kg groups ($p < 0.05$). This shows that the loss in percent bone volume, trabecular thickness and trabecular number in the RSG 10mg/kg group was prevented with ALN treatment.

Cortical Bone Structural Properties

The MicroCT results from the right femora were used to evaluate the structural properties of cortical bone. These parameters are displayed in Table 3-7.

Table 3-7. MicroCT results for cortical bone for all male groups

Cortical Bone	Control	RSG 3mg/kg	RSG 10mg/kg	RSG 10mg/kg + ALN
Length (mm)	37.41 ± 0.54	37.54 ± 0.80	37.98 ± 1.05	37.38 ±0.98
Mean Polar moment of inertia (mm^4)	21.22 ± 3.08	19.84 ± 2.38	21.63 ± 3.15	22.93 ± 2.14
Cross – sectional area (mm^2)	8.74 ± 0.50	8.3 ± 0.56	**8.8 ± 0.57** [b]	**9.33 ± 0.48** [c]
Moment of area (mm^4)	8.1 ± 1.06	7.35 ± 1.01	8.31 ± 1.28	8.84 ± 0.97
Cortical Thickness (mm)	0.94 ± 0.09	0.89 ± 0.09	0.93 ± 0.07	**1.00 ± 0.05** [c]

Data are presented as mean ± standard deviation. [a] *indicates significance vs. male controls ($p<0.05$).* [b] *indicates significance vs. male RSG 3mg/kg group ($p<0.05$).* [c] *indicates significance vs. male RSG 10mg/kg group ($p<0.05$).*

The RSG 10mg/kg + ALN group demonstrated significantly increased femoral cross-sectional area and cortical thickness compared to the RSG 10mg/kg group. The RSG 10mg/kg group showed significantly increased femoral cross-sectional area compared to RSG 3mg/kg rats ($p<0.05$). There were no other significant results.

Porosity Measurements

MicroCT analysis also allowed for an evaluation of total porosity (%) for all 81 female right femur samples. The results for this test are found in Table 3-8.

Table 3-8. Femoral porosity results for all male groups

Cortical Bone	Control	RSG 3mg/kg	RSG 10mg/kg	RSG 10mg/kg + ALN
Total Porosity (%)	1.88 ± 1.02	1.24 ± 0.84	2.27 ± 1.75	0.73 ± 0.34

Data are presented as mean ± standard deviation.

Although the RSG 10mg/kg group did show increased total femoral porosity compared to the control group (Figure 3-1), these results were not statistically significant.

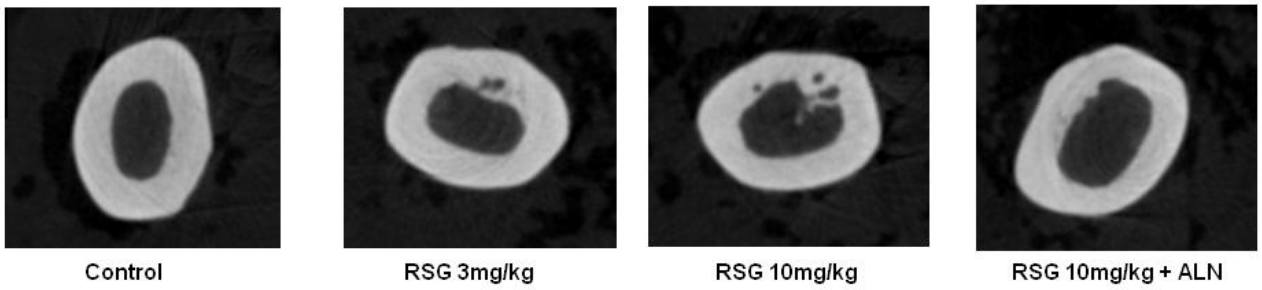

Figure 3-1. Femoral cross sectional images showing total porosity

3.5 The Effect of Rosiglitazone on Mechanical Properties of Cortical Bone

3.5.1 Three-point Bending Results

39 three point bending tests were successfully performed. The unnormalized and normalized results from these tests are displayed in Table 3-9. The unnormalized parameters that were evaluated are ultimate load (N), failure load (N), failure deformation (mm), energy to failure (mJ) and stiffness (N/mm). The parameters that were evaluated via normalization were Ultimate stress (Mpa), Failure Stress (Mpa), Toughness (mJ/mm^3) and Modulus (Mpa).

The RSG 10mg/kg + ALN group demonstrated significantly higher ultimate load and failure load than all other groups ($p<0.05$). The RSG 10mg/kg + ALN group also demonstrated significantly higher failure deformation and energy to failure than the control group ($p<0.05$). The RSG 10mg/kg group showed a trend of higher failure deformation than the control group ($p=0.06$). The RSG 3mg/kg group demonstrated a trend of lower stiffness than the control group whereas the RSG 10mg/kg group demonstrated a significantly lower stiffness than the control group ($p=0.8$ and $p=0.009$ respectively).

Table 3-9. Structural and material properties of cortical bone following 3-point bending for all male groups

Structural Properties	**Control**	**RSG 3mg/kg**	**RSG 10mg/kg**	**RSG 10mg/kg + ALN**
ultimate load (N)	183.41±10.97	181.69±12.53	179.05±22.69	**203.15±21.23**[a]
failure load (N)	178.38±13.23	176.22±14.86	174.68±25.65	**197.29±18.47** [a]
failure deformation(mm)	0.58±0.09	0.64±0.10	0.69±0.16	**0.71±0.11** [a]
energy to failure (mJ)	71.14±18.62	78.18±17.24	83.25±21.18	**93.98±24.57** [a]
stiffness (N/mm)	584.88±50.30	535.17±47.49	**521.78±61.37**[a]	542.63±60.47
Material Properties				
ultimate stress (Mpa)	152.71±14.89	160.20±9.36	**147.01±18.35** [b]	154.82±13.4
failure stress (Mpa)	148.83±18.33	155.36±11.22	143.81±20.89	151.03±14.21
Toughness (mJ/mm^3)	4.98±1.30	5.60±1.23	5.66±1.16	5.93±1.35
Modulus (Mpa)	5784.18± 792.43	5829.78± 723.80	**4951.07±838.11** [ab]	**4907.28±584.13** [a]

Data are presented as mean ± standard deviation. [a] *indicates significance vs. male controls (p<0.05).).* [b] *indicates significance vs. male RSG 3mg/kg group (p<0.05).*

The RSG 10mg/kg group demonstrated lower ultimate stress (p = 0.044) than the RSG 3mg/kg group. The RSG 10mg/kg group also showed a significant decrease in modulus (p < 0.02) compared to the 3mg/kg group and the Control group. Interestingly, the RSG 10mg/kg + ALN group also showed a significant decrease in modulus (p < 0.02) compared to the Control group.

3.5.2 Torsion Results

38 Torsion tests were successfully performed on the left femora. The results from this test are displayed in Table 3-10. The unnormalized parameters that were evaluated are Failure Torque (N·mm), Angular Deformation at Failure (rad), Energy to Failure (N·mm·rad) and Stiffness (N/mm). The normalized parameters that were evaluated are Shear Stress (Mpa), Shear Strain (%), Toughness (mJ/mm^3) and Shear Modulus (Mpa).

The RSG 3mg/kg demonstrated a trend of lower stiffness than the Control group (p < 0.1). The RSG 10mg/kg group demonstrated a trend of lower angular deformation at failure compared to the RSG 3mg/kg group (p < 0.1). The RSG 10mg/kg + ALN group showed a significant

increase in failure torque and stiffness as well as a trend of increased energy to failure compared to the RSG 3mg/kg and RSG 10mg/kg groups.

Following normalization, the RSG 10mg/kg + ALN group demonstrated a trend of higher shear stress than the RSG 10mg/kg group ($p < 0.1$). There were no other significant results.

Table 3-10. Structural and material properties of cortical bone following torsion testing for all male groups

Structural Properties	**Control**	**RSG 3mg/kg**	**RSG 10mg/kg**	**RSG 10mg/kg + ALN**
Failure Torque (N·mm)	449.26 ± 63.85	411.94 ± 145.29	387.85 ± 131.15	**513.36 ± 120.86** [c]
Angular Deformation (rad)	0.23 ± 0.06	0.27 ± 0.08	0.23 ± 0.04	0.24 ± 0.05
Energy to Failure (N·mm·rad)	61.51± 16.79	67.95 ± 35.30	51.22 ± 18.63	70.39 ± 21.52
Stiffness (N/mm)	2146.43 ± 444.34	1681.2 ± 554.89	1760.58 ± 593.07	**2249.77 ± 535.84** [c]
Material Properties				
Shear Stress (MPa)	46.41 ± 7.35	46.02 ± 17.79	39.08 ± 12.28	49.89 ± 14.41
Shear Strain (%)	3.52 ± 0.98	4.24 ± 1.24	3.52 ± 0.70	3.65 ± 0.96
Toughness (mJ/mm^3)	0.5 ± 0.16	0.6 ± 0.32	0.41 ± 0.14	0.54 ± 0.20
Shear Modulus (MPa)	1449.73 ± 324.33	1221.45 ± 479.70	1150.37 ± 337.35	1415.64 ± 389.70

Data are presented as mean ± standard deviation. [c] *indicates significance vs. male RSG 10mg/kg group ($p<0.05$).*

3.6 The Effect of Rosiglitazone on Mechanical Properties of Trabecular Bone

3.6.1 Vertebral Compression

38 vertebral compression tests were successfully performed on the L6 vertebrae. The results from these tests are displayed in Table 3-11. The unnormalized parameters that were evaluated with this test are ultimate load (N), failure load (N), failure deformation (mm), energy to failure (mJ) and stiffness (N/mm). The parameters that were evaluated via normalization are ultimate stress (Mpa), failure stress (Mpa), toughness (mJ/mm^3) and modulus (Mpa).

Table 3-11. Structural and material properties of trabecular bone following vertebral compression for all male groups

Structural Properties	**Control**	**RSG 3mg/kg**	**RSG 10mg/kg**	**RSG 10mg/kg + ALN**
ultimate load(N)	216.12±43.35	183.25±46.24	174.97±28.93	**264.21±76.73**[abc]
failure load (N)	194.20±38.93	163.63±44.20	153.72±25.24	**233.36±73.15**[abc]
failure deformation(mm)	0.44±0.03	0.44±0.14	0.42±0.10	0.43±0.06
energy to failure (mJ)	50.93±9.92	46.8±23.05	37.24±11.20	**59.72±17.36**[c]
stiffness (N/mm)	711.91±223.76	608.30±140.13	601.81±214.66	**842.57±118.26**[abc]
Material Properties				
ultimate stress (Mpa)	32.75±3.03	30.48±8.17	32.36±5.37	**36.82±7.72**[bc]
failure stress (Mpa)	29.43±2.73	27.49±7.82	28.46±4.83	32.66±7.38
Toughnesss (mJ/mm^3)	0.87±0.13	0.88±0.39	0.76±0.25	0.94±0.27
Modulus (Mpa)	966.42±272.15	897.40±272.69	968.61±306.92	**1071.87±118.76**[bc]

Data are presented as mean ± standard deviation. [a] *indicates significance vs. male controls ($p<0.05$).* [b] *indicates significance vs. male RSG 3mg/kg group ($p<0.05$).* [c] *indicates significance vs. male RSG 10mg/kg group ($p<0.05$).*

The RSG 10mg/kg + ALN group demonstrated significantly higher ultimate load, failure load and stiffness than all other groups ($p < 0.05$). The RSG 10mg/kg + ALN group also showed significantly higher energy to failure than the RSG 10mg/kg group ($p = 0.004$) and a trend of higher energy to failure compared to the RSG 3mg/kg group ($p = 0.058$).

The RSG 10mg/kg + ALN group demonstrated significantly higher ultimate stress than the RSG 3mg/kg and RSG 10mg/kg groups ($p = 0.009$ and $p = 0.037$ respectively) and a trend of higher ultimate stress than the Control group ($p = 0.075$). The RSG 10mg/kg + ALN group also showed significantly higher modulus than other groups ($p < 0.05$).

3.6.2 Femoral Neck Fracture

36 femoral neck fracture tests were successfully performed. The results from these tests are displayed in Table 3-12. The parameters that were evaluated are ultimate load (N), failure load (N), failure deformation (mm), energy to failure (mJ) and stiffness (N/mm). Due to the complex geometry of the femoral head and neck, these results cannot be normalized.

Table 3-12. Structural properties for male groups following femoral neck fracture testing

Structural Properties	Control	RSG 3mg/kg	RSG 10mg/kg	RSG 10mg/kg + ALN
ultimate load (N)	89.44±10.40	99.63±14.55	**82.86±11.18** [b]	92.37±12.30
failure load (N)	78.06±17.73	89.89±16.30	79.84±13.73	80.76±12.72
failure deformation (mm)	0.11±0.02	0.14±0.05	0.11±0.03	0.12±0.02
energy to failure (mJ)	5.45±1.06	7.81±3.21	5.24±1.86	6.33±1.73
stiffness (N/mm)	942.62±122.78	905.91±250.22	837.62±198.31	934.07±193.57

Data are presented as mean ± standard deviation. [b] *indicates significance vs. male RSG 3mg/kg group ($p<0.05$).*

The RSG 10mg/kg group showed a significantly lower ultimate load ($p = 0.006$) than the RSG 3mg/kg group. There were no other significant results.

3.7 The Effect of Rosiglitazone on Mineralization and Connectivity

3.7.1 Back-scatter Electron Imaging

Back-scatter electron imaging was completed on 39 male tibiae samples in order to obtain mineralization profiles. The parameters analyzed for this technique are logit, grey level and full width at half maximum height (FWHMH). A mineralization profile is completed for cortical bone, trabecular bone and total (cortical + trabecular) bone. These results are displayed in Table 3-13. Due to excessive amounts of trabecular bone near the tibial growth plate for the RSG 10 + ALN group, only mineralization for total bone could be analyzed for this group as it was difficult to discern between areas of cortical and trabecular bone.

Table 3-13. Mineralization analysis for all male groups

Cortical Bone	**Control**	**RSG 3mg/kg**	**RSG 10mg/kg**	**RSG 10mg/kg + ALN**
logit	-1.00 ± 0.66	-1.14 ± 0.97	-1.29 ± 0.58	--
grey level	167.88 ± 10.19	171.22 ± 17.04	172.60 ± 12.45	--
FWHMH	29.63 ± 7.23	26.78 ± 2.68	28.60 ± 2.95	--
Trabecular Bone				
logit	0.13 ± 0.66	-0.02 ± 0.91	-0.04 ± 0.73	--
grey level	154.38 ± 9.12	159.00 ± 19.42	158.30 ± 12.45	--
FWHMH	37.00 ± 5.71	38.89 ± 9.21	38.20 ± 5.94	--
Total Bone				
logit	-0.38 ± 0.60	-0.55 ± 0.87	-0.65 ± 0.58	**-1.38 ± 0.59** [abc]
grey level	163.88 ± 11.80	168.56 ± 18.62	169.50 ± 10.63	**179.00 ± 15.35** [a]
FWHMH	37.88 ± 6.17	35.22 ± 3.49	38.40 ± 7.65	**30.11 ± 4.94** [abc]

Data are presented as mean ± standard deviation. [a] *indicates significance vs. male controls ($p<0.05$).* [b] *indicates significance vs. male RSG 3mg/kg group ($p<0.05$).* [c] *indicates significance vs. male RSG 10mg/kg group ($p<0.05$).*

Only the RSG 10mg/kg + ALN group demonstrated a significantly different mineralization profile when examining total bone mineralization. The values for logit and FWMHM were significantly higher for the ALN group compared to all other groups ($p<0.05$, Figure 3-2). The RSG 10mg/kg + ALN group also showed significantly higher grey level than the control group ($p<0.05$) with a 8.9% shift to the right of the control group.

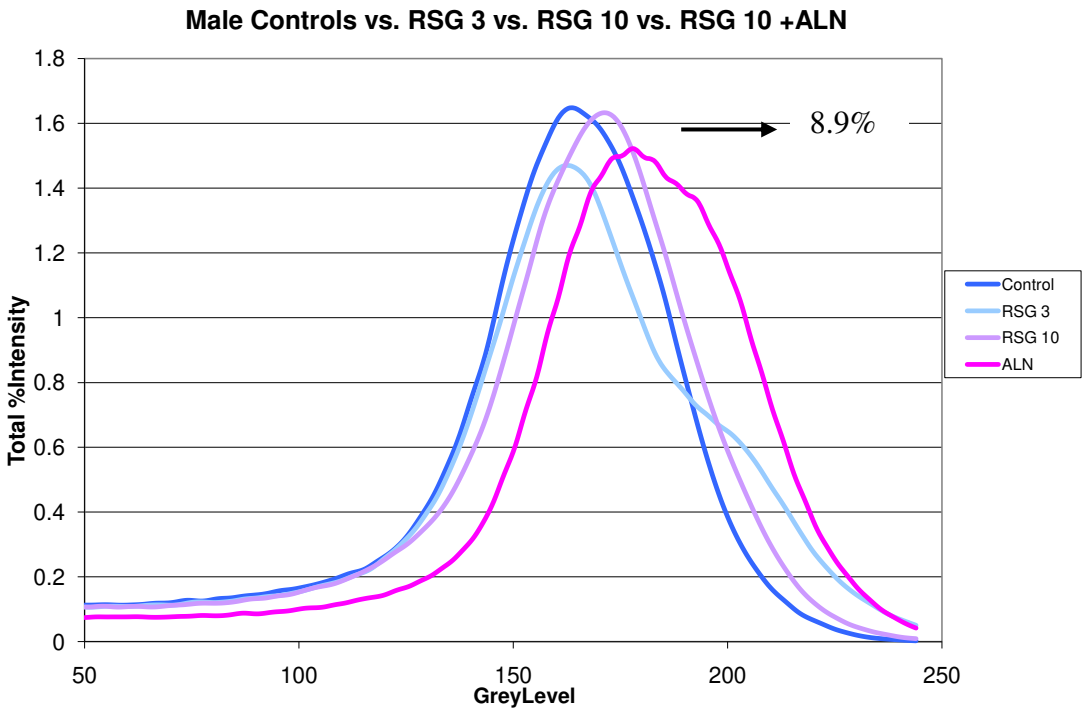

Figure 3-2. Histogram for total mineralization for all male groups

3.7.2 Strut Analysis

Strut analysis was performed on all male tibiae samples from the control, RSG 3mg/kg and RSG 10mg/kg groups in order to evaluate the extent of connectivity of trabeculae. The RSG 10mg/kg + ALN group could not be analyzed due to excessive amounts of trabecular bone near the tibial growth plate. No significant differences were found between groups for any of the parameters analyzed. The results are displayed in Table 3-14.

Table 3-14. Strut analysis for all male groups

Connectivity Parameters	Control	RSG 3mg/kg	RSG 10mg/kg
Total Strut Length (mm/mm^2)	3.09 ± 0.51	2.82 ± 0.43	3.40 ± 1.75
Number of Nodes (mm^{-2})	4.95 ± 1.52	4.15 ± 1.03	5.07 ± 1.97
Length of node-node struts (mm/mm^2)	0.74 ± 0.26	0.59 ± 0.30	0.76 ± 0.38
Length of free-node struts (mm/mm^2)	0.84 ± 0.15	0.79 ± 0.21	0.96 ± 0.31
Dis-connectivity Parameters			
Number of free ends (mm^{-2})	7.60 ± 1.06	7.69 ± 1.12	8.14 ± 2.43
Length of free-free struts (mm/mm^2)	0.50 ± 0.21	0.47 ± 0.17	0.40 ± 0.17

Data are presented as mean ± standard deviation.

3.8 The Effect of Rosiglitazone on Bone Remodelling

3.8.1 Static Histomorphometry

Static histomorphometry analysis was completed on all 39 male proximal tibiae samples. The results are displayed in Table 3-15. No significant differences were found for any parameters.

Table 3-15. Static histomorphometry results for all male groups

Structural Properties	Control	RSG 3mg/kg	RSG 10mg/kg	RSG 10mg/kg + ALN
%TBV (%)	15.27 ± 3.68	14.73 ± 3.01	14.07 ± 2.22	17.42 ± 4.22
Tb.Th. (µm)	54.10 ± 5.71	54.39 ± 4.80	55.00 ± 9.57	55.30 ± 9.03
Tb.N. (mm^{-1})	2.80 ± 0.46	2.71 ± 0.51	2.58 ± 0.37	3.13 ± 0.51
Tb.Sp. (µm)	311.94 ± 63.17	325.54 ± 67.33	339.07 ±49.70	273.36 ±67.94
Formation Parameters				
%OV (%)	0.48 ± 0.47	0.68 ± 0.55	0.71 ± 1.11	0.19 ± 0.52
O.Th. (µm)	5.73 ± 2.55	7.29 ± 2.00	5.30 ± 3.07	2.63 ± 5.37
OS/BS (%)	1.95 ± 1.80	2.89 ± 2.11	3.33 ± 5.22	0.52 ± 1.44
Resorption				
ES (%)	0.43 ± 0.48	0.58 ± 0.43	0.43 ± 0.57	0.31 ± 0.44

Data are presented as mean ± standard deviation.

3.8.2 Dynamic Histomorphometry

Dynamic histomorphometry was completed on all 39 male proximal tibiae samples. The results are displayed in Table 3-16. The formation parameters that were analyzed are mineralizing surface (%), mineral aposition rate (mcm/day) and bone formation rate (mcm/day). The RSG 10mg/kg + ALN group demonstrated significantly decreased mineralizing surface and bone formation rate (Figure 3-3) compared to all other groups ($p<0.05$). There were no other significant results.

Table 3-16. Dynamic histomorphometry results for all male groups

Formation Parameters	Control	RSG 3mg/kg	RSG 10mg/kg	RSG 10mg/kg + ALN
Mineralizing Surface (%)	18.58 ± 5.79	18.36 ± 4.02	17.76 ± 5.71	**5.69 ± 1.83** [abc]
Mineral Apposition Rate (mcm/day)	1.47 ± 0.11	1.55 ± 0.29	1.60 ± 0.53	1.40 ± 0.66
Bone Formation Rate (mcm/day)	0.28 ± 0.10	0.29 ± 0.10	0.31 ± 0.22	**0.08 ± 0.04** [abc]

Data are presented as mean ± standard deviation. . [a] indicates significance vs. male controls ($p<0.05$). [b] indicates significance vs. male RSG 3mg/kg group ($p<0.05$). [c] indicates significance vs. male RSG 10mg/kg group ($p<0.05$). denotes a trend ($p < 0.1$).*

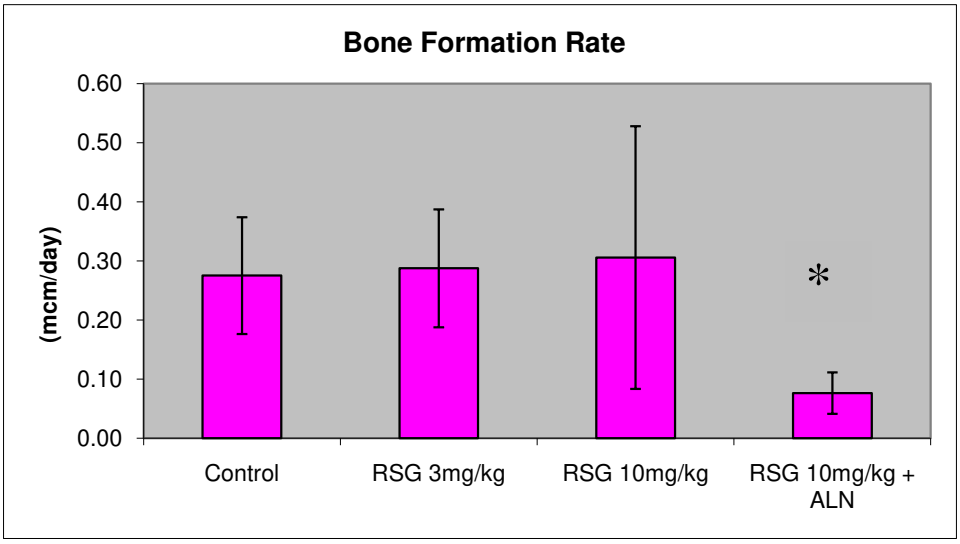

Figure 3-3. Bone formation rate for male groups
(* indicates significant difference compared to all other groups)

3.9 Male Results Summary

All rats gained weight throughout the treatment period regardless of administration of RSG or ALN. Rats given a dose or 10mg/kg RSG demonstrated lower levels of blood glucose as the treatment period progressed despite showing no difference in blood insulin levels from the beginning to the end of the treatment period. The Control group was the only group that demonstrated an increase in blood serum triglycerides and cholesterol at termination of the experiment suggesting that RSG may have an effect on lowering blood levels of cholesterol and triglycerides.

The RSG 10mg/kg group demonstrated lower vertebral BMD and BMC than the controls and the RSG 10mg/kg + ALN group demonstrated higher femoral and vertebral BMD and BMC than all groups suggesting that RSG may negatively influence bone mass and that ALN prevents the loss of bone mass.

The RSG 10mg/kg group also demonstrated decreases in some mechanical properties of cortical bone suggesting a decrease in bone strength. Interestingly, despite increases in unnormalized mechanical properties for the RSG 10mg/kg + ALN group, this group also showed decreases in mechanical properties following normalization. The RSG 10mg/kg + ALN group showed increases in many mechanical properties of trabecular bone before and after normalization. The RSG 10mg/kg group demonstrated decreases in many structural properties compared to controls whereas the group treated with ALN showed an increase in these parameters.

ALN treatment had an effect on total bone mineralization parameters with a mineralization profile shifted to the right compared to all other groups. This indicates hypermineralized bone in the ALN group, which is expected. RSG treatment did not appear to have any effect on mineralization or connectivity in the male study. ALN also appeared to have an effect on bone growth, where decreases in bone formation parameters were observed following treatment. This is expected following chronic administration of ALN. In addition to its anti-resorptive capabilities, ALN slows the entire bone remodeling process which could indirectly result in decreased bone formation. RSG did not appear to have any effect on bone formation in the male rat model which, interstingly, is consistent with the tendency of RSG to only affect the bone quality of women in clinical trials.

Chapter 4: Results from the Female Study

4.1 The Effect of Rosiglitazone on Body Weight

A summary of the 4 weights taken for each rat throughout the treatment period is displayed in Table 4-1. At the onset of treatment as well as for the 3 other weight tests, there were no significant differences in weight (g) between any of the groups. The average weight for all 8 treatment groups increased throughout the experiment (Figure 4-1). All groups demonstrated significantly increased final weight compared to the onset of treatment.

Table 4-1. Weight results for all female groups

	Weight (g) baseline	**Weight (g) #2**	**Weight (g) #3**	**Weight (g) #4**
Sham Control	561 ± 81.01	617.8 ± 116.01	**705.89 ± 73.63** *	**732.89 ± 71.26** *
Sham RSG 10mg/kg	573.7 ± 54.24	**694.1 ± 75.27** *	**798.2 ± 94.55** *	**843.56 ± 108.34** *
OVX Control	663.6 ± 28.10	**762.6 ± 48.35** *	**824.44 ± 43.36** *	**843.44 ± 67.15** *
OVX ALN	640.67 ± 45.87	**757.42 ± 64.26** *	**818.33 ± 58.70** *	**837.83 ± 66.90** *
OVX RSG 3mg/kg	634.25 ± 48.26	**767.83 ± 68.90** *	**826.67 ± 84.10** *	**868.50 ± 101.62** *
OVX RSG 3mg/kg + ALN	644 ± 58.91	**756.45 ± 68.75** *	**807.8 ± 72.32** *	**820.33 ± 80.31** *
OVX RSG 10mg/kg	638.33 ± 54.66	**770.08 ± 70.38** *	**826.17 ± 109.42** *	**878.00 ± 101.31** *
OVX RSG 10mg/kg + ALN	667 ± 47.97	**782.15 ± 72.05** *	**835.23 ± 93.14** *	**867.83 ± 99.32** *

Data are presented as mean ± standard deviation. * indicates significance vs. glucose test #1 ($p<0.05$).*

4.2 The Effect of Rosiglitazone on Blood Biochemistry

4.2.1 Glucose Testing

A summary for the 4 glucose tests performed on each rat throughout the treatment period is displayed in Table 4-2. The OVX RSG 3mg/kg and OVX RSG 10mg/kg groups as well as the Sham controls demonstrated significantly lower blood glucose ($p<0.05$) as treatment progressed. The Sham RSG 10mg/kg group also showed decreased serum glucose for tests 2 and 3 compared to onset.

Table 4-2. Blood serum glucose results for all female groups

	Glucose (mmol/L)	**Glucose (mmol/L)**	**Glucose (mmol/L)**	**Glucose (mmol/L)**
	baseline	**#2**	**#3**	**#4**
Sham Control	7.13 ± 1.28	6.6 ± 0.81	**6.14 ± 0.80** *	**6.16 ± 0.47** *
Sham RSG 10mg/kg	7.52 ±1.81	**6.14 ± 0.57** *	**6.26 ± 0.59** *	6.68 ± 0.92
OVX Control	6.46 ± 1.04	6.99 ± 0.90	7.34 ± 2.07	7.02 ± 1.14
OVX ALN	6.86 ± 1.13	6.35 ± 0.76	6.27 ± 0.76	6.48 ± 0.97
OVX RSG 3mg/kg	6.69 ± 0.94	6.27 ± 0.69	**6.03 ± 0.70** *	**6.44 ± 0.36** *
OVX RSG 3mg/kg + ALN	6.64 ± 0.75	6.83 ± 0.80	6.46 ± 0.94	6.20 ± 0.63
OVX RSG 10mg/kg	7.42 ± 1.60	**6.37 ± 0.38** *	**6.46 ± 0.62** *	**5.76 ± 0.69** *
OVX RSG 10mg/kg + ALN	6.76 ± 0.87	6.58 ± 0.45	6.80 ± 1.19	6.50 ± 0.81

Data are presented as mean ± standard deviation. * indicates significance vs. glucose test #1 ($p<0.05$).*

4.2.2 Remaining Blood biochemistry

A summary of the remaining blood testing results are displayed in Table 4-3. Blood serum was tested for total cholesterol, total triglycerides, insulin, osteocalcin and serum CTX at baseline and at termination of the experiment. At experiment termination, serum was also testing for leptin and adiponectin.

The Sham Control group was the only group that demonstrated significantly higher serum triglycerides at termination compared to baseline ($p < 0.05$). The OVX Control group demonstrated a significant increase in serum insulin at termination compared to baseline whereas the RSG treated groups showed no changes in these parameters. All 5 treated OVX groups showed increased Serum CTX at termination compared to onset. This result is questionable since ALN treatment is known to inhibit bone resorption and should thus cause decreased levels of Serum CTX, a marker of bone resorption. Osteocalcin, a marker for bone formation was significantly decreased in the Sham RSG 10mg/kg group as well as in the OVX control, RSG 3mg/kg, RSG 3mg/kg + ALN and RSG 10mg/kg + ALN groups. The bone marker results are not what we would expect following RSG and ALN treatment. Possible explanations are discussed in Chapter 5.

Table 4-3. Blood biochemistry results for all female groups, B= baseline, T= termination

		Sham		OVX					
		Control	**RSG 10mg/kg**	**Control**	**ALN**	**RSG 3mg/kg**	**RSG 3mg/kg + ALN**	**RSG 10mg/kg**	**RSG 10mg/kg + ALN**
Cholesterol (mmol/L)	B	9.79 ± 7.48	9.02 ± 8.62	14.00 ± 7.16	11.92 ± 4.41	9.63 ± 1.64	13.77 ± 8.41	13.18 ± 5.07	14.72 ± 6.93
Cholesterol (mmol/L)	T	11.07 ± 19.31	6.38 ± 2.54	16.72 ± 9.10	15.92 ± 5.93	**13.25 ± 3.52***	25.46 ± 20.07	13.91 ± 5.41	15.11 ± 8.55
Triglycerides (mmol/L)	B	16.66 ± 5.20	16.11 ± 4.52	11.41 ± 6.96	10.46 ± 4.42	8.92 ± 3.84	11.17 ± 6.79	9.10 ± 5.01	10.18 ± 6.39
Triglycerides (mmol/L)	T	**38.48 ± 25.03***	11.70 ± 8.35	18.20 ± 24.70	12.41 ± 7.36	8.99 ± 7.12	23.62 ± 22.45	9.42 ± 8.40	9.03 ± 5.89
Insulin (ng/mL)	B	15.31 ± 7.33	14.56 ± 6.95	12.20 ± 5.99	10.54 ± 2.41	13.36 ± 6.10	15.23 ± 6.83	13.07 ± 5.43	10.76 ± 7.29
Insulin (ng/mL)	T	15.40 ± 12.49	14.40 ±6.34	**19.74 ± 9.09***	14.00 ± 7.32	17.84 ± 11.10	11.91 ± 7.64	14.06 ± 8.52	11.95 ± 6.63
Osteocalcin (ng/mL)	B	170.32 ± 81.84	123.87 ± 25.92	175.12 ± 46.66	186.29 ± 30.83	190.78 ± 46.22	201.09 ± 42.69	196.10 ± 42.15	173.48 ± 26.37
Osteocalcin (ng/mL)	T	150.34 ± 77.44	**58.12 ± 16.39***	**126.59 ± 49.09***	39.88 ± 22.78	**107.56 ± 27.57***	**65.84 ± 39.87***	125.04 ± 77.48	**72.15 ± 80.94***
Serum CTX (ng/mL)	B	22.67 ± 12.36	15.05 ± 5.43	35.81 ± 26.11	22.62 ± 16.06	18.51 ± 5.28	20.43 ± 8.54	22.14 ± 8.74	23.08 ± 8.63
Serum CTX (ng/mL)	T	**38.31 ± 17.65***	16.83 ± 3.03	36.89 ± 22.05	**38.34 ± 11.51***	**32.82 ± 8.10***	**34.67 ± 9.42***	**32.04 ± 12.31***	**36.03 ± 15.65***
Adiponectin (µg/mL)	T	15.68 ± 3.51	19.84 ± 2.54	18.18 ± 3.47	19.51 ± 3.77	20.13 ± 2.17	17.90 ± 5.24	20.26 ± 4.94	21.04 ± 3.84
Leptin(ng/mL)	T	109.35 ± 39.71	81.14 ± 15.91	123.61 ± 116.26	120.57 ± 61.40	127.71 ± 26.69	142.11 ± 73.17	120.78 ± 32.48	147.89 ± 64.99

Data are presented as mean ± standard deviation. * indicates significance vs. baseline blood serum test ($p<0.05$).*

4.3 The Effect of Rosiglitazone on Bone Mineral Density

Areal Bone Mineral Density

Areal bone mineral density was analyzed via DEXA analysis. A summary of the results from Dual Energy X-Ray Absorptiometry is displayed in Table 4-4. One scan was performed on each right femur and another scan was performed on each L5 and L6 lumbar vertebrae. For L5 and L6, the average values for BMD (g/cm^2), BMC (g) and Bone area (cm^2) were taken and are displayed in Table 4-4. There were no significant differences in femoral or vertebral BMD and BMC between the Sham Control and the Sham RSG 10mg/kg group. However, the Sham control group did demonstrate higher femoral and vertebral BMD and BMC than OVX controls, confirming the effects of ovariectomy in this rat model.

Following 2-way ANOVA, RSG and ALN both had an effect on femoral BMD ($p=0.022$ and $p=0.00$ respectively) and vertebral BMD ($p=0.001$ and $p=0.00$ respectively). There was no significant interaction effect of ALN and RSG in either case ($p=0.816$ and $p = 0.955$). The OVX RSG 10mg/kg group had significantly lower femoral and vertebral BMD compared to OVX controls and the OVX ALN group ($p<0.05$). The OVX ALN group had significantly higher femoral and vertebral BMD than all OVX groups except for RSG 3mg/kg + ALN group ($p<0.05$). ALN treatment caused higher values for BMD compared to OVX control and OVX RSG-treated groups however, BMD values did still decrease with increasing RSG dose. The OVX RSG 3mg/kg + ALN and OVX RSG 10mg/kg + ALN both had significantly higher femur BMC than OVX Controls ($p<0.05$). There were no significant differences in femoral or vertebral bone area between any of the groups.

Table 4-4. DEXA results for all female groups

		Sham		OVX					
	Sample	**Control**	**RSG 10mg/kg**	**Control**	**ALN**	**RSG 3mg/kg**	**RSG 3mg/kg + ALN**	**RSG 10mg/kg**	**RSG 10mg/kg + ALN**
BMD(g/cm^2)	RF	0.20 ± 0.01	0.20 ± 0.01	**0.19 ± 0.01** ^{h}	**0.22 ± 0.01** ^{dfg}	0.19 ± 0.01	**0.22 ± 0.01** ^{d}	**0.18 ± 0.01** ^{de}	**0.21 ± 0.00** ^{dfg}
BMC(g)	RF	0.43 ± 0.02	0.44 ± 0.03	0.43 ± 0.04	**0.49 ± 0.05** ^{d}	0.42 ± 0.04	**0.50 ± 0.05** ^{d}	**0.41 ± 0.02** ^{e}	**0.47 ± 0.02** ^{dfg}
B Area(cm^2)	RF	2.13 ± 0.10	2.17 ± 0.13	2.21 ± 0.08	2.23 ± 0.11	2.21 ± 0.13	2.25 ± 0.12	2.24 ± 0.10	2.22 ± 0.04
BMD(g/cm^2)	L5 & L6	0.11 ± 0.01	0.11 ± 0.01	**0.10 ± 0.01** ^{h}	**0.13 ± 0.01** ^{dfg}	0.10 ± 0.01	**0.13 ± 0.01** ^{d}	**0.09 ± 0.01** ^{d}	**0.12 ± 0.01** ^{dfg}
BMC(g)	L5 & L6	0.05 ± 0.00	0.05 ± 0.01	0.05 ± 0.01	**0.06 ± 0.01** ^{d}	0.05 ± 0.01	0.06 ± 0.01	0.04 ± 0.01	0.06 ± 0.01
B Area(cm^2)	L5 & L6	0.45 ± 0.02	0.46 ± 0.03	0.45 ± 0.03	0.48 ± 0.03	0.46 ± 0.03	0.48 ± 0.03	0.46 ± 0.02	0.47 ± 0.03

Data are presented as mean ± standard deviation. ^{d} *indicates significance vs. OVX controls (p<0.05).* ^{e} *indicates significance vs. OVX ALN group (p<0.05).).* ^{f} *indicates significance vs. OVX RSG 3mg/kg group (p<0.05).* ^{g} *indicates significance vs. OVX RSG 10mg/kg group (p<0.05).* ^{h} *indicates significance vs. Sham Control group (p<0.05).RF=right femur, L5&L6=lumbar vertebrae 5 and 6.*

Volumetric Bone Mineral Density

MicroCT analysis allowed for an analysis of volumetric BMD. MicroCT was completed on all 81 L6 vertebrae and all 81 right femora from the female rats. The results from these tests are displayed in Table 4-5.

Table 4-5. Volumetric BMD results for all female groups

	Sham		**OVX**					
Volumetric BMD	**Control**	**RSG 10**	**Control**	**ALN**	**RSG 3**	**RSG 3 +ALN**	**RSG 10**	**RSG 10 +ALN**
Trabecular	0.57 ± 0.06	0.54 ± 0.02	**0.52 ± 0.06**[h]	**0.62 ± 0.05**[dfg]	0.50 ± 0.07	**0.63 ± 0.07**[dfg]	**0.44 ± 0.04**[de]	**0.59 ± 0.04**[dfg]
Cortical	1.16 ± 0.03	1.16 ± 0.01	1.15 ± 0.02	1.16 ± 0.01	1.15 ± 0.02	1.16 ± 0.01	1.15 ± 0.01	**1.17 ± 0.01**[fg]

Data are presented as mean ± standard deviation. [d] *indicates significance vs. OVX controls (p<0.05).* [e] *indicates significance vs. OVX ALN group (p<0.05).* [f] *indicates significance vs. OVX RSG 3mg/kg group (p<0.05).* [g] *indicates significance vs. OVX RSG 10mg/kg group (p<0.05.)* [h] *indicates significance vs. Sham Control group (p<0.05).*

The OVX control group showed decreased volumetric vertebral BMD compared to Sham controls, once again confirming the effect of ovariectomy in our rat model. There were no significant differences in vertebral or femoral BMD between the two Sham groups.

Following 2-way ANOVA, RSG had no effect on femoral BMD in the OVX groups but did have an effect on vertebral volumetric BMD (p=0.006). ALN did have an effect on femoral and vertebral volumetric BMD (p=0.003 and p=0.000). There was no interaction between RSG and ALN for either parameter (p=0.668 and p=0.403). The RSG 10mg/kg group demonstrated decreased vertebral volumetric BMD compared to OVX controls and the OVX ALN group (p<0.05), confirming the results obtained from DEXA analysis. There were no differences, however, when comparing femoral volumetric BMD of the OVX RSG 10mg/kg group to the other OVX groups. All 3 OVX ALN groups showed increased vertebral volumetric BMD

compared to OVX controls, OVX RSG 3mg/kg and OVX RSG 10mg/kg groups ($p<0.05$). The OVX RSG 10mg/kg + ALN group also had increased femoral volumetric BMD compared to the two OVX RSG-treated groups ($p < 0.05$).

4.4 Effect of Rosiglitazone on Bone Structural Properties

Trabecular Bone Microarchitecture

The MicroCT results from the L6 vertebrae were used to evaluate the microarchitecture of trabecular bone. These parameters include percent bone volume (BV/TV), trabecular thickness (Tb.Th.). trabecular number (Tb.N.) and trabecular separation (Tb.Sp.). The results from these tests are displayed in Table 4-6.

There were no significant differences for any parameters between the Sham controls and Sham RSG 10 groups. The OVX control group demonstrated significantly decreased BV/TV, Tb.N. and increased Tb.Sp. than Sham controls which is expected of OVX treatment.

Following 2-way ANOVA, RSG and ALN both had an effect on BV/TV, Tb.Th., Tb.N. and Tb.Sp. ($p<0.05$ and $p=0.00$ respectively). There was no significant interaction effect between RSG and ALN for any parameter. The OVX RSG 3mg/kg group showed a decrease in trabecular thickness ($p<0.05$) compared to OVX controls and the OVX ALN group. The OVX RSG 10mg/kg group demonstrated decreases in percent bone volume (Figure 4-1), trabecular thickness, trabecular number and an increase in trabecular separation compared to the OVX control group as well as the OVX ALN group ($p<0.05$).

The OVX ALN and OVX RSG 3mg/kg + ALN group showed the opposite result with increased percent bone volume, increased trabecular number and decreased trabecular separation compared to the OVX controls, OVX RSG 3mg/kg and OVX RSG 10mg/kg. The OVX RSG 10mg/kg + ALN group also showed increased percent bone volume and trabecular number compared to OVX controls and the 2 OVX RSG treated groups ($p < 0.05$), demonstrating that trabecular bone loss due to RSG can be prevented by ALN treatment in this model.

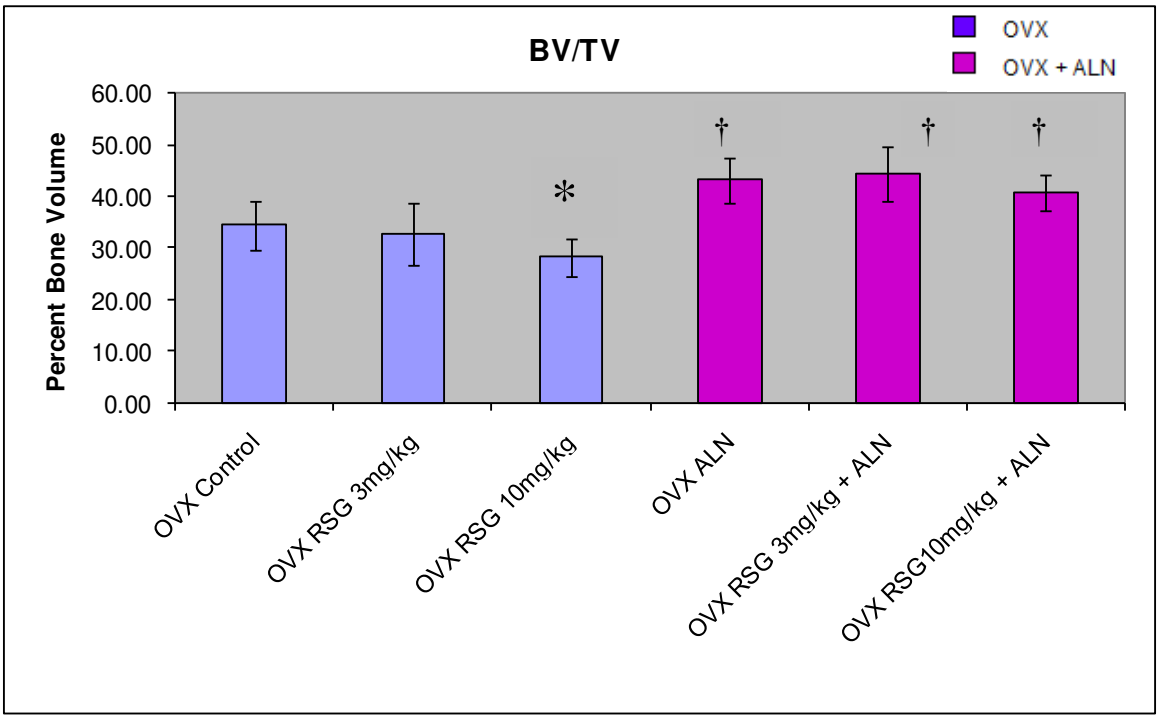

Figure 4-1. Percent bone volume for female OVX groups
(* indicates significantly lower than OVX Controls, † indicates significantly higher than controls)

Cortical Bone Structural Properties

The MicroCT results from the right femora were used to evaluate the structural properties of cortical bone. These parameters are displayed in Table 4-6. Following 2-way ANOVA, only ALN had an effect on cortical geometrical parameters ($p<0.05$). There was no interaction effect between RSG or ALN for any parameter. The OVX ALN and OVX RSG 3mg/kg + ALN groups demonstrated significantly increased cortical thickness compared to OVX RSG 3mg/kg and OVX RSG 10mg/kg groups ($p<0.05$). The OVX RSG 10mg/kg + ALN group also had significantly higher cortical thickness compared to the OVX RSG 10mg/kg group ($p<0.05$). Lastly, the OVX RSG 3mg/kg + ALN group showed significantly higher cross-sectional area than the OVX RSG 3mg/kg and 10mg/kg groups ($P<0.05$). There were no other significant findings.

Table 4-6. MicroCT results for trabecular and cortical bone for all female groups

	Sham		**OVX**					
Cortical Bone	**Control**	**RSG 10mg/kg**	**Control**	**ALN**	**RSG 3mg/kg**	**RSG 3mg/kg + ALN**	**RSG 10mg/kg**	**RSG 10mg/kg + ALN**
Length (mm)	33.98 ± 0.98	34.09 ± 0.56	34.39 ± 0.99	34.60 ± 0.70	34.72 ± 1.10	34.49 ± 1.28	34.35 ± 0.64	34.47 ± 0.97
Mean Polar moment of inertia (mm^4)	14.72 ± 2.17	14.89 ± 2.15	16.19 ± 2.62	16.57 ± 3.08	15.85 ± 2.96	16.53 ± 3.14	15.66 ± 2.00	15.92 ± 2.25
Cross – sectional area (mm^2)	7.64 ± 0.39	7.73 ± 0.37	8.01 ± 0.73	8.27 ± 0.75	7.81 ± 0.63	**8.40 ± 0.75** [fg]	7.80 ± 0.42	8.05 ± 0.55
Moment of area (mm^4)	5.86 ± 0.95	5.74 ± 0.91	6.01 ± 1.01	6.39 ± 1.36	6.10 ± 1.25	6.30 ± 1.35	5.94 ± 0.75	6.07 ± 1.01
Cortical Thickness (mm)	0.83 ± 0.07	0.86 ± 0.02	0.86 ± 0.05	**0.90 ± 0.08** [fg]	0.84 ± 0.05	**0.90 ± 0.04** [fg]	0.82 ± 0.05	**0.88 ± 0.06** [g]
Trabecular Bone								
Percent bone volume	39.54 ± 4.78	37.25 ± 2.12	**34.46 ± 4.75** [h]	**43.17 ± 4.38** [dfg]	32.73 ± 6.02	**44.28 ± 5.36** [dfg]	**28.17 ± 3.73** [de]	**40.67 ± 3.44** [dfg]
Trabecular thickness	0.11 ± 0.01	0.11 ± 0.00	0.11 ± 0.01	0.11 ± 0.00	**0.10 ± 0.01** [de]	0.11 ± 0.01	**0.10 ± 0.01** [de]	0.11 ± 0.00
Trabecular number	3.54 ± 0.27	3.54 ± 0.14	**3.13 ± 0.30** [h]	**3.83 ± 0.33** [dfg]	3.13 ± 0.37	**3.86 ± 0.33** [dfg]	**2.82 ± 0.23** [de]	**3.67 ± 0.21** [dfg]
Trabecular separation	0.20 ± 0.03	0.22 ± 0.01	**0.24 ± 0.02** [h]	**0.20 ± 0.02** [dfg]	0.25 ± 0.03	**0.20 ± 0.02** [dfg]	**0.27 ± 0.02** [de]	0.21 ± 0.02

Data are presented as mean ± standard deviation. [d] *indicates significance vs. OVX controls (p<0.05).* [e] *indicates significance vs. OVX ALN group (p<0.05).).* [f] *indicates significance vs. OVX RSG 3mg/kg group (p<0.05).* [g] *indicates significance vs. OVX RSG 10mg/kg group (p<0.05).* [h] *indicates significance vs. Sham control group (p<0.05).*

Porosity Measurements

MicroCT analysis also allowed for an evaluation of total porosity (%) for all 81 female right femur samples. The results for this test are found in Table 4-7.

Table 4-7. Porosity results for all female groups

	Sham		**OVX**					
	Control	**RSG 10**	**Control**	**ALN**	**RSG 3**	**RSG 3 +ALN**	**RSG 10**	**RSG 10 +ALN**
Porosity (%)	1.29 ± 1.23	0.75 ± 0.57	1.08 ± 0.93	**0.57 ± 0.53** [fg]	1.47 ± 1.03	**0.88 ± 0.64** [g]	**2.20 ± 1.41** [d]	**1.1 ± 1.46** [g]

Data are presented as mean ± standard deviation. [d] *indicates significance vs. OVX controls (p<0.05).* [e] *indicates significance vs. OVX ALN group (p<0.05).* [f] *indicates significance vs. OVX RSG 3mg/kg group (p<0.05).* [g] *indicates significance vs. OVX RSG 10mg/kg group (p<0.05.)*

There were no significant differences in porosity between the two Sham groups or between the Sham controls and OVX controls. Follwing 2-way ANOVA, RSG and ALN both had an effect on total porosity (p=0.05 and p=0.009 respectively). There was no significant interaction effect between RSG and ALN. The OVX RSG 10mg/kg group demonstrated significantly higher femoral total porosity than OVX controls (p = 0.023) (Figure 4-2). The OVX ALN group had significantly lower total porosity than both OVX RSG treated groups (p < 0.05). The OVX RSG 3mg/kg + ALN and OVX RSG 10mg/kg + ALN groups had significantly lower total porosity than the OVX RSG 10mg/kg group (p < 0.02).

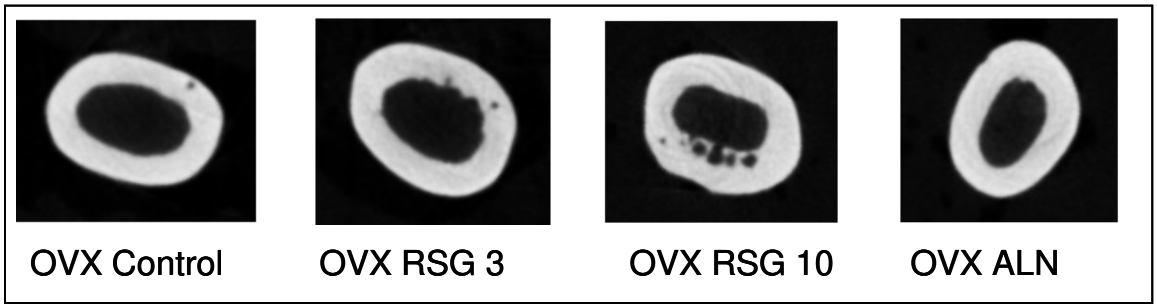

Figure 4-2. Femoral cross sectional images showing total porosity

4.5 The Effect of Rosiglitazone on Mechanical Properties of Cortical Bone

4.5.1 Three-point Bending Results

81 three point bending tests were successfully performed on the right femora. The unnormalized and normalized results from these tests are displayed in Table 4-8. The unnormalized parameters that were evaluated are ultimate load (N), failure load (N), failure deformation (mm), energy to failure (mJ) and stiffness (N/mm). The parameters that were evaluated via normalization were Ultimate stress (Mpa), Failure Stress (Mpa), Toughness (mJ/mm^3) and Modulus (Mpa).

There we no significant differences for any parameters between the two Sham groups or between the Sham controls and OVX controls. Follwing 2-way ANOVA, ALN had an effect on ultimate load, ultimate stress and toughness ($p<0.045$). RSG alone had no effect on any parameters and there was no interaction between RSG and ALN. The OVX RSG 3mg/kg + ALN group showed increased ultimate load and failure load compared to both the OVX RSG 3mg/kg and 10mg/kg groups ($p < 0.05$). The OVX RSG 10mg/kg + ALN group showed significantly higher ultimate load and failure load compared to the OVX RSG 10mg/kg group ($p < 0.05$).

Once normalized, The OVX RSG 3mg/kg + ALN group had significantly higher ultimate stress compared to both the OVX RSG 3mg/kg and 10mg/kg groups ($p < 0.05$). The OVX RSG 10mg/kg + ALN demonstrated significantly higher ultimate stress and toughness than the OVX RSG 10mg/kg group ($p < 0.05$).

Table 4-8. Structural and material properties of cortical bone following 3-point bending for all female groups

	Sham		OVX					
Structural Properties	**Control**	**RSG 10mg/kg**	**Control**	**ALN**	**RSG 3mg/kg**	**RSG 3mg/kg + ALN**	**RSG 10mg/kg**	**RSG 10mg/kg + ALN**
ultimate load (N)	151.26 ± 10.12	156.16 ± 14.00	163.14 ± 17.54	170.79 ± 21.68	160.38 ± 17.14	**177.06 ± 24.51[fg]**	154.72 ± 8.69	**173.79 ± 20.12[g]**
failure load (N)	150.25 ± 11.67	149.84 ± 12.80	161.13 ± 16.72	169.86 ± 21.80	158.77 ± 16.97	**175.90 ± 23.51[fg]**	154.39 ± 8.68	**169.17 ± 20.61[g]**
failure deformation(mm)	0.46 ± 0.07	0.47 ± 0.03	0.51 ± 0.07	0.50 ± 0.06	0.50 ± 0.07	0.51 ± 0.10	0.47 ± 0.02	0.56 ± 0.09
energy to failure (mJ)	41.78 ± 7.35	46.08 ± 7.66	52.27 ± 13.20	52.97 ± 12.83	51.16 ± 13.03	56.60 ± 19.91	45.35 ± 3.68	62.60 ± 15.86
stiffness (N/mm)	514.29 ± 28.68	529.07 ± 37.79	558.99 ± 42.48	549.06 ± 73.10	536.23 ± 50.50	589.17 ± 59.82	542.23 ± 28.43	557.62 ± 56.22
Material Properties								
ultimate stress (Mpa)	160.37 ± 13.72	168.15 ± 15.63	168.94 ± 14.06	169.64 ± 10.24	167.07 ± 10.72	**185.52 ± 26.03[fg]**	162.34 ± 11.46	**176.70 ± 13.00[g]**
Toughness (mJ/mm^3)	3.43 ± 0.64	3.85 ± 0.70	4.21 ± 1.02	4.14 ± 0.83	4.20 ± 0.91	4.72 ± 1.99	3.71 ± 0.23	**5.01 ± 1.30[g]**
Modulus (Mpa)	7100.00 ± 1146.60	7384.38 ± 865.89	7474.98 ± 881.30	6926.95 ± 828.75	7144.05 ± 1190.70	7873.64 ± 1076.38	7291.97 ± 749.67	7235.93 ± 714.72

Data are presented as mean ± standard deviation.[f] indicates significance vs. OVX RSG 3mg/kg group ($p<0.05$).[g] indicates significance vs. OVX RSG 10mg/kg group ($p<0.05$).

4.5.2 Torsion Results

81 Torsion tests were successfully performed on the left femora. The results from these tests are displayed in Table 4-9. The unnormalized parameters that were evaluated are Failure Torque (N·mm), Angular Deformation at Failure (rad), Energy to Failure (N·mm·rad) and Stiffness (N/mm). The normalized parameters that were evaluated are Shear Stress (Mpa), Shear Strain (%), Energy to Failure (mJ/mm^3) and Shear Modulus (Mpa).

There were no significant differences between the two Sham groups or between the Sham controls and OVX controls. Following 2-way ANOVA, RSG had an effect on failure torque, stiffness, shear stress and shear modulus ($p<0.05$). There was no interaction effect between RSG and ALN for any parameters. The OVX RSG 10mg/kg group demonstrated significantly lower failure torque and stiffness compared to OVX controls and the OVX ALN group ($p < 0.05$). Interestingly, the OVX RSG 10mg/kg + ALN group also demonstrated significantly lower failure torque and stiffness compared to OVX controls and the OVX ALN group ($p < 0.05$) suggesting that ALN does not protect against the effects of RSG in this case.

Once normalized, the OVX RSG 10mg/kg group still showed significantly decreased shear stress (Figure 4-3) compared to OVX controls and the OVX ALN group and also showed decreased shear modulus compared to OVX controls ($p < 0.05$). The OVX RSG 3mg/kg + ALN and OVX RSG 10mg/kg + ALN groups also showed decreased shear modulus compared to OVX controls ($p < 0.05$). Additionally, the OVX RSG 10mg/kg + ALN group demonstrated increased shear stress compared to the OVX ALN group and increased toughness compared to the OVX RSG 10mg/kg group ($p < 0.05$).

Table 4-9. Structural and material properties of cortical bone following torsion testing for all female groups

	Sham		**OVX**					
Structural Properties	**Control**	**RSG 10mg/kg**	**Control**	**ALN**	**RSG 3mg/kg**	**RSG 3mg/kg + ALN**	**RSG 10mg/kg**	**RSG 10mg/kg + ALN**
Failure Torque (N·mm)	389.27 ± 95.35	425.59 ± 104.50	449.70 ± 93.04	512.39 ± 124.97	443.47 ± 102.32	446.67 ± 95.67	**364.78 ± 97.23** [de]	**415.45 ± 106.07** [de]
Angular Deformation at Failure (rad)	0.19 ± 0.07	0.20 ± 0.03	0.21 ± 0.0	0.19 ± 0.03	0.19 ± 0.03	0.24 ± 0.03	0.23 ± 0.07	0.24 ± 0.09
Energy to Failure (N·mm·rad)	44.55 ± 12.71	51.95 ± 13.40	58.35 ± 27.28	56.80 ± 18.1	51.47 ± 16.41	64.61 ± 11.72	46.99 ± 9.45	61.59 ± 25.05
Stiffness (N/mm)	1687.75 ± 469.61	1926.66 ± 575.91	2267.25 ± 636.49	2395.43 ± 514.30	2028.05 ± 546.14	1861.69 ± 524.86	**1680.64 ± 833.62** [de]	**1747.02 ± 721.45** [e]
Material Properties								
Shear Stress (MPa)	52.36 ± 15.79	57.05 ± 12.19	56.99 ± 9.17	68.05 ± 15.29	58.23 ± 14.09	55.11 ± 6.40	**47.99 ± 9.95** [de]	**52.77 ± 11.26** [e]
Shear Strain (%)	2.87 ± 0.94	3.25 ± 0.59	3.35 ± 1.23	2.90 ± 0.39	3.07 ± 0.63	3.82 ± 0.38	3.61 ± 0.92	3.89 ± 1.36
Toughness (mJ/mm^3)	0.46 ± 0.16	0.54 ± 0.16	0.57 ± 0.27	0.54 ± 0.15	0.53 ± 0.18	0.57 ± 0.09	0.47 ± 0.09	**0.61 ± 0.25** [g]
Shear Modulus (MPa)	1517.24 ± 494.54	1610.57 ± 400.89	1743.70 ± 381.29	2035.92 ± 466.66	1650.65 ± 488.10	**1448.59 ± 182.49**[d]	**1372.87 ± 495.96**[d]	**1339.80 ± 462.56**[d]

Data are presented as mean ± standard deviation. [d] *indicates significance vs. OVX controls ($p<0.05$).* [e] *indicates significance vs. OVX ALN group ($p<0.05$).* [g] *indicates significance vs. OVX RSG 10mg/kg group ($p<0.05$).*

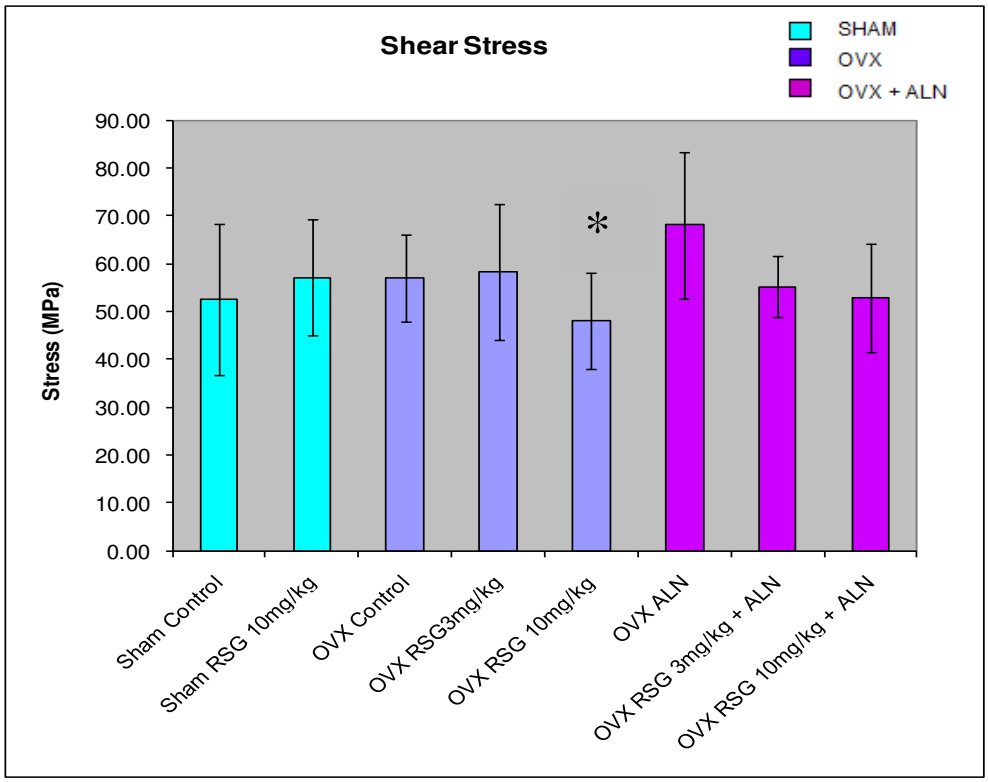

Figure 4-3. Shear stress for all female groups
(* indicates significantly lower than OVX Controls)

4.6 The Effect of Rosiglitazone on Mechanical Properties of Trabecular Bone

4.6.1 Vertebral Compression

81 vertebral compression tests were successfully performed on the L6 vertebrae. The results from these tests are displayed in Table 4-10. The unnormalized parameters that were evaluated with this test are ultimate load (N), failure load (N), failure deformation (mm), energy to failure (mJ) and stiffness (N/mm). The parameters that were evaluated via normalization are ultimate stress (Mpa), failure stress (Mpa), toughness (mJ/mm^3) and modulus (Mpa).

There were no significant differences between the Sham controls and OVX controls or between the two Sham groups for any parameters. Following 2-way ANOVA, RSG and ALN both had an effect on ultimate load, failure deformation, ultimate stress and toughness ($p<0.05$).

Additionally, ALN had an effect on stiffness (p=0.00). There was no significant interaction between RSG and ALN. The OVX RSG 10mg/kg group showed significantly decreased ultimate load than OVX controls. All 3 OVX ALN groups had increased ultimate load compared to controls. For the OVX RSG 3mg/kg + ALN group, this difference in ultimate load was significantly higher than the OVX RSG 3mg/kg and 10mg/kg groups as well. The OVX RSG 3mg/kg + ALN groups showed significantly higher failure deformation than both the OVX RSG 3mg/kg and 10mg/kg groups. Interestingly, the OVX RSG 10mg/kg + ALN group showed lower failure deformation than OVX controls. The OVX ALN and OVX RSG 10mg/kg + ALN groups also had significantly increased stiffness compared to OVX controls. For the OVX RSG 10mg/kg + ALN group, this difference was also significant compared to both OVX RSG 3mg/kg and 10mg/kg groups.

Once normalized, the OVX RSG 10mg/kg group demonstrated significantly decreased ultimate stress, failure stress and toughness compared to OVX controls ($p < 0.05$). The OVX ALN and OVX RSG 3mg/kg + ALN groups both showed significantly increased ultimate stress, failure stress and toughness compared to both the OVX RSG 3mg/kg and 10 mg/kg groups ($p < 0.05$). Lastly, the OVX RSG 10mg/kg + ALN group had significantly increased ultimate and failure load compared to the OVX RSG 10mg/kg + ALN group ($p < 0.05$).

Table 4-10. Structural and material properties of trabecular bone following vertebral compression for all female groups

	Sham		OVX					
Structural Properties	**Control**	**RSG 10mg/kg**	**Control**	**ALN**	**RSG 3mg/kg**	**RSG 3mg/kg + ALN**	**RSG 10mg/kg**	**RSG 10mg/kg + ALN**
ultimate load (N)	219.03 ± 18.38	205.02 ± 30.28	181.25 ± 45.00	**282.08 ± 58.64** [d]	171.98 ± 33.91	**274.41 ± 50.26** [dfg]	**146.55 ± 34.38** [de]	**234.59 ± 51.01** [dfg]
failure load (N)	196.15 ± 13.20	183.78 ± 27.26	170.83 ± 36.80	231.10 ± 94.55	147.04 ± 25.78	246.91 ± 45.09	130.53 ± 32.44	197.27 ± 34.20
failure deformation(mm)	0.89 ± 0.16	0.81 ± 0.16	0.82 ± 0.19	0.80 ± 0.30	**0.70 ± 0.14** [d]	**0.97 ± 0.17** [fg]	**0.76 ± 0.23** [d]	**0.77 ± 0.12**[d]
energy to failure (mJ)	124.54 ± 32.62	103.43 ± 36.12	95.35 ± 35.44	132.34 ± 45.02	68.10 ± 15.68	153.11 ± 46.97	68.94 ± 26.78	97.86 ± 24.14
stiffness (N/mm)	403.89 ± 99.34	365.01 ± 136.66	368.54 ± 71.62	**429.15 ± 117.08** [g]	360.79 ± 89.50	430.03 ± 77.35	301.60 ± 92.91	**471.34 ± 50.48** [dfg]
Material Properties								
ultimate stress (Mpa)	34.21 ± 4.14	34.12 ± 4.76	35.03 ± 6.56	**41.50 ± 6.73** [fg]	30.87 ± 3.33	**40.64 ± 3.77** [fg]	**27.89 ± 4.78** [de]	**36.95 ± 7.09** [fg]
failure stress (Mpa)	30.63 ± 3.73	30.59 ± 4.30	32.13 ± 5.98	**37.40 ± 6.30** [fg]	26.89 ± 2.34	**36.57 ± 3.41** [fg]	**24.81 ± 4.43** [de]	**32.37 ± 6.46** [fg]
Toughness (mJ/mm^3)	2.44 ± 0.79	2.11 ± 0.70	2.31 ± 0.82	**2.60 ± 0.63** [fg]	**1.56 ± 0.28**[d]	**2.83 ± 0.72** [fg]	**1.60 ± 0.63**[de]	1.97 ± 0.42
Modulus (Mpa)	498.14 ± 99.77	495.58 ± 186.39	556.21 ± 133.59	508.42 ± 123.45	534.34 ± 193.36	509.24 ± 69.57	474.36 ± 128.58	610.78 ± 104.14

Data are presented as mean ± standard deviation. [d] *indicates significance vs. OVX controls ($p<0.05$).* [e] *indicates significance vs. OVX ALN group ($p<0.05$).* [f] *indicates significance vs. OVX RSG 3mg/kg group ($p<0.05$).* [g] *indicates significance vs. OVX RSG 10mg/kg group ($p<0.05$).*

4.6.2 Femoral Neck Fracture

81 femoral neck fracture tests were successfully performed. The results from these tests are displayed in Table 4-11. The parameters that were evaluated are ultimate load (N), failure load (N), failure deformation (mm), energy to failure (mJ) and stiffness (N/mm). Due to the complex geometry of the femoral head and neck, these results cannot be normalized.

The Sham RSG 10 group showed decreased ultimate load compared to Sham controls ($p<0.05$). Following 2-way ANOVA, RSG and ALN both showed a trend of having an effect on ultimate load ($p<0.1$). The OVX RSG 10mg/kg group showed significantly decreased ultimate load compared to OVX controls ($p < 0.05$). The OVX RSG 10mg/kg + ALN group showed significantly increased ultimate load and energy to failure compared to the OVX RSG 10mg/kg group ($p < 0.05$). There were no other significant results.

Table 4-11. Structural properties for all female groups following femoral neck fracture testing

	Sham		OVX					
Structural Properties	**Control**	**RSG 10mg/kg**	**Control**	**ALN**	**RSG 3mg/kg**	**RSG 3mg/kg + ALN**	**RSG 10mg/kg**	**RSG 10mg/kg + ALN**
ultimate load (N)	82.39 ± 10.70	78.63 ± 7.73	78.37 ± 10.10	78.16 ± 11.83	77.19 ± 11.39	**79.17 ± 8.83** [g]	**67.77 ± 10.93** [d]	**80.57 ± 10.28** [g]
failure load (N)	75.03 ± 8.52	74.69 ± 7.83	72.65 ± 13.93	72.12 ± 8.96	69.61 ± 12.86	74.94 ± 11.04	63.27 ± 11.24	64.02 ± 16.15
failure deformation(mm)	0.51 ± 0.18	0.39 ± 0.12	0.48 ± 0.17	0.49 ± 0.18	0.40 ± 0.07	0.47 ± 0.16	0.41 ± 0.07	0.50 ± 0.18
energy to failure (mJ)	25.09 ± 13.57	**18.13 ± 7.56** [h]	21.45 ± 6.13	22.06 ± 8.06	18.08 ± 5.75	21.08 ± 7.52	16.45 ± 4.77	**24.34 ± 10.63** [g]
stiffness (N/mm)	186.63 ± 44.73	224.57 ± 42.21	205.98 ± 66.37	204.33 ± 62.48	226.25 ± 29.22	190.11 ± 71.12	178.88 ± 37.16	200.89 ± 71.24

Data are presented as mean ± standard deviation. [d] *indicates significance vs. OVX controls (p<0.05).* [g] *indicates significance vs. OVX RSG 10mg/kg group (p<0.05) .* [h] *indicates significance vs. sham controls (p<0.05).*

4.7 The Effect of Rosiglitazone on Mineralization and Connectivity

4.7.1 Back-scatter Electron Imaging

Back-scatter electron imaging was completed on 81 female tibiae samples in order to obtain mineralization profiles. The parameters analyzed for this technique are logit, grey level and full width at half maximum height (FWHMH). A mineralization profile is completed for cortical bone, trabecular bone and total (cortical + trabecular) bone. These results are displayed in Table 4-12.

For total mineralization analysis, the OVX control group demonstrated a 1.8% shift towards lower mineralization compared Sham controls (Figure 4-4) which we would expect of OVX. This shift was also reflected by an increased logit value for the OVX control group. This increase, however, was not statistically significant. The OVX control group also showed significantly decreased FWHMH than Sham controls. Following 2-way ANOVA, RSG and ALN both had an effect on FWHMH ($p<0.05$) but there was no interaction between the two factors. The OVX RSG 10mg/kg + ALN group also showed significantly decreased FWHMH compared to the OVX ALN group.

The OVX RSG 10 group had a mineralization profile that was shifted 0.6% to the right of OVX controls indicating a more hypermineralized distribution (Figure 4-5). This was once again reflected in the logit score which was decreased for the OVX RSG 10 group versus OVX controls. Lastly, the OVX ALN group had a mineralization profile that was shifted 4.1% to the right of OVX controls (Figure 4-6) which is expected of ALN treatment. None of these differences, however, were statistically significant.

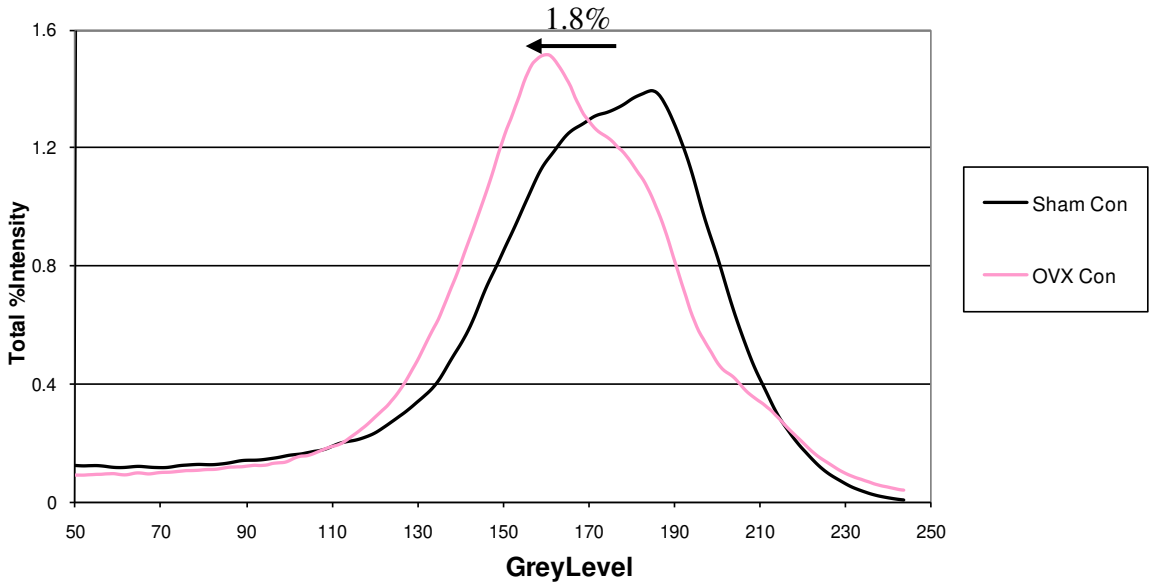

Figure 4-4. Total mineralization histograms for female control groups

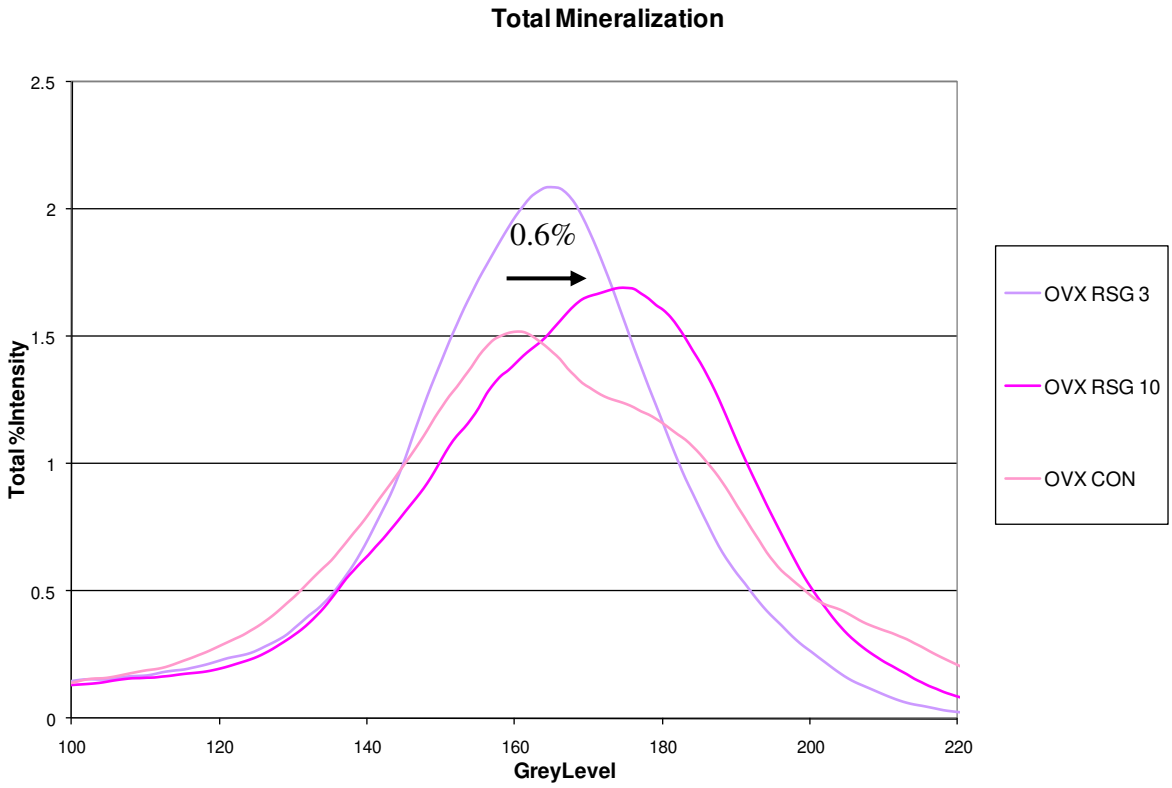

Figure 4-5. Total mineralization histograms for female OVX groups

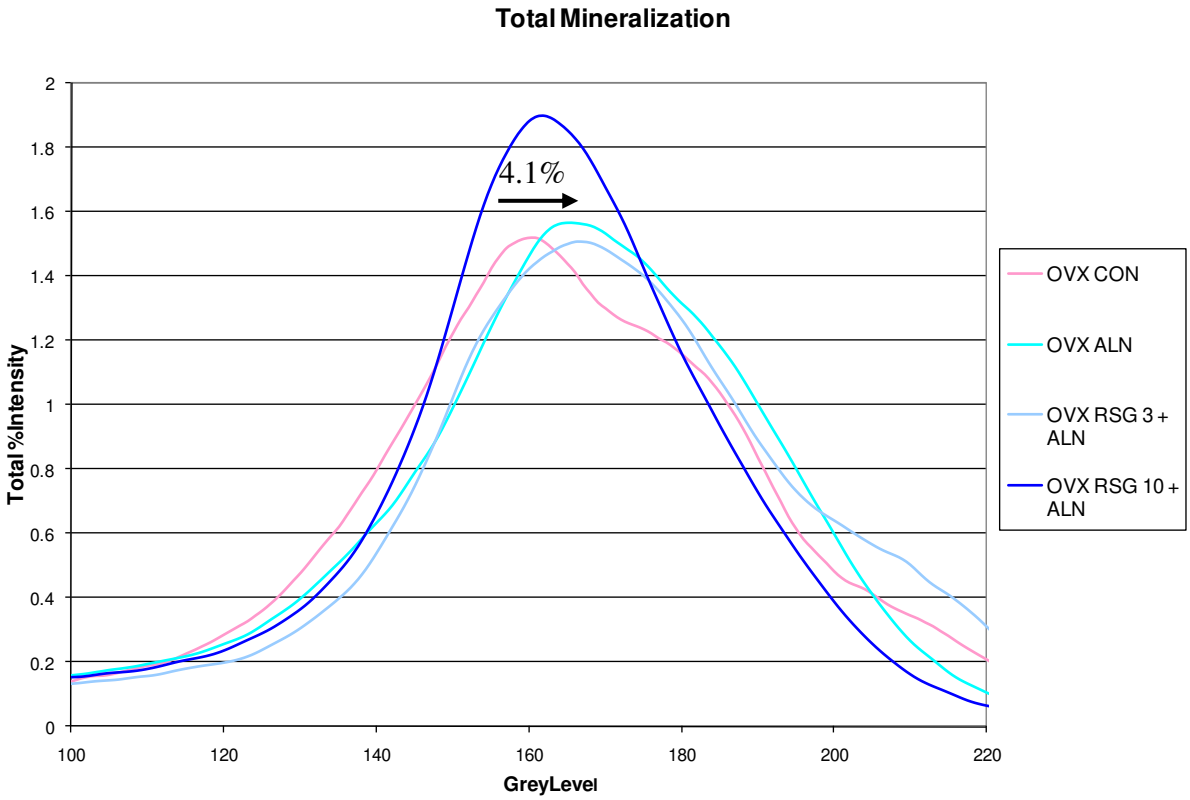

Figure 4-6. Total mineralization histograms for female OVX groups

Table 4-12. Mineralization analysis for all female groups

	Sham		OVX					
Cortical Bone	**Control**	**RSG 10mg/kg**	**Control**	**ALN**	**RSG 3mg/kg**	**RSG 3mg/kg + ALN**	**RSG 10mg/kg**	**RSG 10mg/kg + ALN**
logit	0.08 ± 1.36	0.20 ± 1.58	0.59 ± 1.95	0.84 ± 1.27	1.25 ± 0.85	0.51 ± 1.59	0.49 ± 1.58	1.51 ± 1.24
grey level	175.29 ± 14.85	175.38 ± 18.23	172.33 ± 20.49	164.67 ± 12.90	165.00 ± 7.98	172.00 ± 18.97	171.50 ± 12.54	162.25 ± 8.20
FWHMH	31.71 ± 6.24	26.88 ± 6.22	27.11 ± 5.90	29.89 ± 10.01	25.67 ± 3.61	25.43 ± 2.23	25.50 ± 2.39	26.08 ± 3.99
Trabecular Bone								
logit	0.08 ± 0.75	0.09 ± 0.95	0.47 ± 1.25	0.36 ± 0.99	0.81 ± 0.39	0.15 ± 0.91	0.31 ± 0.66	0.51 ± 0.76
grey level	**169.43 ± 18.64** [f]	171.75 ± 20.47	161.78 ± 21.32	162.89 ± 14.30	153.56 ± 7.62	166.29 ± 17.06	158.50 ± 11.25	158.92 ± 10.66
FWHMH	46.29 ± 3.50	45.13 ± 8.53	**36.22 ± 12.51** [h]	40.89 ± 3.59	39.56 ± 7.47	**42.14 ± 5.05** [g]	34.50 ± 5.21	38.83 ± 6.49
Total Bone								
logit	0.45 ± 1.06	0.55 ± 1.23	0.77 ± 1.71	0.89 ± 1.15	1.36 ± 0.67	0.63 ± 1.34	0.73 ± 1.11	1.30 ± 0.97
grey level	174.71 ± 15.45	175.13 ± 19.31	171.56 ± 22.01	164.44 ± 16.27	163.00 ± 8.00	170.71 ± 18.30	170.50 ± 11.40	162.25 ± 8.04
FWHMH	39.00 ± 8.37	35.00 ± 6.61	**32.78 ± 6.28** [h]	34.67 ± 9.19	31.11 ± 3.37	30.57 ± 3.10	32.25 ± 3.06	**29.58 ± 2.84** [e]

Data are presented as mean ± standard deviation. [d] *indicates significance vs. OVX controls ($p<0.05$).* [e] *indicates significance vs. OVX ALN group ($p<0.05$).* [f] *indicates significance vs. OVX RSG 3mg/kg group ($p<0.05$).* [g] *indicates significance vs. OVX RSG 10mg/kg group ($p<0.05$) .* [h] *indicates significance vs. sham controls ($p<0.05$).*

4.7.2 Strut Analysis

Strut analysis was performed on 81 female tibiae samples in order to evaluate the extent of connectivity of trabeculae. The results are displayed in Table 4-13.

The OVX control group demonstrated significantly decreased total strut length, number of nodes, length of node-node struts, length of free-node struts, and number of free ends compared to Sham controls ($p < 0.05$). There were no significant differences between the two Sham groups for any parameters. Following 2-way ANOVA, only ALN had an effect on connectivity parameters ($p<0.05$) with no significant interaction between RSG and ALN. The OVX ALN and OVX RSG 10mg/kg + ALN groups showed significant increases in all of the aforementioned parameters compared to OVX controls, OVX RSG 3mg/kg and OVX RSG 10mg/kg groups ($p < 0.05$), indicating that trabeculae in the ALN groups are more connected than in the RSG-treated groups. The OVX RSG 3mg/kg + ALN group showed significantly increased total strut length, length of free node struts and number of free ends compared to OVX controls, OVX RSG 3mg/kg and OVX RSG 10mg/kg groups ($p < 0.05$). Additionally, the OVX ALN and OVX RSG 3mg/kg + ALN group showed significantly increased length of free free struts compared to OVX controls ($p < 0.05$).

Table 4-13. Strut analysis for all female groups

	Sham		OVX					
Connectivity Parameters	**Control**	**RSG 10mg/kg**	**Control**	**ALN**	**RSG 3mg/kg**	**RSG 3mg/kg + ALN**	**RSG 10mg/kg**	**RSG 10mg/kg + ALN**
Total Strut Length (mm/mm^2)	3.83 ± 0.79	3.83 ± 0.89	**2.52 ± 0.35** [h]	**4.18 ± 1.01** [dfg]	2.65 ± 1.12	**3.54 ± 0.57** [dfg]	2.05 ± 0.48	**3.90 ± 1.31** [dfg]
Number of Nodes (mm^{-2})	8.61 ± 2.82	8.33 ± 2.99	**4.33 ± 0.94** [h]	**9.37 ± 4.05** [dfg]	4.69 ± 4.60	6.28 ± 2.21	2.72 ± 1.04	**8.61 ± 6.19** [dfg]
Length of node-node struts (mm/mm^2)	1.60 ± 0.59	1.66 ± 0.69	**0.63 ± 0.19** [h]	**1.60 ± 0.91** [dfg]	0.71 ± 0.84	0.99 ± 0.40	0.28 ± 0.18	**1.34 ± 1.09** [dfg]
Length of free-node struts (mm/mm^2)	1.12 ± 0.27	1.13 ± 0.25	**0.66 ± 0.17** [h]	**1.26 ± 0.29** [dfg]	0.79 ± 0.50	**1.10 ± 0.23** [dfg]	0.65 ± 0.32	**1.30 ± 0.32** [dfg]
Dis-connectivity Parameters								
Number of free ends (mm^{-2})	8.60 ± 2.33	8.91 ± 0.64	**5.95 ± 1.30** [h]	**11.10 ± 2.21** [dfg]	**7.79 ± 1.28**[d]	**10.28 ± 1.93** [dfg]	6.52 ± 1.30	**10.01 ± 2.00** [dfg]
Length of free-free struts (mm/mm^2)	0.33 ± 0.15	0.32 ± 0.13	0.32 ± 0.19	**0.51 ± 0.23**[d]	0.40 ± 0.20	**0.54 ± 0.15**[d]	0.35 ± 0.15	0.44 ± 0.22

Data are presented as mean ± standard deviation. [d] *indicates significance vs. OVX controls ($p<0.05$).* [e] *indicates significance vs. OVX ALN group ($p<0.05$).* [f] *indicates significance vs. OVX RSG 3mg/kg group ($p<0.05$).* [g] *indicates significance vs. OVX RSG 10mg/kg group ($p<0.05$).* [h] *indicates significance vs. OVX RSG 3mg/kg group ($p<0.05$).* [g] *indicates significance vs. Sham control group ($p<0.05$).*

4.8 The Effect of Rosiglitazone on Bone Remodelling

4.8.1 Static Histomorphometry

Static histomorphometry analysis was completed on 81 female proximal tibiae samples. The results are displayed in Table 4-14.

The Sham control group showed significantly decreased % osteoid volume and OS/BS compared to OVX controls. There were no significant differences between the two Sham groups for any parameters. Following 2-way ANOVA, RSG and ALN had an effect on BV/TV, Tb.N. and Tb.Sp. ($p<0.034$). They both also had an effect on % osteoid volume and OS/BS while only RSG had an effect on eroded surface. Once again, there was no interaction effect between the two drugs. The OVX RSG 3mg/kg and OVX RSG 10mg/kg groups both demonstrated significantly lower % osteoid volume and % osteoid surface/bone surface compared to OVX controls ($p < 0.05$). Additionally, all 3 OVX ALN groups showed decreased % osteoid volume and % osteoid surface/bone surface compared to OVX controls ($p < 0.05$). The OVX RSG 10mg/kg group also had significantly increased % eroded surface (Figure 4-7) compared to OVX controls, OVX ALN and OVX RSG 3mg/kg groups ($p < 0.05$).

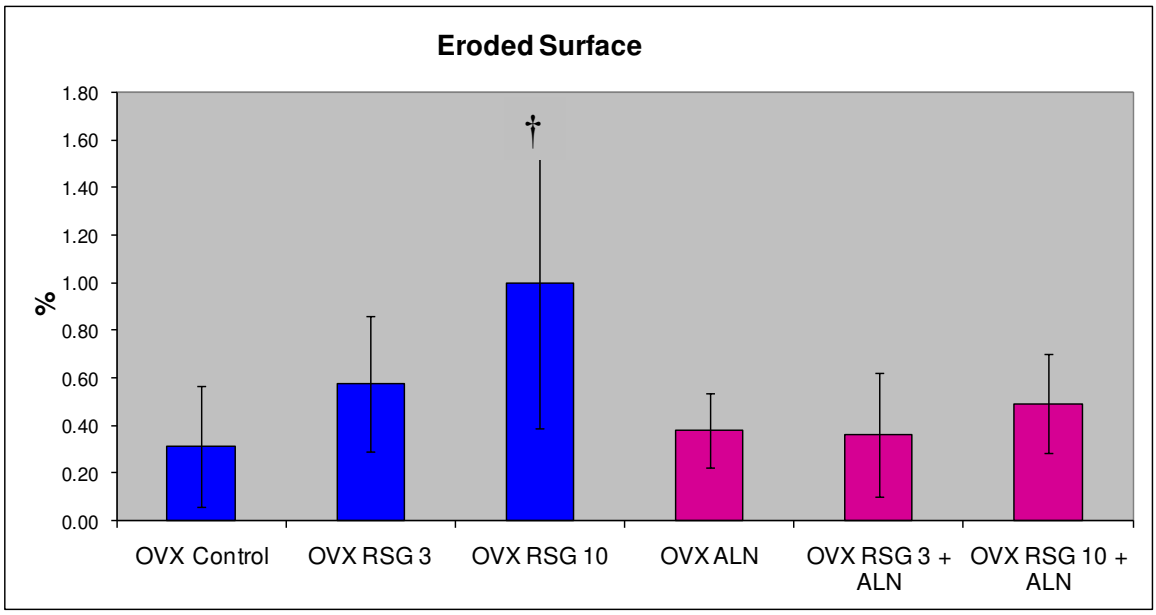

Figure 4-7. Eroded surface for female OVX groups
(† indicates significantly higher than OVX Controls)

Table 4-14. Static histomorphometry for all female groups

	Sham		OVX					
Structural Properties	**Control**	**RSG 10mg/kg**	**Control**	**ALN**	**RSG 3mg/kg**	**RSG 3mg/kg + ALN**	**RSG 10mg/kg**	**RSG 10mg/kg + ALN**
%TBV (%)	**26.19 ± 5.37** [d]	23.21 ± 5.78	**12.86 ± 4.68**[e]	**24.78 ± 4.07** [dfg]	**14.20 ± 6.41** [e]	**23.80 ± 9.14** [dfg]	**8.96 ± 1.98** [e]	**17.31 ± 7.87**[ge]
Tb.Th. (µm)	**68.69 ± 8.41** [h]	58.90 ± 4.70	61.31 ± 9.81	60.18 ± 3.84	57.45 ± 6.04	59.51 ± 16.58	**52.26 ± 6.58** [d]	53.36 ± 9.77
Tb.N. (mm^{-1})	3.80 ± 0.61	3.90 ± 0.75	2.07 ± 0.64	**4.12 ± 0.61** [dfg]	2.41 ± 0.89	**3.94 ± 0.61** [dfg]	1.71 ± 0.31	**3.12 ± 1.03** [dfg]
Tb.Sp. (µm)	**200.87 ± 48.41**[d]	205.56 ± 53.64	468.94 ± 186.61	**187.76 ± 39.00**[d]	409.24 ± 168.51	**199.83 ± 50.20**[d]	**549.64 ± 115.02**[f]	**318.55 ± 196.61**[dg]
Formation Parameters								
%OV (%)	**0.13 ± 0.14** [d]	0.05 ± 0.04	1.41 ± 2.54	**0.06 ± 0.07** [d]	**0.20 ± 0.16** [d]	**0.08 ± 0.17** [d]	**0.49 ± 0.45** [d]	**0.26 ± 0.59** [d]
O.Th. (µm)	7.17 ± 4.69	5.47 ± 3.51	7.65 ± 1.55	8.28 ± 9.52	6.59 ± 4.60	6.14 ± 6.78	7.33 ± 3.10	7.53 ± 6.43
OS/BS (%)	**0.52 ± 0.55** [d]	0.23 ± 0.23	4.70 ± 6.34	**0.11 ± 0.13** [d]	**1.02 ± 0.93** [d]	**0.68 ± 0.99** [d]	**1.73 ± 1.61** [d]	**0.78 ± 1.88** [d]
Resorption								
ES (%)	0.30 ± 0.22	0.51 ± 0.35	0.31 ± 0.25	0.38 ± 0.15	0.57 ± 0.28	0.36 ± 0.26	**1.00 ± 0.61** [d e f]	0.49 ± 0.21

Data are presented as mean ± standard deviation. [d] *indicates significance vs. OVX controls (p<0.05).* [e] *indicates significance vs. OVX ALN group (p<0.05).* [f] *indicates significance vs. OVX RSG 3mg/kg group (p<0.05).* [g] *indicates significance vs. OVX RSG 10mg/kg group (p<0.05).*

4.8.2 Dynamic Histomorphometry

Dynamic histomorphometry was completed on 81 female proximal tibiae samples. The results are displayed in Table 4-15. The formation parameters that were analyzed are mineralizing surface (%), mineral apposition rate (mcm/day) and bone formation rate (mcm/day). Due to ALN treatment, it was not possible to see any fluorescent labeling in any of the 3 OVX ALN groups, and so these groups could not be analyzed.

OVX controls showed significantly increased % mineralized surface compared to Sham controls ($p < 0.05$). The OVX RSG 3mg/kg and 10mg/kg groups both showed significantly decreased mineralized surface (%) compared to OVX controls ($p < 0.05$). These 2 groups also demonstrated significantly slower bone formation rate (Figure 4-8) compared to OVX controls ($p < 0.05$).

Table 4-15. Dynamic histomorphometry for all female groups

Formation Parameters	Sham Control	Sham RSG 10mg/kg	OVX Control	OVX RSG 3mg/kg	OVX RSG 10mg/kg
Mineralizing Surface (%)	8.07 ± 4.33	**6.59 ± 1.01** [d]	**13.15 ± 6.28** [h]	**7.14 ± 1.84** [d]	**6.83 ± 4.09** [d]
Mineral Apposition Rate (mcm/day)	1.40 ± 0.26	1.37 ± 0.14	1.32 ± 0.26	1.21 ± 0.15	1.05 ± 0.44
Bone Formation Rate (mcm/day)	0.12 ± 0.09	**0.09 ± 0.02** [d]	0.18 ± 0.10	**0.09 ± 0.02**[d]	**0.08 ± 0.06**[d]

Data are presented as mean ± standard deviation. [d] *indicates significance vs. OVX controls ($p<0.05$).* [e] *indicates significance vs. OVX ALN group ($p<0.05$).* [f] *indicates significance vs. OVX RSG 3mg/kg group ($p<0.05$).* [h] *indicates significance vs. Sham control group ($p<0.05$).*

4.9 Female Results Summary

All rats gained weight throughout the treatment period regardless of administration of RSG or ALN. Both Sham groups (Control and RSG 10mg/kg) showed a decrease in blood glucose as the treatment period progressed. For the OVX groups, only the RSG 3mg/kg and RSG 10mg/kg groups demonstrated a decrease in blood glucose throughout the treatment period. The Sham Control group was the only group that demonstrated an increase in blood serum triglycerides at termination of the experiment and the OVX controls demonstrated a significant increase in serum insulin at termination compared to baseline.

The OVX control and OVX RSG 10mg/kg groups exhibited decreased femoral and vertebral areal BMD and BMC compared to both Sham groups suggesting that OVX has a negative effect on bone mass. The OVX RSG 10mg/kg group demonstrated significantly lower areal femoral and vertebral BMD than OVX controls suggesting that RSG treatment may influence bone mass in both cortical and trabecular bone. All three OVX ALN groups exhibited increased areal femoral BMD and BMC as well as vertebral BMD which indicates that ALN may prevent the loss of bone mass.

There were no significant differences in bone geometrical properties following RSG treatment. Some parameters (medial/lateral diameter, polar moment of inertia, cross-sectional area, and moment of area) did decrease in the OVX groups following RSG treatment however, these findings were not statistically significant. The OVX RSG 3mg/kg + ALN group demonstrated significantly higher cross-sectional area than the OVX RSG 3mg/kg and OVX RSG 10mg/kg groups. RSG treatment in OVX rats resulted in a significant increase in total porosity compared to OVX controls. This increased porosity may be contributing to some of the decreased

structural and material properties that were observed in cortical bone following mechanical testing.

The OVX RSG 10mg/kg group demonstrated decreases in the unnormalized and normalized mechanical properties (failure torque, stiffness, shear stress) of cortical bone suggesting a decrease in bone strength compared to OVX controls. RSG treatment in OVX rats also resulted in decreased mechanical properties of trabecular bone (ultimate load, failure load) compared to OVX Controls.

ALN treatment resulted in increases in some unnormalized mechanical properties (ultimate load, stiffness, failure torque) and normalized mechanical properties (ultimate stress, failure stress) of cortical bone compared to OVX controls. OVX groups treated with both RSG and ALN exhibited decreases in some cortical bone parameters (shear stress, shear modulus) when compared to OVX Controls or OVX ALN rats suggesting that RSG may still result in decreased bone strength in these groups. The OVX RSG 10 + ALN group showed increases in trabecular bone mechanical properties (ultimate load, energy to failure, stiffness) compared to OVX controls as well as OVX RSG 10 rats.

RSG and ALN treatment did not appear to have a significant effect on bone mineralization in the female rat model (Sham and OVX). OVX did result in decreased connectivity as assessed by strut analysis with ALN treatment causing an increase in these parameters. RSG treatment did appear to decrease some bone formation parameters while also significantly increasing eroded surface, a marker for bone resorption. ALN treatment caused an even more significant decrease in bone formation parameters as assessed by static histomorphometry. This is expected

following chronic administration of ALN. In addition to its anti-resorptive capabilities, ALN slows the entire bone remodeling process which could indirectly result in decreased bone formation.

Chapter 5: Discussion

5.1 Introduction

This study sought to evaluate the effects of RSG on bone loss and bone quality in a male rat model of insulin resistance as well as in an ovariectomized female rat model of post-menopausal osteoporosis combined with insulin resistance. The study also focused on examining the combined effects of RSG and a bisphosphonate, ALN, in the male and female rat model. Measurements of bone density, structural and mechanical properties, bone remodeling and mineralization were used to evaluate bone quality.

We found that RSG treatment resulted in cortical and trabecular bone loss in the female OVX model. Congruent with this bone loss were decreased mechanical properties in both cortical and trabecular bone following RSG treatment. Lastly, RSG treatment appeared to cause decreased bone formation as well as large increases in bone resorption suggesting a possible mechanism by which RSG induces bone loss and leads to inferior bone quality in our OVX female model. ALN appeared to prevent the bone loss caused by RSG and partially prevented decreases in mechanical strength of cortical and trabecular bone in the male and female model. This result is expected of ALN's anti-resorptive capabilities. Additional studies should be conducted to further analyze the resorptive effect of RSG on the skeleton.

5.2 Current T2DM Treatments

The detrimental effect of Type 1 diabetes on bone quality is widely accepted, however, there is also emerging data suggesting an increased fracture risk associated with T2DM as well (Rosen, 2008). Currently, there are various treatments available to help control the symptoms of T2DM. At the earliest stage, diet and exercise can be very effective at controlling as well as reversing the effects of the disease (Knowler, 2002). If diet and exercise are insufficient, oral therapeutic treatments become necessary. The biguanide class of drugs are the first line of defense for T2DM treatment. Metformin belongs to this drug class and is the most commonly prescribed treatment. It acts by improving hyperglycemia through the suppression of glucose production by liver cells (Holman, 1988). It also increases insulin sensitivity, peripheral glucose uptake and the oxidation of fatty acids (Bailey, 1996). Metformin is also prescribed in combination with rosiglitazone in order to actively reduce insulin resistance (Fonseca, 2000).

Sulfonylureas are another class of oral anti-diabetic drugs used specifically to treat T2DM. These drugs act by facilitating the release of insulin from the pancreatic beta cells through interaction with the beta cell membrane itself. In addition to their effects on insulin release, sulfonylureas can also sensitize the beta cells of the pancrease to glucose and inhibit hepatic glucose production (Bailey, 1996).

Rosiglitazone (RSG) is an insulin-sensitizing drug used to treat patients with T2DM to improve glycemic control. RSG is a member of the thiazolidinedione (TZD) class of drugs and is an agonist for the peroxisome proliferator-activated receptor isoform γ (PPARγ). PPAR γ is a member of the nuclear receptor family of transcription factors (Mayerson, A.B. et al, 2002).

Activation of this receptor by RSG allows for the regulation of insulin-responsive genes (Rzonca, S.O. et al., 2005).

5.3 Skeletal Effects of RSG

While TZDs like RSG are a commonly prescribed treatment for T2DM patients, there are conflicting studies regarding the influence of RSG on bone quality. Some *in vitro* studies suggest that RSG acts by decreasing bone formation. Adipocytes and osteoblasts share a common mesenchymal precursor cell. PPAR-γ is a known positive adipocyte differentiation regulator (Takada and Kato, 2007) so activation of PPAR-γ by RSG could reduce bone formation through inhibition of the osteoblastogenesis pathway. Conversely, *in vivo* studies have shown that PPAR-γ may affect osteoclast differentiation (Wan et al., 2007). Osteoclasts are derived from hematopoietic stem cells. Previous studies suspect that the effect of PPAR-γ activation is specific to osteoclast genes that function along the osteoclast differentiation pathway. This suggests that RSG binding to PPAR-γ may promote osteoclastogenesis, subsequently influencing bone resorption, as well as formation.

5.4 The Effect of RSG on Cortical Bone in the ZF Rat

In the female OVX model, both cortical BMD and BMC were decreased following RSG treatment. Cortical BMD and BMC were not affected in the male model. Cortical bone is more dense and compact and thus, less susceptible to potential increases in bone turnover (Cowin, 2001). In the females, it is possible that the combination of OVX and RSG treatment allowed for both cortical and trabecular bone to be affected. Similarly, Sottile et al (2004) performed a study with OVX estrogen-deprived female Wistar rats and saw enhanced bone loss with RSG treatment in tibia, femur and lumbar spine. ALN treatment resulted in increased cortical BMD suggesting that ALN may prevent the loss of bone mass associated with RSG treatment.

ALN treatment caused an increase in cortical thickness in female OVX rats whereas RSG did not have an effect on any geometrical parameters of cortical bone. The female OVX model, however, did show increased cortical bone porosity with RSG treatment. Total porosity was increased by more than 100% in the OVX RSG 10mg/kg treated group compared to OVX controls. Total porosity was also increased in the male RSG-treated groups but not to levels that were significant. This cortical bone porosity is especially important as even small increases in porosity can decrease bone strength substantially (Turner, 2002) and increased cortical bone porosity is not usually seen in OVX rats. Important to note is that most of the porosity was located close to the endosteal surface of the femur which is the surface closest to the bone marrow. This raises an interesting possibility that adipokines secreted by the fat cells in the bone marrow could be affecting either formation or resorption of the cortical bone adjacent to it. ALN treatment resulted in significantly decreased porosity in both the male and female model, which is expected of its anti-resorptive capabilities.

Following mechanical testing, RSG treatment resulted in decreased structural and material properties of cortical bone (failure torque, stiffness, shear stress and modulus) in the female OVX model. These decreases are congruent with the decreased areal BMD and the significantly increased cortical bone porosity which is known to decrease bone strength (Turner, 2002). While ALN treatment did allow for increases in these parameters, they did not improve to the levels seen in OVX controls suggesting that ALN treatment does not completely prevent the decrease in material parameters seen with RSG treatment. It would be useful to explore higher doses of ALN to determine if material properties would increase. These findings, along with the porosity results are important within the scope of this study as previous studies have

demonstrated an increased incidence of limb fractures in T2DM women being treated with RSG. Also, the influence of ALN on cortical bone and the effect of RSG on cortical porosity add to our hypothesis that RSG is influencing bone resorption in addition to bone formation in the female OVX model.

Important to note is that most of the significance observed was seen in rats dosed with 10mg/kg RSG, suggesting a dose-dependent effect of RSG in our rat model. There were some significant results seen with the RSG 3mg/kg groups however, these results were sporadic among different tests and inconsistent among parameters within a test. While previous studies have shown that RSG given at doses of 3mg/kg and 10mg/kg to obese rats was sufficient to lower blood glucose, insulin, free fatty acids and triglycerides (Pickavance et al., 1999), we mostly saw bone quality differences in rats treated with RSG 10mg/kg.

5.5 The Effect of RSG on Trabecular Bone in the ZF rat

RSG appeared to have an effect on trabecular BMD and BMC in both the male and female ZF rat model where both BMD and BMC were decreased following RSG treatment. It is possible that only trabecular bone was affected in males due to trabecular bone's increased susceptibility to bone turnover due to greater bone surface area. Soronceanu et al (2004) also observed decreased vertebral BMD and lower trabecular bone volume following RSG treatment in mice. ALN treatment resulted in increased BMD and BMC trabecular bone suggesting that ALN may prevent the loss of bone mass associated with RSG treatment.

RSG also appeared to have an effect on bone architecture and volumetric density. In the male ZF and female OVX ZF rat models, trabecular architecture was negatively affected by RSG treatment. Recently, Ma et al (2010) also demonstrated decreased BV/TV, Tb.N. and Tb.Th. in

OVX spontaneous hypertensive rats treated with RSG. Similar to our study, these trabecular architecture results corresponded to decreased BMD. Vertebral volumetric BMD was also affected by RSG treatment in our female OVX model. ALN treatment prevented the effects of RSG in both males and females which we expected.

The female OVX model also demonstrated decreases in structural and material properties of trabecular bone (ultimate load, ultimate stress and energy to failure) as a result of RSG treatment. Lazarenco et al (2007) similarily observed decreased vertebral bone strength in an aged rat model treated with RSG which correlated with decreased trabecular BMD. In our study, ALN treatment did cause increases in ultimate load and ultimate stress but only to levels that were significantly higher than groups treated with RSG, not to levels significantly higher than female OVX controls. We speculate that RSG is causing decreased strength and increased brittleness in trabecular bone of the female OVX model resulting in an increased susceptibility to fracture.

No significant differences in bone formation or resorption parameters were observed in the male ZF rats following static or dynamic histomorphometry. There were also no changes in trabecular connectivity parameters following histomorphometry in the males which made it difficult to confirm the connectivity changes that were observed following MicroCT analysis. This may suggest a limitation of the histomorphometry technique as it measures connectivity parameters in 2 dimensions as opposed to MicroCT which provides a 3-dimensional measurement. Histomophometry analysis revealed decreases in bone formation parameters (% OV, %OS/BS, bone formation rate) of trabecular bone in the female OVX model following RSG administration. ALN treatment resulted in decreased bone formation parameters as well. Since

ALN slows down bone resorption, which is closely coupled with bone formation, it is expected that ALN treatment would decrease bone formation following long term use (Graham, 2007). Eroded surface was also significantly increased following RSG 10mg/kg treatment in the female OVX model suggesting an increase in bone resorption. These results suggest that bone formation and bone resorption are both being affected by RSG treatment in our female OVX model. This, along with ALN's ability to prevent losses of trabecular architecture and bone mass in males and females leads us to suspect that RSG may be strongly influencing bone resorption in our rat model.

5.6 Possible Mechanisms of Action for RSG

There has been much debate over the mechanism by which RSG leads to bone loss and inferior bone quality. Some studies have shown that decreased bone formation is to blame whereas others suggest that an excess of bone resorption causes bone loss and increased fracture risk following RSG treatment. A combination of *in vitro* and *in vivo* analysis has been performed in an attempt to answer this question.

Rzonca et al (2004) showed evidence to support the hypothesis that activation of PPARγ by RSG causes the preferential differentiation of mesenchymal cells into adipocytes at the expense of osteoblasts therefore decreasing bone formation and leading to bone loss. This study used an *in vivo* model consisting of non-diabetic B6 mice dosed with RSG 20µg/g·d, to show significantly decreased BMD and trabecular structural properties following RSG administration. Histomorphometry also showed a decrease in bone formation with simultaneous increase in fat content, thus supporting the argument for decreased osteoblast differentiation following RSG treatment. Similarly, Soronceanu et al (2004) found that activation of PPARγ by RSG in mice

(RSG 3mg/kg/day) had lower vertebral BMD and lower trabecular bone volume, however, this study revealed no change in bone marrow adiposity. They did see decreased osteoblast number and activity that the authors attributed to increased apoptotic death of osteoblasts and osteocytes. Ali et al (2002) also based their study on the concept of the common mesenchymal precursor that is shared by adipocytes and osteoblasts. Their previous *in vitro* studies showed decreased osteoblastogenesis following activation of PPARγ by RSG. In their *in vivo* study using Swiss-Webster mice, they saw that RSG (given at a dose of 25 μg/g·d) caused bone loss and increased adipogenesis as well as a decreased ratio of osteoblasts to osteoclasts and a reduction in bone formation rate compared to controls leading to their conclusion that RSG attenuates osteoblast differentiation. Lazarenco et al (2007) identified PPARγ as both a regulator of glucose metabolism and bone mass. Similar to our project, this study used an aged model to assess the skeletal effects of RSG. In both adult and aged C57BL/6 mice, bone volume was significantly decreased by RSG (at a dose of 0.14mg/g chow). In adult animals, bone loss correlated with attenuated bone formation, whereas in aged animals, bone loss was associated with increased osteoclastogenesis, mediated by increased RANKL expression. This is an important finding in the scope of our study which seeks to explain the effects of RSG in an aged rat model of osteoporosis. Our study supports many of these previous findings as we similarily observed decreased bone mass, increased marrow adiposity and decreased bone formation in our female OVX ZF rat model, indicating that bone formation is being affected by RSG treatment.

Enhanced osteoclast differentiation could be another mechanism by which TZDs contribute to bone loss. A study by Wan et al (2007) supports the hypothesis that RSG activation of PPARγ causes an increase in bone resorption. This study discovered a pro-osteoclastogenic effect of PPARγ using a TieCre/flox mouse model where PPARγ was deleted in osteoclasts but not in

osteoblasts and showed that these mice developed osteoporosis. They found that activating PPARγ with RSG further exacerbated osteoclast differentiation and this effect was dependent on the PPARγ receptor. They could verify that these effects were due to osteoclasts because PPARγ was not deleted in the mesenchymal lineages that give way to osteoblasts. They found that decreased osteoclast number in their PPARγ -negative mutant was not due to lack of progenitor cells but was due to defects in the RANKL signalling pathways which mediates osteoclast differentiation. Sottile et al (2004) also found evidence supporting increased osteoclastogenesis and they did so using Wistar rats. This study reported both an increase in marrow adipogenesis and increased bone resorption on Wistar rats after activation of PPAR with RSG (at a dose of 10mg/kg). They also did a study with OVX estrogen-deprived Wistar rats and saw enhanced bone loss in tibia, femur and lumbar spine with RSG treatment and increased fat marrow volume compared to OVX controls. They also observed increased bone resorption parameters in the RSG treatment group whereas osteoblast number was comparable to controls. Giaginis et al (2007) also demonstrated a decrease in bone formation and increased osteoclast formation in OVX Wistar rats whereas they saw no change in intact rats following RSG administration (at doses of 5, 10 and 20 μg/g b.w./day). Our study also supports these findings as we observed increased eroded surface, increased cortical porosity and the ability of estrogen and ALN to protect against the negative effects of RSG on the skeleton, indicating that bone resorption is being affected by RSG treatment as well.

Only the study by Ma et al (2010), however, has used a model of obesity and insulin resistance in combination with OVX. This is especially relevant since in the ADOPT clinical trial, increased limb fractures were reported specifically in women with T2DM and many women treated with RSG are post-menopausal. The aforementioned studies also did not evaluate the

mechanical integrity of bone nor did they administer bisphosphonates (commonly prescribed treatment for osteoporosis) in conjunction with RSG. Using alendronate in combination with RSG not only allows us to examine a possible counter measure to the deleterious effects of RSG on the skeleton but also provides insight into the mechanism by which RSG is inducing bone loss in this in vivo system. We have observed the ability of ALN to alleviate the effects of RSG in both the male and female model *in vivo*. Since ALN is known to enhance the mechanical strength of bone through decreasing resorption and increasing mineralization, we suggest that RSG's seemingly detrimental effect on bone may be due to excess resorption in addition to decreased formation.

5.7 The Protective Effects of Estrogen and Alendronate on RSG Treated Bone

It appears that both estrogen and Alendronate provide protective effects against RSG on the skeleton. For many parameters of both cortical and trabecular bone, OVX female rats showed decreases compared to Sham females suggesting a positive effect of estrogen on the skeleton. For the male and female study, ALN treatment also had a positive effect on both cortical bone and trabecular bone, with the exception of female torsion testing. The loss of estrogen leads to increases in cytokines such as IL-1, IL-6 and TNF (Shevde, 2000). Increases in these cytokines are known to stimulate osteoclastogenesis causing an increase in bone resorption (Roodman, 1999). The reduction of estrogen following OVX results in the aforementioned effect through removal of the inhibitory effect that estrogen normally exerts on RANKL induced osteoclastogenesis (Shevde, 2000). The fact that estrogen protects against the negative effects of RSG on bone suggests a potential mechanism by which RSG leads to bone loss. RSG activation of PPARγ may be interfering with RANKL resulting in increased osteoclastogenesis and increased bone resorption.

ALN, as previously mentioned, inhibits resoprtion thus resulting in increased bone mass and strength. The fact that even with the removal of estrogen, ALN is largely able to protect bone against the negative effects of RSG once again suggests that RSG is having an effect on bone resorption. Following our 2-way ANOVA statistical analysis for the female OVX study we found no interaction effect between RSG and ALN. For example, following torsion testing, failure torque decreased with increasing RSG dose. While ALN did cause increased values for failure torque, this parameter still decreased with increasing RSG dose even in the presence of ALN. The data for many parameters appeared as in Figure 5-1.

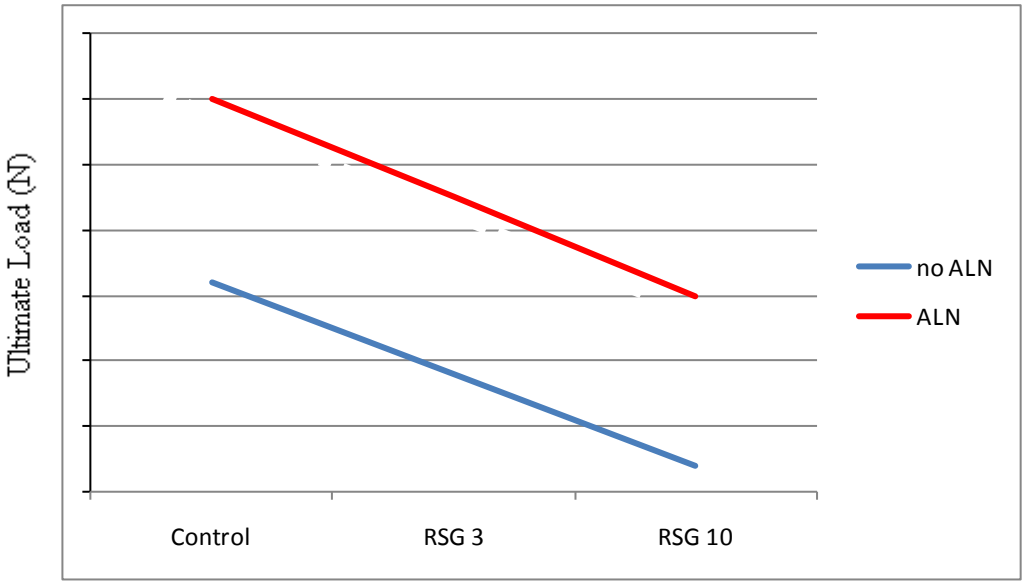

Figure 5-1. Schematic diagram showing pattern for RSG and ALN data

Figure 5-1 shows that RSG is having an effect on the parameter in question (eg. ultimate load) and ALN is having an effect as well. Both parameters are showing a similar effect and thus, there is no interaction between the two. So, ALN does protect against the effects of OVX . ALN does not completely protect against the effects of RSG on the skeleton, as this protection is less effective as RSG dose increases.

5.8 Blood Biochemistry and Bone Markers in the ZF Rat

Male and female RSG treated rats demonstrated lower levels of blood serum glucose as the treatment period progressed. RSG treatment also appeared to maintain serum cholesterol and triglyceride levels in males and females throughout the experiment, which is expected of the drug (Mayerson et al., 2002). Insulin levels were maintained in all RSG treated male and female groups throughout the experiment whereas OVX controls showed increased insulin levels at termination. Since RSG should combat insulin resistance (Rzonca et al., 2009), we would expect to see controlled insulin levels in our RSG-treated rats. Male RSG treated rats showed increased adiponectin results compared to male controls at experiment termination. We would expect that RSG treated rats would show increased levels of adiponectin since serum levels of adiponectin should correlate with systemic insulin sensitivity (Yang, W.S. et al., 2002). No differences in leptin were seen between any of the male or female groups at experiment termination. Previous findings on the effects of RSG on leptin are inconclusive with some studies showing decreased leptin with TZD treatment and some showing no change (Mayerson et al., 2002).

The bone marker results were less conclusive. Osteocalcin levels decreased in RSG treated rats as treatment progressed, however, osteocalcin decreased in OVX control rats as well. Previous studies have shown a reduction in serum osteocalcin following RSG treatment in post-menopausal women (Grey, et al., 2007). Osteocalcin is a marker of bone formation. Osteocalcin was reduced at termination in two of the ALN treated groups as well. While ALN is an inhibitor of bone resorption, bone formation may be indirectly reduced following chronic usage (12 weeks) due to reduced bone remodelling rate. The results of our study would then suggest that RSG is negatively affecting bone remodeling in our ZF rat model. However, the decreased osteocalcin in control rats suggests that this test may not be reliable. It is possible that the extent

of obesity in these ZF rats affected the bone marker results. Lipemia and hemolysis are known to falsely decrease osteocalcin results (Grey, 2008). It is reduced in lipemic serum because osteocalcin can bind to lipids in the serum (Watts, 1999) which could explain why it was reduced in female controls as well. Rats were not fasted prior to blood serum testing however, food intake is not known to have an effect on osteoclacin (Grey, 2008).

Serum CTX, a by-product of collagen breakdown and a marker of bone resorption (Grey et al., 2008) was significantly increased at experiment termination in RSG treated rats but also in female sham controls. This could indicate that RSG is facilitating bone resorption. ALN treated rats, however, also showed increased serum CTX whereas we would expect lower CTX since ALN is known to prevent the loss of bone mass through decreasing bone resorption. It is possible that the serum test that was performed was not adequate for the assessment of CTX and should not necessarily be trusted. As mentioned previsouly, rats were not fasted prior to blood serum testing. Fasting is a requirement for testing serum CTX (Grey, 2008) and could explain the questionable results. Previous studies have also shown that serum CTX increases with increased weight (Villareal, 2008) and that other bone resorption markers increase after menopause (Watts, 1999). Similarily, Anderson et al (2003) found that OVX treatment in rats caused an increase in serum CTX and Mollard et al (2004) saw no changes in serum CTX in ZF rats compared to healthy controls indicating that the marker is not sensitive enough to detect resorption rates in this ZF model. These two factors could have caused the increased CTX readings in the 3 ALN groups which is an unexpected result. Lastly, there is a known diurnal variation for serum CTX and other bone resorption markers of up to 20% (Watts, 1999) which could have affected our results. Other markers for bone resorption include the TRAP enzyme as well as serum NTX.

Taken together, these results suggest that using osteocalcin and serum CTX as markers for bone turnover may not provide adequate assessments of bone formation and resorption in our ZF rat model. In our study, these markers did not provide an accurate prediction of fracture risk and conflicted with the results from assessments of bone architecture, mechanical strength and remodelling. In the future, blood serum testing should be more standardized in order to eliminate any factors that could skew results. Rats should be fasted prior to testing and sampling should be performed at the same time of day for each test. Urine testing, as opposed to blood testing could be used for serum CTX as some studies have shown this to be more effective (Watts, 1999). This, however, was not feasible in our study.

5.9 Methodological Concerns

RSG Dosage

Some of the parameters from tests performed in this study had very large standard deviations. One possible explanation lies in the administration of RSG to the rats. As mentioned in the methods section, RSG was administered orally via 1mL pieces of Jello. RSG powder was dissolved in warm Jello and vortexed to dissolve. However, the amounts of RSG that we were using were not completely soluble in water at lower temperatures and using higher temperatures or boiling water could have negatively affected the properties of the drug (Glaxo Smith Kline). We were confident that each stock solution contained the correct RSG concentration but it is possible that the concentration in each 1ml piece of Jello varied very slightly from one piece to the next. This slight variation in concentration could have influenced the large standard deviations observed within some of the groups. This could be improved by administering RSG to the rats by gavage.

Male Project Design

Unfortunately, for the male study, there was no group that was treated with ALN by itself. It would have been ideal to have a male ALN group which would have been the proper control for the male RSG 10 + ALN group. The addition of an ALN control group would have given us greater insight into the protective effect that ALN has on RSG treated bones in the male study.

DEXA

DEXA is a 2-dimensional analysis of bone mineral density. While it is the current "gold standard" for this type of analysis in clinical practice, it is not necessarily the best determinant of fracture risk as it is a density measurement based on bone area and not bone volume. All of the other factors that influence bone quality need to be taken into account for an adequate assessment of fracture risk. MicroCT analysis provides a more accurate assessment of BMD as it is a 3-dimensional measurement (Bagi, 2005).

Mechanical Testing

While care is taken to ensure consistency of techniques throughout mechanical testing, there are various factors that can affect the results from these tests. Specimen storage and preparation are of upmost importance. Factors such as specimen preservation, hydration and temperature can all effect results from mechanical testing (Turner, 1993). If bone dries out, strength has been shown to increase while toughness decreases (Evans 1973). For this reason, it is important to keep specimens hydrated with saline, however, bone are removed from their saline soaked gauze immediately prior to testing. While this minimizes the effects of drying, this may also slightly affect results. The temperature at which specimens are tested is also important. Ideally, bones should be tested at physiological body temperature (37°C). However, bones for this study were

all tested at room temperature which could also affect results as it has been shown that testing at room temperature increases Young's Modulus (Ashman, 1982).

Most importantly, care should be taken to ensure that bones are stored, hydrated and tested in the same conditions every time. This will minimize the effects of the aforementioned factors that may affect mechanical properties. It should be kept in mind that results from these tests are relative and not necessarily absolute.

Histomorphometry

Static and dynamic histomorphometry are 2-dimentional analyses of trabecular connectivity. It is difficult to ensure that the depth within the bone at which the 2D sample is taken is consistent from sample to sample. Static histomorphometry also allows for possible human error throughout the process of staining, cover slipping and analyzing each individual slide. These errors could explain the lack of congruity between MicroCT and static histomorphometry results. Studies have shown that 3-dimensional MicroCT measurements of trabecular architecture do not always correlate with results from 2-dimensional histomorphometry (Ito, 1998).

5.10 Conclusions

1. RSG treatment differentially affects male, female and female OVX rats.
2. RSG treatment causes decreased bone mass, trabecular bone connectivity and structural and material properties in OVX female ZF rats.
3. ALN treatment prevents the loss of bone mass, structural and material properties as well as bone connectivity parameters in OVX female ZF rats. However, ALN does not always increase these parameters to levels seen in OVX control rats.
4. RSG treatment caused significantly increased long bone porosity in the OVX ZF model indicating that RSG may increase the likelihood of limb fractures in post-menopausal women.
5. RSG treatment may be influencing bone resorption as well as bone formation, with cortical bone being especially affected in our ZF rat model.

5.11 Future Work

In order to further examine the effect of RSG on bone resorption, Tartrate-resistant Acidic Phosphatase (TRAP) staining should be performed on proximal tibia samples to quantify osteoclasts in the male and female models. Osteoclasts stain positive for the TRAP enzyme, providing an indication of bone resorption. Another way to analyze bone resorption involves the use of dentin slices. Osteoclasts can be extracted from the Zucker rats and placed on slides containing bone (dentin) slices with or without RSG. The activity of the osteoclasts can then be assessed based on how much dentin in resorbed.

It would also be useful to perform a recovery experiment in addition to the 12 week RSG treatement experiments. It is possible that the skeletal effects of RSG are diminished after cessation of administration so it would be useful to explore this possibility. The duration of dose treatment could be crucial for evaluating the effects of TZDs on bone (Giaginis, 2007).

References

Ali A, Weinstein RS, Stewart SA, Parfitt AM, Manolagas SC, Jilka RL. Rosiglitazone Causes Bone Loss in Mice by Suppression Osteoblast Differentiation and Bone Formation. *Endocrinology* 2005; 146: 1226-1235.

An YH, Martin KL. Handbook of Histology Methods for Bone and Cartilage. Humana Press Inc., 2003.

Azuma, Y, Sato H, Oue Y, Okabe K, Ohta T, Tsuchimoto M, Kiyoki M. Alendronate distributed on bone surfaces inhibits osteoclastic bone resorption in vitro and in experimental hypercalcemia models. *Bone* 1995;16: 235 – 45.

Bagi CM, Hanson N, Andresen C, Pero R, Lariviere R, Turner CH, Laib A. The use of micro-CT to evaluate cortical bone geometry and strength in nude rats: Correlation with mechanical testing, pQCT and DXA. *Bone* 2006; 38: 136 – 44.

Bailey CJ and Turner RC. Metformin. *New England Journal of Medicine* 1996; 334: 574 – 9.

Bray GA. The Zucker-fatty rat: a review. *Federation Proceedings* 1977; 36: 148 – 53.

Carruthers M, Trinick TR, Jankowska E, Traish AM. Are the adverse effects of glitazones linked to induced testosterone deficiency? *Cardiovascular Diabetology* 2008; 15: 30.

Chachra D, Kasra M, Vanin CM, MacLusky NJ, Casper RF, Grynpas MD. Hormone replacement therapy regimens and rat vertebral biomechanics. *Calcified Tissue International* 1995; 56: 130 – 4.

Cheng AYY, Fantus IG. Oral antihyperglycemic therapy for type 2 diabetes mellitus. *Canadian Medical Association Journal* 2005; 172: 213 – 26.

Cornish J, Costa JL, Naot D. The Bone-fat mass relationship: laboratory studies. *International Bone and Mineral Society* 2009; 6: 311 – 22.

Cowin, S.C. Bone Biomechanics Handbook. CRC Press., (2001).

Cummings, S.R. et al. Improvement in Spine Bone Density and Reduction in Risk of Vertebral Fractures During Treatment with Antiresorptive Drugs. *American Journal of Medicine* 2002; 112: 281 – 89.

Epstein FH. Bone marrow, cytokines and bone remodeling. *Mechanisms of Disease* 1995; 332: 305 – 11.

Eriksen EF, Hodgson SF, Eastell R, Riggs BL, Cedel SL, O'Fallon WM. Cancellous bone remodeling in type i (postmenopausal) osteoporosis: Quantitative assessment of rates of

formation, resorption, and bone loss at tissue and cellular levels. *Journal of Bone and Mineral Research* 1990; 5: 311 – 19 .

Giaginis C, Tsantili-Kakoulidou A, Theocharis S. Peroxisome proliferator-activated receptors (PPARs) in the control of bone metabolism. *Fundamental and Clinical Pharmacology* 2007; 21: 231 – 44.

Giustina A, Mazzioti G, Canalis E. Growth hormone, insulin-like growth factors and the skeleton. *Endocrinology Review* 2008; 29: 535 – 59.

Graham R, Russell G. Bisphosphonates: Mode of action and pharmacology. *Pediatrics* 2007; 119: S150 – S162.

Green S and Shambon P. Nuclear receptors enhance our understanding of transcription regulation. *Trends in Genetics* 1988;4: 309 – 14.

Grey A. The Peroxisome Proliferator-Activated Receptor-γ Agonist Rosiglitazone Decreases Bone Formation and Bone Mineral Density in Healthy Postmenopausal Women: A Randomized, Controlled Trial. *Journal of Clinical Endocrinology & Metabolism* 2007; 92: 1305 – 10.

Grey A. Skeletal consequences of thiazolidinedione therapy. *Osteoporosis International* 2008; 19: 129 – 37.

Grigoriadis AE, Wang ZQ, Cecchini MG, Hofstetter W, Felix R, Fleisch HA, Wagner EF. C-Fos: a key regulator of osteoclast-macrophage lineage determination and bone remodeling. *Science* 1994; 266: 443 – 8.

Grynpas MD, Chachra D, Lundon K. Bone quality in animal models of osteoporosis. *Drug Development Research* 2000; 49: 146 – 58.

Hampson G, Evans C, Petitt RJ, Evans WD, Woodhead SJ, Peters JR, Ralston SH. Bone mineral density, collagen type 1 α 1 genotypes and bone turnover in premenopausal women with diabetes mellitus. *Diabetologia* 1998; 41: 1314 – 20.

Hamrick MW, Ferrari SL. Leptin and the sympathetic connection of fat to bone. *Osteoporosis International* 2008; 19: 905 – 12.

Heaney RP. Is there a role for bone quality in fragility fractures? *Calcified Tissue International* 1993; 53: S3 – S6.

Hill PA. Bone remodelling. *British Journal of Orthodontics* 1998; 25: 101 – 7.

Høegh-Andersen P, Tanko LB, Andersen TL, Lundberg CV, Mo JA, Heegaard AM, Delaisse JM, Christgau S. Ovariectomized rats as a model of postmenopausal osteoarthritis: validation and application. *Arthritis Research and Therapy* 2004: 6: 169 – 80.

Hofbauer LC, Brueck CC, Singh SK, Dobnig H. Osteoporosis in patients with diabetes mellitus. *Journal of Bone and Mineral Research* 2007; 22: 1317 – 28.

Holmes C, Khan TS, Owen C, Ciliberti N, Grynpas MD, Stanford WL. Longitudinal analysis of mesenchymal progenitors and bone quality in the stem cell antigen-1-null osteoporotic mouse. *Journal of Bone and Mineral Research* 2007; 22:1373 – 86.

Ionova-Martin SS, Do SH, Barth HD, Szadkowska M, Porter AE, Ager III JW, Ager Jr. JW, Alliston T, Vaisse C, Ritchie RO.. Reduced size-independent mechanical properties of cortical bone in high-fat diet-induced obesity. *Bone* 2010; 46: 217 – 25.

Ito M, Nakamure T, Matsumoto T, Tsurusaki K, Hayashi K. Analysis of trabecular microarchitecture of human iliac bone using microcomputed tomography in patients with hip arthrosis with or without vertebral fracture. *Bone* 1998; 23: 163 – 69.

Iwaniec UT and Turner RT. Animal models for osteoporosis. In: Marcus R, Feldman D, Nelson DA, Rosen CJ, editors. *Osteoporosis*. 3rd ed. Boston:Elsevier; 2008; 985 – 1009.

Jennermann C, Triantafillou J, Cowan D, Pennick BGA, Connolly KM, Morris DC. Effects of thiazolidinediones on bone turnover in the rat. *Endocrinology* 1995; 145: 401 – 6.

Jiang G, Dallas-Yang Q, Li Z, Szalkowski D, Liu F, Shen X, Wu M, Zhou G, Doebber T, Berger J, Moller DE, Zhang BB. Potentiation of insulin signaling in tissues of Zucker obese rats after acute and long-tern treatment with PPARγ agonists. *Diabetes* 2002; 51: 2412 – 19.

Karsenty G. Convergence between bone and energy homeostatis: leptin regulation of bone mass. *Cell Metabolism* 2006; 4: 341 – 8.

Kasra M, Vanin CM, MacLusky NJ, Casper RF, Grynpas MD. The effects of different estrogen and progestin regimens on the mechanical properties of rat femur. *Journal of Orthopaedic Research* 1997; 15: 118 – 23.

Kawai M, Devlin MJ, and Rosen CJ. Fat targets for skeletal health. *Nature Reviews Rheumatology* 2009;5: 365 – 72.

Kawashima Y, Fritton JC, Yakar S, Epstein S, Schaffler MB, Jepsen KJ, LeRoith D. Type 2 diabetic mice demonstrate slender long bones with increased fragility secondary to increased osteoclastogenesis. *Bone*, 2009; 44: 648 – 55.

Khan E, Abu-Amer Y. Activation of peroxisome proliferator-activated receptor-γ inhibits differentiation of preosteoblasts. *Journal of Laboratory and Clinical Medicine* 2003;: 29 – 34.

Kurtz TW, Morris RC, Pershadsingh HA. The Zucker fatty rat as a genetic model of obesity and hypertension. *Hypertension* 1989; 13: 896 – 901.

Lanyon LE and Ruben CT. Static vs dynamic loads as an influence on bone remodeling. *Journal of Biomechanics* 1984; 17: 897 – 905.

Lazarenco OP, Rzonca SO, Hogue WR, Swain FL, Suva LJ, Lecka-Czernik B. Rosiglitazone induces decreased in bone mass and strength that are reminiscent of aged bone. *Endocrinology* 2007; 148: 2669 – 80.

Lehmann JM, Moore LB, Smith-Oliver TA, Wilkinson WO, Willson TM, Kliewer SA. An antidiabetic thiazolidinedione is a high affinity ligand for peroxisome proliferator-activated receptor-γ (PPAR-γ). Journal of Biological Chemistry 1995; 270: 12953 – 56.

Ma L, Ji JL, Ji H, Yu X, Ding LJ, Liu K, Li YQ. Telmisartan alleviates rosiglitazone-induced bone loss in ovariectomized spontaneous hypertensive rats. *Bone* 2010; 47: 5 – 11.

Lecka-Czernik B, Ackert-Bicknell C, Adamo ML, Marmolejos V, Churchill GA, Shockley JR, Reid IR, Grey A, Rosen CJ. Activation of peroxisome proliferator-activated receptor gamma (PPARgamma) by rosiglitazone suppresses components of the insulin-like growth factor regulatory system in vitro and in vivo. *Endocrinology* 2007; 148: 903 – 11.

Leidig-Bruckner G and Ziegler R. Diabetes mellitus a risk for osteoporosis? *Experimental and Clinical Endocrinology and Diabetes* 2001; 109: S493 – S514.

Liefde II, Vanderclift M, de Laet CEDH, can Daele PLA, Hofman A, Pols HAP. Bone mineral density and fracture risk in type-2 diabetes mellitus: the Rotterdam study. *Osteoporosis International* 2005; 16: 1713 – 20.

Lin TH, Yang RS, Tang CH, Lin CP, Fu WM. PPARγ inhibits osteogenesis via the down-regulation of the expression of COX-2 and iNos in rats. *Bone* 2007; 41: 562 – 74.

Loke YK, Singh S, Furberg CD. Long-term use of thiazolidinediones and fractures in type 2 diabetes: a meta-analysis. *Canadian Medical Association Journal* 2009; 180: 32 – 9.

Mancini T, Mazziotti G, Doga M, Carpinteri R, Simetovic N, Vescovi PP, Giustine A. Vertebral fractures in males with type 2 diabetes treated with rosiglitazone. *Bone* 2009; 45: 784 – 788.

Martine EA, Ritman EL, Turner RT. Time course of epiphyseal growth plate fusion in rat tibiae. *Bone* 2003; 32: 261 – 7.

Mayerson AB, Hundal RS, Dufour S, Lebon V, Befroy D, Cline GW, Enocksson S, Inzucchi SE, Shulman GI, Petersen KF. The Effects of Rosiglitazone on Insulin Sensitivity, Lipolysis, and Hepatic and Skeletal Muscle Triglyceride Content in Patients With Type 2 Diabetes. *Diabetes* 2002; 51: 797 – 802.

Meier C, Kraenzlin ME, Bodmer M et al. Chronic use of thiazolidinediones increases fracture risk. *Journal of Scientific Outcomes* 2008; 15: 322 – 23.

Mollard RC, Gillam ME, Wood TM, Taylor CG, Weiler HA. (n-3) Fatty Acids Reduce the Release of Prostaglandin E_2 from Bone but Do Not Affect Bone Mass in Obese (*fa/fa*) and Lean Zucker Rats. *The American Society for Nutritional Sciences* 2005; 135: 499 – 504.

Moller D. New drug targets for type 2 diabetes and the metabolic syndrome. *Nature* 2001; 414: 821 – 27.

Nagy TR, Prince CW, Li J. Validation of peripheral dual-energy X-ray absorptiometry for the measurement of bone mineral in intact and excised long bones of rats. *Journal of Bone and Mineral Research* 2001; 16: 1682 – 7.

Natali A, Balbeweg S, Toschi E, Capaldo B, Barbaro D, Gastaldelli A, Yudkin JS, Ferrannini E. Vascular effects of improving metabolic control with metformin or rosiglitazone in type 2 diabetes. *Diabetes Care* 2004; 27:1349 – 57.

Parfitt AM, Drezner MK, Glorieux FH, Kanis JA, Malluche H, Meunier PJ, et al. Bone histomorphometry: standardization of nomenclature, symbols, and units. Report of the ASBMR Histomorphometry Nomenclature Committee. *Journal of Bone and Mineral Research* 1987; 2: 595 – 610.

Peng ZQ, Vaananen HK, Zhang HX, Tuukkanen J. Long-term effect of ovariectomy on the mechanical properties and chemical composition of rat bone. *Bone* 1997; 20: 207 – 12.

Petit MA, Beck TJ, Lin HM, Bentley C, Legro R, Lloyd T. Femoral bone structural geometry adapts to mechanical loading and is influenced by sex steroids: the Penn State Young Women's Health Study. *Bone* 2004; 35: 750 – 9.

Pickavance LC, Tadayyon M, Widdowson PS, Buckingham RE, Wilding JPH . Therapeutic index for rosiglitazone in dietary obese rats: separation of efficacy and haemodilution. *British Journal of Pharmacology* 1999; 128: 1570 – 76.

Redd GK, Stehno-Bittel L, Hamade S, Enwemeka CS. The Biomechanical integrity of bone in experimental diabetes. *Diabetes Research and Clinical Practice* 2001; 54: 1 – 8.

Reid IR. Relationships between fat and bone. *Osteoporosis International* 2008;19: 595 – 606.

Rho JY, Kuhn-Spearing L, Zioupos P. Mechanical properties and the hierarchical structure of bone. *Medical Engineering and Physics* 1998; 20: 92 – 102.

Roodman G. Cell biology of the osteoclast. *Experimental Hematology* 1999; 27: 1229 – 41.

Rosen CJ. Sugar and Bone : A not-so sweet story. *Journal of Bone and Mineral Research* 2008; 23: 1881 – 83.

Rosen ED, Spiegelman BM. PPARγ: a nuclear regulator of metabolism, differentiation and cell growth. *Journal of Biological Chemistry* 2001; 12: 37731 – 4.

Rzonca SO, Suva LJ, Gaddy D, Montague DC, Lecka-Czernik B. Bone is a target for the antidiabetic compound rosiglitazone. *Endocrinology* 145, 401-406 (2005).

Sahni M, Guenther HL, Fleisch H, Collin P, Martin TJ. Bisphosphonates act on rat bone resorption through the mediation of osteoblasts. *Journal of Clinical Investigation* 1993; 91: 2004–2011.

Schwartz, A.V. Diabetes Mellitus: Does it Affect Bone? *Calcified Tissue International* 2003; 73: 515 – 19.

Schwartz AV, Sellmeyer DE. Women, type 2 diabetes, and fracture risk. *Current Diabetes Reports* 2004; 4: 364 – 369.

Schwartz AV, Sellmeyer DE, Vittinghoff E, Palermo L, Lecka-Czernik B, Feingold KR, Strotmeyer ES, Resnick HE, Carbone L, Beamer BA, Park SW, Lane NE, Harris TB, Cummings SR, for the health, Aging and Body Composition (Health ABC) Study. Thiazolidinedione use and bone loss in older diabetic adults. *Journal of Clinical Endocrinology and Metabolism* 2006; 91: 3349 – 54.

Shevde NK, Bendixen AC, Dienger KM, Pike JW. Estrogens suppress RANK ligand-induced osteoclast differentiation via a stromal cell independent mechanical involving c-Jun repression. *Proceedings of the National Academy of Sciences* 2000; 97: 7829 – 34.

Soronceau MA, Miao D, Bai XY. Rosiglitazone impacts negatively on bone by promoting osteoblast/osteocyte apoptosis. *Journal of Endocrinology* 2004; 183: 203 – 16.

Sottile V, Seuwen K, Kneissel M. Enhanced Marrow Adipogenesis and Bone Resorption in Estrogen-Deprived Rats Treated with the PPARgamma Agonist BRL49653 (Rosiglitazone). *Calcified Tissue International* 2004; 75: 325 – 37.

Takada, I. and Kato, S. A new PPAR-γ Function in Bone. *International Bone and Mineral Society* 2008; 5: 258 – 61.

Thomsen JS, Laib A, Koller B, Prohaska S, Mosekilde LI, Gowin W. Stereological measures of trabecular bone structure: comparison of 3D micro computed tomography with 2D histological sections in human proximal tibial bone biopsies. *Journal of Microscopy* 2005; 218: 171 – 9.

Tontonoz P and Spiegelman BM. Fat and Beyond: the diverse biology of PPARγ. *Annual Review Biochemistry* 2008; 77: 289 – 312.

Turner CH, Hsieh YF, Muller R, Bouxsien ML, Baylink DJ, Rosen DJ, Grynpas MD, Donahue LR, Beamer WG. Genetic regulation of cortical and trabecular bone strength and microstructure in inbred strains of mice. *Journal of Bone and Mineral Research* 2000; 15: 1126 – 31.

Turner CH. Biomechanics of Bone: Determinants of skeletal fragility and bone quality. *Osteoporosis International* 2002; 13: 97 – 104.

Turner CH. Three rules for bone adaptation to mechanical stimuli. *Bone* 1998; 23: 399 – 407.

Turner RT and Iwaniec UT. Moderate weight gain does not influence bone metabolism in skeletally mature female rats. *Bone* 2010, doi:10.1016/j.bone.2010.06.010

Viberti G, Kahn SE, Greene DA, Herman WH, Zinman B, Holman RR, Haffner SM, Levy D, Lachin JM, Berry RA, Heise MA, Jones NP, Freed MI. ADOPT An international multicenter study of the comparative efficacy of rosiglitazone, glyburide, and metformin in recently diagnosed type 2 diabetes. *Diabetes Care* 2002; 25; 1737 – 43.

Villareal DT, Shah K, Banks MR, Sinacore DR, Klein S. Effect of Weight Loss and Exercise Therapy on Bone Metabolism and Mass in Obese Older Adults: A One-Year Randomized Controlled Trial. *Journal of Clinical Endocrinology & Metabolism* 2008; 93: 2182 – 218.

Walker AB, Chattington PD, Buckingham RE, Williams G. The thiazolidinedione rosiglitazone (BRL-49653) lowers blood pressure and protects against impairment of endothelial function in zucker fatty rats. *Diabetes* 1999; 48: 1448 – 53.

Wan Y, Chong LW, Evans RM. PPAR-gamma regulates osteoclastogenesis in mice. *Nature Medicine* 2007; 13: 1496 – 1503.

Watts NB. Treatment of osteoporosis with bisphosphonates**.** *Endocrinology and Metabolism Clinics* 1998; 27

Watts, NB. Clinical utility of biomarkers of bone remodeling. *Clinical Chemistry* 1999; 45: 1359 – 1369.

Williams GA, Wang Y, Callon KE, Watson M, Lin J, Lam JBB, Costa JL, Orpe A, Broom N, Naot D, Rien IR, Cornish J. In vitro and in vivo effects of adiponectin on Bone. *Endocrinology* 2009; 150: 3603 – 10.

Wood AJ. Drug therapy: Metformin. *The New England Journal of Medicine* 1996; 334: 574 – 79.

Yang WS, Jeng CY, Wu TJ, Tanaka S, Funahashi T, Matsuzawa Y, Wang JP, Chen CL, Tai TY, Chuang LM. Synthetic peroxisome proliferator-activated receptor-γ agonist, rosiglitazone, increases plasma levels of adiponectin in type 2 diabetic patients. *Diabetes Care* 2002; 25: 376 – 380.

Ye JM, Dzamko N, Cleasby ME, Hegarty BD, Furler SM, Cooney GJ, Kraegen EW. Direct demonstration of lipid sequestration as a mechanism by which rosiglitazone prevents fatty-acid-induced insulin resistance in the rat: comparison with metformin. *Diabetologia* 2004; 47: 1306 – 13.